

SEQUENTIAL GROWTH FACTOR DELIVERY FROM
POLYMERIC SCAFFOLDS FOR BONE TISSUE ENGINEERING

A THESIS SUBMITTED TO
THE GRADUATE SCHOOL OF NATURAL AND APPLIED SCIENCES
OF
MIDDLE EAST TECHNICAL UNIVERSITY

BY

PINAR YILGÖR

IN PARTIAL FULFILLMENT OF THE REQUIREMENTS
FOR
THE DEGREE OF DOCTOR OF PHILOSOPHY
IN
BIOTECHNOLOGY

SEPTEMBER 2009

Approval of the thesis:

**SEQUENTIAL GROWTH FACTOR DELIVERY FROM
POLYMERIC SCAFFOLDS FOR BONE TISSUE ENGINEERING**

submitted by **PINAR YILGÖR** in partial fulfillment of the requirements for the degree of **Doctor of Philosophy in Department of Biotechnology, Middle East Technical University** by,

Prof. Dr. Canan Özgen
Dean, Graduate School of **Natural and Applied Sciences**

Prof. Dr. Gülay Özcengiz
Head of Department, **Biotechnology**

Prof. Dr. Nesrin Hasırcı
Supervisor, **Chemistry Dept., METU**

Prof. Dr. Vasıf Hasırcı
Co-Supervisor, **Biological Sciences Dept., METU**

Examining Committee Members:

Prof. Dr. Rui L. Reis
Polymer Engineering Dept., Minho Univ., Portugal

Prof. Dr. Nesrin Hasırcı
Chemistry Dept., METU

Prof. Dr. Gülay Özcengiz
Biological Sciences Dept., METU

Prof. Dr. İsmet Gürhan
Bioengineering Dept., Ege Univ.

Prof. Dr. Meral Yücel
Biological Sciences Dept., METU

Date: 28.09.2009

I hereby declare that all information in this document has been obtained and presented in accordance with academic rules and ethical conduct. I also declare that, as required by these rules and conduct, I have fully cited and referenced all material and results that are not original to this work.

Name, Last name: Pınar Yılgör

Signature:

ABSTRACT

SEQUENTIAL GROWTH FACTOR DELIVERY FROM POLYMERIC SCAFFOLDS FOR BONE TISSUE ENGINEERING

Yılıgör, Pınar

Ph.D., Department of Biotechnology

Supervisor : Prof. Dr. Nesrin Hasırcı

Co-Supervisor: Prof. Dr. Vasıf Hasırcı

September 2009, 152 pages

Tissue engineering is a promising alternative strategy to produce artificial bone substitutes; however, the control of the cell organization and cell behavior to create fully functional 3-D constructs has not yet been achieved. To overcome these, activities have been concentrated on the development of multi-functional tissue engineering scaffolds capable of delivering the required bioactive agents to initiate and control cellular activities. The aim of this study was to prepare tissue engineered constructs composed of polymeric scaffolds seeded with mesenchymal stem cells (MSCs) carrying a nanoparticulate growth factor delivery system that would sequentially deliver the growth factors in order to mimic the natural bone healing process. To achieve this, BMP-2 and BMP-7, the osteogenic growth factors, were encapsulated in different polymeric nanocapsules (poly(lactic acid-co-glycolic acid) (PLGA) and poly(3-hydroxybutyrate-co-3-hydroxyvalerate)

(PHBV)) with different properties (degradation rates, crystallinity) and, therefore, different release rates to achieve the early release of BMP-2 followed by the release of BMP-7, as it is in nature. Initially, these nanoparticulate delivery systems were characterized and then the effect of single, simultaneous and sequential delivery of BMP-2 and BMP-7 from these delivery systems was studied *in vitro* using rat bone marrow MSCs. The effect of using these two growth factors in a sequential manner by mimicking their natural bioavailability timing was shown with maximized osteogenic activity results. BMP-2 loaded PLGA nanocapsules were subcutaneously implanted into Wistar rats and according to initial results, their biocompatibility as well as the positive effect of BMP-2 release on the formation of osteoclast-like cells was shown. To complete the construction of the bioactive scaffold, this nanoparticulate sequential delivery system was incorporated into two different types of polymeric systems; natural (chitosan) and synthetic (poly(ϵ -caprolactone) (PCL)). 3-D fibrous scaffolds were produced using these materials by wet spinning and 3-D plotting. Incorporation of nanocapsules into 3-D chitosan scaffolds was studied by two different methods: incorporation within and onto chitosan fibers. Incorporation into 3-D PCL scaffolds was achieved by coating the nanocapsules onto the fibers of the scaffolds in an alginate layer. With both scaffold systems, incorporation of nanocapsule populations capable of delivering BMP-2 and BMP-7 in single, simultaneous and sequential fashion was achieved. As with free nanocapsules, the positive effect of sequential delivery on the osteogenic differentiation of MSCs was shown with both scaffold systems, creating multi-functional scaffolds capable of inducing bone healing.

Keywords: Bone Tissue Engineering, Mesenchymal Stem Cells, Nanoparticles, 3-D Plotting, Wet Spinning, Biodegradable Polymers.

ÖZ

KEMİK DOKU MÜHENDİSLİĞİ AMAÇLI SIRALI BÜYÜME FAKTÖRÜ SALAN POLİMERİK DOKU İSKELELERİ

Yılgör, Pınar

Doktora, Biyoteknoloji Bölümü

Tez Yöneticisi : Prof. Dr. Nesrin Hasırcı

Ortak Tez Yöneticisi : Prof. Dr. Vasıf Hasırcı

Eylül 2009, 152 sayfa

Doku mühendisliği yapay kemik dokusu oluşturulması için alternatif umut verici bir yöntemdir, ancak tamamen fonksiyonel üç boyutlu yapıların oluşturulması için gerekli hücre organizasyonu ve aktivitelerinin kontrolü henüz sağlanamamıştır. Bu sorunu çözmek amacıyla, çalışmalar hücre davranışlarını tetikleyecek ve kontrol edecek gerekli biyoaktif ajanların salımını sağlayabilen multi-fonksiyonel doku iskeleleri oluşturmak üzerine konsantre olmuştur. Bu çalışmanın amacı, kemik iyileşme sürecini taklit edebilmek amacıyla hazırlanmış bir sıralı salım sistemi ile yüklü ve mezenşimal kök hücre (MSC) ekilmiş fonksiyonel polimerik doku iskeleleri oluşturmaktır. Bunun elde edilmesi için izlenen yöntem, osteojenik büyüme faktörleri olan BMP-2 ve BMP-7'nin doğada olduğu gibi sıralı salımını sağlayabilmek amacıyla bunların farklı bozunma hızı ve özelliklere sahip iki farklı polimerik nanokapsül (poli(laktik asit-ko-glikolik asit)

(PLGA) ve poli(3-hidroksibütirat-ko-3-hidroksivalerat) (PHBV)) içerisine hapsedilmesi ve erken BMP-2, geç BMP-7 salımı sağlayabilen bir sistem oluşturulmasıdır. Öncelikle bu nanopartiküllerden oluşan sıralı salım sistemi karakterize edilmiş ve daha sonra BMP-2 ve BMP-7'nin tek, birlikte ve sıralı salımının etkileri *in vitro* ortamda kemik iliği MSC hücreleri ile incelenmiştir. Bu iki büyüme faktörünün doğal oluşma sıralarını taklit ederek sıralı şekilde salınmasının etkisi maksimum osteojenik aktivite sonuçları ile gösterilmiştir. BMP-2 taşıyan PLGA nanokapsülleri Wistar sıçanlarının deri altına implante edilmiş ve elde edilen ilk sonuçlara göre, nanokapsüllerin biyoyumluluğu ile birlikte *in vivo* BMP-2 salımının osteoklast-benzeri hücre oluşmasına pozitif etkileri gözlemlenmiştir. Biyoaktif doku iskelelerinin yapımının tamamlanması için, bu sıralı salım sağlayan nanopartikül sistemi, doğal (kitosan) ve sentetik (poli(ϵ -kaprolakton) (PCL)) iki farklı polimerik sistem içerisine yüklenmiştir. Üç-boyutlu lifsi doku iskeleleri bu malzemeler kullanılarak ıslak eğirme ve 3-boyutlu çizim yöntemleriyle hazırlanmıştır. Nanopartiküllerin kitosan doku iskelelerine yüklenmesi fiberlerin içerisine veya üzerine olmak üzere iki farklı yöntemle çalışılmıştır. PCL doku iskelelerine yükleme ise, nanopartiküllerin bir aljinat tabakası içerisinde fiber yüzeylerine kaplanması ile elde edilmiştir. Her iki sisteme de tek, birlikte ve sıralı BMP-2 ve BMP-7 salımı yapabilen nanopartikül popülasyonları yüklenmiştir. Tek başına nanopartiküllerde olduğu gibi, her iki polimerik sistemde de sıralı salımın osteojenik aktivite üzerine pozitif etkisi gösterilmiş olup kemik iyileşme sürecini tetikleyebilecek multi-fonksiyonel doku iskeleleri hazırlanmıştır.

Anahtar Kelimeler: Kemik Doku Mühendisliği, Mezenşimal Kök Hücre, Nanopartiküller, 3-Boyutlu Çizim, Islak Eğirme, Biyobozunur Polimerler.

Dedicated to Lena and Esat Yulgör...

ACKNOWLEDGEMENTS

I would like to express my most sincere gratitude to my supervisor Prof. Dr. Nesrin Hasırcı for her continuous guidance, support and encouragement throughout my thesis. I am grateful for the time and effort she has spent to improve my scientific experience during my graduate years.

I am deeply indebted to my co-supervisor Prof. Dr. Vasıf Hasırcı who has supported, encouraged and inspired me the most during these years. I was fortunate to work with him; with whom I've had the opportunity to get training at an international level which indeed improved this thesis as well as my own scientific insight. I am very much grateful to him for his efforts to improve my scientific skills, for his being an accessible source of knowledge, and for all his patience towards my "interior design attacks" to reorganize his lab.

I wish to express my deeply felt gratitude to Prof. Dr. Rui Reis for giving me a wonderful opportunity to work in his lab, which definitely changed the course of this study. I also would like to thank to all members of 3B's Research Group for making my life in Portugal easier, fruitful and worth remembering. I especially would like to acknowledge the efforts of Dr. Kadriye Tuzlakođlu and Dr. Rui Amandi de Sousa who helped and guided my experiments in Portugal as well as for their contributions in the preparation of my publications.

I am also very grateful to Assoc. Prof. Dr. Gamze Torun Kse for her guidance and encouragement throughout this thesis.

I would like to express my sincere gratitude to Prof. Dr. Semih Keskil (Bayındır Hospital, Ankara, Turkey), Dr. Blent nal (GATA Military Hospital, Ankara, Turkey), Prof. Dr. Sadi Gndođdu (Ufuk University, Ankara, Turkey), Assist. Prof. Dr. Gldal Yılmaz (Gazi University, Ankara, Turkey), Prof. Dr. James Kirkpatrick and Dr. Shahram Ghanaati (Johannes Gutenberg University, Mainz, Germany) for making the *in vivo* part of this thesis possible.

My sincere acknowledgements go to my thesis progress committee members, Prof. Dr. Meral Yücel and Prof. Dr. İsmet Gürhan for their useful comments and suggestions throughout this thesis.

I would like to thank Dr. Pınar Zorlutuna for her invaluable friendship, for all the brainstormings and critical thinking on science and on life in general.

I am grateful to Dr. Halime Kenar and Dr. Deniz Yücel for their kind friendship and for their suggestions and help throughout this thesis. It was a pleasure to work with them as well as to organize the *in vivo* studies.

I wish to thank to all members of METU BIOMAT Research Group who helped and influenced this study in many ways; Arda Büyüksungur, Erkin Aydın, Albana Ndreu, Buket Başmanav, Aysel Kızıltay, Tuğba Endoğan, Hayriye Özçelik, Beste Kımıkoğlu, Birsen Demirbağ, Özge Karadaş, Sinem Kardeşler, Gizem Altay, Gökhan Bahçecioğlu, Gözde Eke, Aysu Küçükürhan and Bilgenur Kandemir. It was an honor to work with such qualified scientists. I also would like to thank Mr. Zeynel Akın for his technical support throughout my thesis.

This study was conducted within the scope of the EU FP6 NoE Project EXPERTISSUES. I gratefully acknowledge the support of EXPERTISSUES in the form of an integrated PhD grant. I also would like to acknowledge the support from TUBITAK through projects TBAG 105T508 and 108T805.

Special thanks to my brother, my “petit” surgeon, Dr. Çağlar Yılgör for his help in the design of my *in vivo* experiments, for his endless energy that always cheers me up, and for his support and love with whom I’ve learned to share things in life.

I would like to thank my husband Dr. Gazi Huri for his help and support in every possible way; mentally, physically and scientifically and, above all, for giving me peace in a lifetime of war.

Finally, I would like to thank from the depth of my heart my dear parents Lena Yılgör and Prof. Dr. Esat Yılgör for their understanding, love, care and support during this study as well as all throughout my life.

TABLE OF CONTENTS

ABSTRACT.....	iv
ÖZ.....	vi
ACKNOWLEDGEMENTS.....	ix
TABLE OF CONTENTS.....	xi
LIST OF TABLES.....	xv
LIST OF FIGURES.....	xvi
LIST OF ABBREVIATIONS.....	xxii
CHAPTERS	
1. INTRODUCTION.....	1
1.1. Bone.....	1
1.1.1. Structure and Organization of Bone.....	1
1.1.2. Bone Repair Process.....	3
1.2. Clinical Approaches in Bone Repair and Regeneration.....	4
1.2.1. Biological Grafts.....	5
1.2.2. Synthetic Grafts.....	8
1.3. Emerging Alternative in Bone Repair: Tissue Engineering.....	11
1.3.1. Cells in Bone Tissue Engineering.....	12
1.3.1.1. Mesenchymal Stem Cells.....	13
1.3.2. Scaffolds in Bone Tissue Engineering.....	15
1.3.2.1. Materials Used in Scaffold Production.....	15
1.3.2.1.1. Natural Polymers.....	16
1.3.2.1.2. Synthetic Polymers.....	17
1.3.2.2. Scaffold Production Techniques.....	18
1.3.2.2.1. Rapid Prototyping.....	20
1.3.2.2.2. Wet Spinning.....	22
1.3.3. Growth Factors in Bone Tissue Engineering.....	23

1.3.3.1. Bone Morphogenetic Proteins.....	25
1.4. Controlled Growth Factor Delivery in Tissue Engineering.....	26
1.4.1. Impact of Nanotechnology in Controlled Delivery.....	28
1.4.2. Multiple Growth Factor Delivery from Tissue Engineering Constructs.....	30
1.5. Aim, Novelty and Approach of the Study.....	31
2. MATERIALS AND METHODS.....	33
2.1. Materials.....	33
2.2. Methods.....	34
2.2.1. Preparation of Scaffolds for Bone Tissue Engineering.....	34
2.2.1.1. Production of Chitosan Fiber Mesh Scaffolds by Wet Spinning....	34
2.2.1.2. Production of Poly(ϵ -caprolactone) (PCL) Scaffolds.....	36
2.2.1.2.1. PCL Scaffold Fabrication by 3-D Plotting.....	36
2.2.1.2.2. PCL Scaffold Fabrication by Wet Spinning.....	42
2.2.2. Preparation of Nanocapsules for Growth Factor Delivery.....	43
2.2.3. Incorporation of Nanocapsules into/onto the Carriers.....	45
2.2.3.1. Incorporation of Nanocapsules into Chitosan Scaffolds (NP-IN)..	45
2.2.3.2. Incorporation of Nanocapsules onto Chitosan Scaffolds (NP-ON)	46
2.2.3.3. Incorporation of Nanocapsules onto PCL Scaffolds.....	46
2.2.4. Characterization.....	47
2.2.4.1. Scanning Electron Microscopy (SEM).....	47
2.2.4.2. Particle Size Distribution Analysis.....	48
2.2.4.3. Assessment of in situ Degradation.....	48
2.2.4.3.1. Degradation of PLGA and PHBV Nanocapsules.....	48
2.2.4.3.2. Swelling and Degradation of Chitosan Scaffolds.....	48
2.2.4.3.3. Degradation of PCL Scaffolds.....	49
2.2.4.4. Microcomputed Tomography (μ -CT).....	49
2.2.4.5. Dynamic Mechanical Analysis (DMA).....	50
2.2.5. In situ Release Studies.....	50
2.2.5.1. BSA Release from Nanocapsules in Free Form and in Scaffolds..	50
2.2.5.2. BMP Release from Free Nanocapsules.....	51
2.2.6. <i>In vitro</i> Studies.....	52

2.2.6.1. Isolation of Bone Marrow Mesenchymal Stem Cells.....	52
2.2.6.2. Bone Marrow MSC Culture.....	53
2.2.6.3. Cell Seeding.....	53
2.2.6.3.1. Cell Seeding for Free Nanocapsules.....	54
2.2.6.3.2. Cell Seeding on Chitosan and PCL Scaffolds.....	54
2.2.6.4. Determination of Cell Proliferation.....	54
2.2.6.5. ALP Assay for the Assessment of MSC Differentiation.....	56
2.2.6.6. Determination of Cell Phenotype.....	57
2.2.7. <i>In vivo</i> Studies.....	57
2.2.7.1. <i>In vivo</i> Evaluation of BMP-2 Loaded PLGA Nanocapsules.....	57
2.2.7.2. <i>In vivo</i> Evaluation of BMP-2/BMP-7 Releasing Tissue Engineered PCL Constructs.....	59
2.2.8. Statistical Analysis.....	63
3. RESULTS AND DISCUSSION.....	64
3.1. Preparation of Nanoparticulate Sequential Delivery System.....	64
3.1.1. Particle Structure and Size.....	64
3.1.2. Degradation of Loaded PLGA and PHBV Nanocapsules.....	66
3.1.3. Encapsulation Efficiency and Release Kinetics.....	68
3.1.4. Influence of Sequential BMP-2/BMP-7 Delivery on MSC Proliferation and Differentiation.....	73
3.2. Growth Factor Delivery from Chitosan Scaffolds.....	76
3.2.1. Chitosan Fiber Mesh Scaffold Production.....	76
3.2.2. Characterization of the Scaffolds.....	79
3.2.3. MSC Culture on Chitosan Scaffolds.....	82
3.2.4. Incorporation of Nanoparticles into Chitosan Scaffolds.....	85
3.2.5. The Release Behavior.....	88
3.2.6. Effect of BMP-2 dose on the Proliferation and Differentiation of MSCs.....	89
3.2.7. Influence of BMP-2/BMP-7 Delivery from Constructs on MSC Proliferation and Differentiation.....	91
3.3. Growth Factor Delivery from PCL Scaffolds.....	95
3.3.1. PCL Scaffold Production and Characterization.....	95

3.3.1.1. Scaffold Porosity.....	95
3.3.1.2. Mechanical Properties.....	99
3.3.2. Degradation of PCL Scaffolds.....	101
3.3.3. MSC Culture on PCL Scaffolds.....	103
3.3.4. Incorporation of Sequential Delivery System into PCL Scaffolds.....	109
3.3.5. Effect of Sequential BMP-2/BMP-7 Delivery from PCL Scaffolds with Different Fiber Orientations on the Proliferation and Differentiation of MSCs.....	113
3.4. <i>In vivo</i> Evaluation of BMP-2 loaded PLGA Nanocapsules.....	118
4. CONCLUSIONS.....	121
REFERENCES.....	123
APPENDICES	
A. CALIBRATION CURVE FOR BSA CONCENTRATION DETERMINATION.....	147
B. CALIBRATION CURVE FOR CELL NUMBER DETERMINATION.....	148
C. ETHICAL COMMITTEE APPROVAL.....	149
CURRICULUM VITAE.....	150

LIST OF TABLES

TABLES

Table 2.1.	Composition of chitosan scaffold preparation media.....	36
Table 2.2.	Experimental groups of <i>in vivo</i> evaluation of BMP releasing PCL scaffolds.....	62
Table 3.1.	BSA encapsulation efficiency of PLGA and PHBV nanocapsules.....	69
Table 3.2.	Kinetic analysis of BSA, BMP-2 and BMP-7 release from PLGA and PHBV nanocapsules according to Higuchi Diffusion Model...	71
Table 3.3.	Changes in chitosan scaffold properties after incubation in sterile PBS (pH 7.4) for 21 days.....	81
Table 3.4.	Mean porosity values of the PCL scaffolds.....	87
Table 3.5.	Storage and loss modulus of oriented and random PCL scaffolds..	100

LIST OF FIGURES

FIGURES

Figure 1.1.	The transverse section of bone (decalcified fibula, x250).....	2
Figure 1.2.	The structure of compact (perimeter) and cancellous (inside) bone	3
Figure 1.3.	Different forms of commercial demineralized bone matrix (Company: Exactech) (a) Optecure® gel allograft; (b) slab, (c) spherical, (d) powder forms of Optecure® allograft, (e) Optecure cortical cancellous chips.....	7
Figure 1.4.	Different shapes and sizes of commercial bovine xenograft Surgibone® (a) disk shaped, (b) rectangular prismatic, (c) cylindrical sponges.....	7
Figure 1.5.	Neobone ® ceramic bone substitutes, (a) the microstructure, (b) various forms including cylindrical and rectangular prismatic sponges, powder and crushed forms.....	9
Figure 1.6.	The potential of MSCs to differentiate into a variety of mesenchymal tissues, such as bone, cartilage, tendon, muscle, marrow, fat, and dermis.....	14
Figure 1.7.	A typical rapid prototyping chain for manufacturing custom-made implants.....	21
Figure 2.1.	Scheme of wet spun chitosan and chitosan/PEO mesh production.....	35
Figure 2.2.	Bioplotter equipment and its components that was used to fabricate oriented PCL scaffolds.....	38

Figure 2.3.	A representative example of Bioplotter CAD/CAM software working window by which the scaffold production parameters were set for the fabrication of basic PCL scaffold (Needle length: 28.1 mm, Needle diameter: 0.5 mm, Dispenser temperature: 140°C, Layer thickness: 0.25 mm, Basic structure, Offset X: 0, Offset Y: 0).....	39
Figure 2.4.	Production of the first two layers of crossed (C) PCL scaffold. (a) production of the first layer, (b) production of the second layer on the first layer, (c) two-layered scaffold (length 20 mm, height 20 mm and thickness 0.5 mm).....	40
Figure 2.5.	The design of oriented PCL scaffolds loaded on Bioplotter software. 3-D and cross sectional views of B (a, b), BO (c, d), C (e, f), CO (g, h).....	41
Figure 2.6.	PCL mesh production by combining 3 layers of PCL fibers.....	42
Figure 2.7.	Preparation of polymeric (PLGA, PHBV) nanocarriers of BMPs by $w_1/o/w_2$ double emulsion method.....	44
Figure 2.8.	Subcutaneous implantation of BMP-2 loaded PLGA nanocapsules to Wistar rats. (a) Pre-op, (b, c, d) shaving, cleaning and disinfection of the subscapular region, (e) subcutaneous implantation, (f) post-op.....	58
Figure 2.9.	The scheme of implantation into the iliac crest.....	60
Figure 2.10.	Implantation of scaffold C into the pelvis of a Sprague-Dawley rat. (a) Incision, (b) iliac crest, (c) creation of the bone defect, (d) bone defect, (e) insertion of the scaffold into the defect site.....	61
Figure 3.1.	BSA loaded capsules (a) PLGA: 10% (x50,000; inset shows wall thickness of 220 nm), (b) PLGA: 20% (x5,000), (c) PHBV: 10% (x20000), (d) PHBV: 20% (x1000).....	65
Figure 3.2.	Particle size distribution of 10% PLGA and 10% PHBV capsules.....	66

Figure 3.3.	pH change of the medium during degradation of PLGA and PHBV nanocapsules.....	67
Figure 3.4.	Degradation of BSA loaded nanocapsules at 37 °C in sterile PBS (pH 7.4) (a) PLGA, day 0 (x50,000), (b) PLGA, day 15 (x50,000), (c) PLGA, day 21 (x50,000), (d) PHBV, day 0 (x10,000), (e) PHBV, day 15 (x10,000), (f) PHBV, day 21 (x10,000).....	68
Figure 3.5.	BSA release from (a) PLGA capsules, (b) PHBV capsules with varying polymer contents.....	70
Figure 3.6.	BMP release from polymeric nanocapsules (BMP-2 from 10% PLGA nanocapsules, BMP-7 from 10% PHBV nanocapsules).....	72
Figure 3.7.	The kinetic analysis of BMP release according to Higuchi Diffusion Model (BMP-2 from 10% PLGA nanocapsules, BMP-7 from 10% PHBV nanocapsules).....	72
Figure 3.8.	Effect of BMP-2 and BMP-7 on MSC proliferation.....	74
Figure 3.9.	Effect of single, simultaneous and sequential delivery of BMP-2 and BMP-7 on MSC differentiation into osteoblastic cells.....	75
Figure 3.10.	CHI4-HAc2 fiber mesh scaffold, (a) x15, (b) x100, (c) x1000; CHI6-HAc2 fiber mesh scaffold, (d) x15, (e) x100, (f) 1000x. Bar represents (a, d) 2 mm, (b, e) 200µm, (c, f) 20µm.....	77
Figure 3.11.	CHI4-PEO2-HAc2 fiber mesh scaffold, (a) 15x, (b) 100x, (c) 1,000x; CHI4-PEO2-HAc5 fiber mesh scaffold, (d) 15x, (e) x100, (f) x1,000. Bar represents (a, d) 2 mm, (b, e) 200µm, (c, f) 20µm.....	78
Figure 3.12.	3-D representations of chitosan scaffolds obtained through µ-CT. (a, b) CHI4-HAc2, (b) CHI4-PEO2-HAc5.....	80
Figure 3.13.	Porosity distribution throughout the thickness of CHI4-HAc2 scaffold.....	80
Figure 3.14.	Fiber structure after 21 days of incubation in PBS. (a) CHI4-HAc2, (b) CHI4-PEO2-HAc5 scaffolds.....	82

Figure 3.15. MSC proliferation on CHI4-HAc2 (■) and CHI4-PEO2-HAc5 (□) scaffolds (n=3, *p<0.05, **p<0.001).....	83
Figure 3.16. Specific ALP activity on CHI4-HAc2 (■) and CHI4-PEO2-HAc5 (□) scaffolds.....	83
Figure 3.17. MSC attachment and spreading on (a, b) CHI4-HAc2; (c, d) CHI4-PEO2-HAc5 scaffolds after 21 days of incubation.....	85
Figure 3.18. PLGA nanocapsules incorporated (NP-IN) in (a, b) CHI4-HAc2 fiber, (c) CHI4-PEO2-HAc5 fiber (x1,000 in all micrographs including insets). Inset are unloaded counterparts.....	86
Figure 3.19. PLGA and PHBV nanocapsules on CHI4-HAc2 scaffold (NP-ON), (a) x200 (t=0), (b) x2000 (t=0), (c) x6,000 (t=21 day), (d) x12,000 (t=21 day).....	87
Figure 3.20. Release of BSA from free and incorporated particles.....	88
Figure 3.21. Effect of BMP-2 dose carried in PLGA nanocapsule loaded scaffolds on the proliferation of MSCs (n=3, *p<0.001, **p<0.01, ***p<0.05).....	90
Figure 3.22. Effect of BMP-2 dose on the differentiation of MSCs.....	91
Figure 3.23. MSC proliferation on chitosan scaffolds carrying BMP loaded nanocapsules. s. (n=3, *p<0.001, **p<0.01, ***p<0.05).....	92
Figure 3.24. Specific ALP Activity on BMP loaded particle incorporated chitosan fiber mesh scaffolds.....	94
Figure 3.25. SEM images of PCL scaffolds produced with 3-D plotting and wet spinning with different architectures, B: (a) and (b) x15, (c) x50; BO: (d) and (e) x15, (f) x50; C: (g) and (h) x15, (i) x50; CO: (j) and (k) x15, (l) x50; R: (m) and (n) x15, (o) x50.....	96
Figure 3.26. 3-D representations of PCL scaffolds. (a) B, (b) BO, (c) C, (d) CO, (e) R.....	97
Figure 3.27. Porosity distribution throughout the thickness of PCL scaffolds...	98
Figure 3.28. Relation between storage moduli and porosity of the oriented PCL scaffolds.....	101

Figure 3.29.	pH change of the medium during degradation of “B” PCL scaffold.....	102
Figure 3.30.	SEM of degradation of “B” PCL scaffold after 6 weeks of incubation in sterile PBS, (a) x250, (b) x500, (c) x1,000, (d) x2,000.....	103
Figure 3.31.	MSC proliferation on PCL scaffolds.....	104
Figure 3.32.	Fluorescence microcopy of MSC seeded PCL scaffolds, (a) B (x5), (b) B (x10), (c) BO (x5), (d) BO (x10). Stain: FITC-labeled phalloidin. Time: Day 21.....	105
Figure 3.33.	Fluorescence microcopy of MSC seeded PCL scaffolds, (a) C (x5), (b) C (x10), (c) CO (x5), (d) CO (x10), (e) R (x5), (f) R (x10). Stain: FITC-labeled phalloidin. Time: Day 21.....	106
Figure 3.34.	SEM of MSC attachment and spreading on PCL scaffolds. (a) BO, (b) C, (c) CO, (d) R. In these figures especially the cell stretching between different fibers is shown. Time: Day 21.....	107
Figure 3.35.	Specific ALP activity on PCL scaffolds.....	108
Figure 3.36.	SEM of PLGA nanocapsules incorporated onto the fiber surfaces of PCL scaffolds. B: (a) x90, (b) x400; BO: (c) x90, (d) x400; R: (e) x250, (f) x1,000.....	108
Figure 3.37.	SEM of “B” scaffold loaded with PLGA and PHBV nanocapsules after 21 days of culture (x20,000).....	111
Figure 3.38.	BSA release from free and incorporated PLGA nanocapsules on PCL scaffolds.....	112
Figure 3.39.	BSA release from free and incorporated PHBV nanocapsules on PCL scaffolds.....	112
Figure 3.40.	Cell proliferation on BMP loaded particle incorporated PCL scaffolds.....	114
Figure 3.41.	PCL scaffolds seeded with MSC on day 21 of incubation incorporated with PLGA and/or PHBV nanocapsules to provide sequential BMP-2/BMP-7 delivery. (a) scaffold B, (b) scaffold BO, (c) scaffold R, (d) x-section of the fiber of BO scaffold	

	showing complete coverage of the fiber surface with MSCs. x10.	115
Figure 3.42.	MSCs on BMP-2 loaded PLGA nanocapsule incorporated (a, b) B, (c, d) BO, (e, f) WS PCL scaffolds at the end of 21 days of incubation.....	116
Figure 3.43.	Specific ALP activity on BMP loaded particle incorporated PCL scaffolds.....	117
Figure 3.44.	Histology of the subcutaneous implantation site in a Wistar rat. Haematoxylin-Eosin staining, x40.....	118
Figure 3.45.	The overall evaluation of the <i>in vivo</i> performance of BMP-2 loaded PLGA nanocapsules.....	120
Figure A.1.	Calibration curve of BSA concentration for Micro-Bradford Assay.....	147
Figure B.1.	Calibration curve of rat bone marrow MSCs for Alamar Blue Assay.....	148
Figure C.1.	Ethical Committee Approval.....	149

LIST OF ABBREVIATIONS

μ -CT	Micro Computed Tomography
3-D	3 Dimensional
ALP	Alkaline Phosphatase
ANOVA	One-Way Analysis of Variance
B	Basic
BMP	Bone Morphogenetic Protein
BO	Basic-Offset
BSA	Bovine Serum Albumin
C	Crossed
CAD/CAM	Computer Aided Design / Computer Aided Manufacturing
CHI	Chitosan
CLSM	Confocal Laser Scanning Microscope
CM	Complete Media
CO	Crossed-Offset
DBM	Demineralized Bone Matrix
DMA	Dynamic Mechanical Analysis
DMEM	Dulbecco's Modified Eagle Medium
DMSO	Dimethyl Sulfoxide
ECM	Extracellular Matrix
ELISA	Enzyme-Linked ImmunoSorbent Assay
ESC	Embryonic Stem Cell
EtO	Ethylene Oxide
FBS	Fetal Bovine Serum
FDA	Food and Drug Administration
FDM	Fused Deposition Modeling
FGF	Fibroblast Growth Factor

FITC	Fluorescein Isothiocyanate
GAG	Glycosaminoglycan
HA	Hydroxyapatite
HAc	Acetic Acid
IGF	Insulin-like Growth Factor
IL	Interleukin
MSC	Mesenchymal Stem Cell
MW	Molecular Weight
NC	Nanocapsule
PBS	Phosphate Buffered Saline
PCL	Poly(ϵ -caprolactone)
PDGF	Platelet Derived Growth Factor
PE	Polyethylene
PEG	Poly(ethylene glycol)
PEO	Poly(ethyleneoxide)
PGA	Poly(glycolic acid)
PHA	Polyhydroxyalkanoate
PHB	Polyhydroxybutyrate
PHBV	Poly(3-hydroxybutyrate-co-3-hydroxyvalerate)
PHEMA	Poly(2-hydroxyethyl metacrylate)
PLA	Poly(lactic acid)
PLGA	Poly(lactic acid-co-glycolic acid)
PM	Primary Media
PMMA	Polymethylmetacrylate
PP	Polypropylene
PPF	Poly(propylene fumarate)
PVA	Polyvinylalcohol
R	Random
RP	Rapid Prototyping
SEM	Scanning Electron Microscope
SLS	Selective Laser Sintering
TCPS	Tissue Culture Polystyrene

TGF- β	Transforming Growth Factor-Beta
THF	Tetrahydrofuran
TRAP	Tartrate Resistant Acid Phosphatase
UHMWPE	Ultra High Molecular Weight Polyethylene
UV	Ultraviolet
VEGF	Vascular Endothelial Growth Factor

CHAPTER 1

INTRODUCTION

The aim of this study was to develop 3-D tissue engineered constructs that would induce natural bone regeneration upon implantation into a defect site by mimicking the *in vivo* conditions with an inherent growth factor delivery system.

1.1. Bone

1.1.1. Structure and Organization of Bone

Bones serve for such important functions of the human body as providing shape, protection of the internal organs, storage of minerals and growth factors and blood production (through the marrow in the medullary cavity of long bones and interstices of the cancellous bone). Other than the mineralized tissue and the marrow, bone contains blood vessels and nerves.

Bone is a complex, constantly changing, highly organized and mineralized connective tissue. The bones of the adult skeleton consist of cortical (compact) bone and cancellous (trabecular) bone (80 and 20% of the total bone mass of an adult skeleton, respectively). Cortical bone is much denser with a porosity ranging between 5-10% and is found primarily in the shaft of the long bones that form the outer shell around cancellous bone (Buckwalter *et. al.*, 1995). Cancellous bone tissue fills the interior which is composed of a network of rod- and plate-like elements that make the overall structure light and provides room for the blood vessels and the marrow.

Bone has a high structural hierarchy made of collagen-based structures and hydroxyapatite minerals that are in association with mature and immature bone cells, osteoblasts, osteocytes and osteoclasts. The basic structural unit is the Haversian system (osteon), roughly cylindrical structure that is typically several millimeters long and around 0.2 mm in diameter (Figure 1.1). Each osteon consists of concentric layers of collagen that surround a central canal, called the Haversian canal. It contains the nerves and blood vessels.

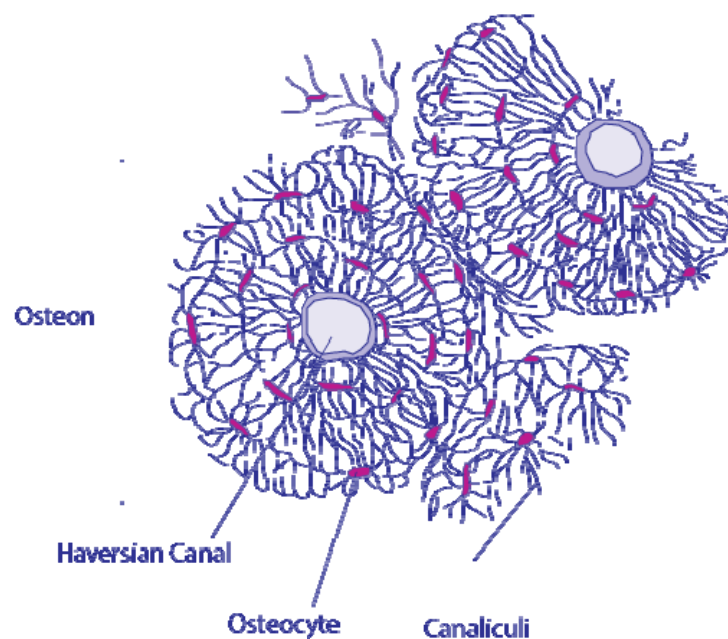


Figure 1.1. The transverse section of bone (decalcified fibula, x250) (Gray, 2000).

Within the shaft of a long bone, many osteons are bundled together in parallel along the axis of the bone, forming the compact bone, which handles the compressive and bending forces applied on them (Figure 1.2). Near the ends of the bones, where the stresses become more complex, the osteons spread out and branch to form a meshwork of cancellous bone.

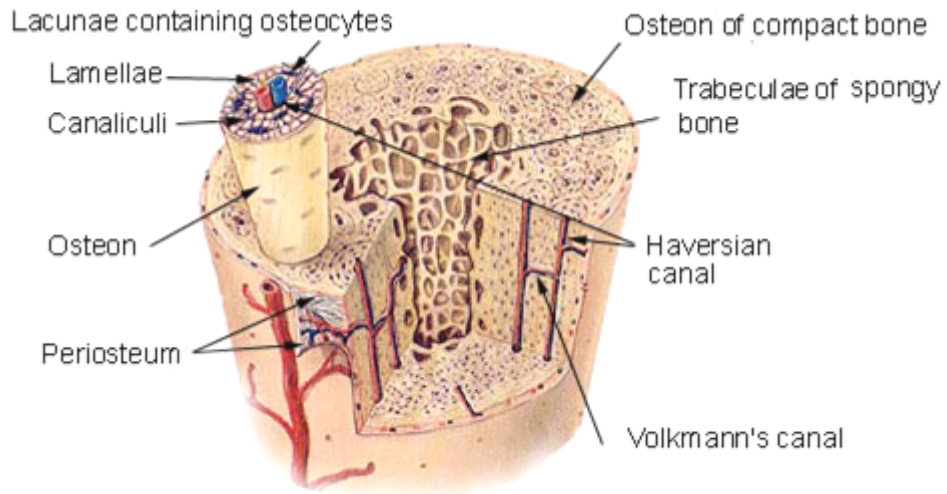


Figure 1.2. The structure of compact (perimeter) and cancellous (inside) bone (Spence, 1990).

1.1.2. Bone Repair Process

Although declining with age, bone remodels itself continuously throughout life; the structure is resorbed by the activity of osteoclasts and subsequently produced by osteoblasts. During this remodeling, calcium homeostasis is regulated, micro damages are repaired and the skeleton is shaped and sculpted. Bone also has the capacity of self-reconstruction and healing upon damage.

Fracture healing occurs in three major steps; inflammatory, reparative and remodeling. The inflammation occurs immediately following the fracture, during which a hematoma (or fibrin clot) occurs at the fracture site. Locally produced cytokines and growth factors within the hematoma promote the migration of osteoprogenitor cells to the defect site, and direct their differentiation into specific lineages (chondroblasts and osteoblasts responsible of hyaline cartilage and woven bone formation, respectively) (Allori *et. al.*, 2008). These factors also control cell proliferation and extracellular matrix (ECM) production. During these processes, multiple growth factors such as those from the transforming growth

factor-beta (TGF- β) superfamily, especially bone morphogenetic proteins (BMPs), insulin-like growth factor (IGF), fibroblast growth factor (FGF), platelet derived growth factor (PDGF) and vascular endothelial growth factor (VEGF) function in unison in a time and concentration dependent manner to regulate different aspects of the bone repair process (Hauschka *et. al.*, 1986). For example, PDGF is expressed predominantly during the early inflammatory stages and was found to stimulate the proliferation of mesenchymal stem cells (Marden *et. al.*, 1993; Rasubala *et. al.*, 2003). Being among the most osteoinductive growth factors presently described capable of inducing osteoblastic differentiation in several cell types (i.e., mesenchymal stem cells and fibroblasts) (Cowan *et. al.*, 2005); BMP-2 was reported to be an early appearing factor, peaking at day 1 after fracture, while BMP-7 was expressed mainly after 2 weeks (Cho *et. al.*, 2002). Expression of other TGF- β s is especially high during active matrix secretion (Sandberg *et. al.*, 1993; Linkhart *et. al.*, 1996). EGF upregulates the production of the matrix metalloproteinases, thus promoting the remodeling (van der Zee *et. al.*, 1998) which is the final phase of bone repair.

In the reparative phase of bone repair, generally at 3 weeks after fracture, a soft callus that bridges the fracture site forms. Then these structures are gradually replaced with lamellar bone, trabecular bone and finally with the compact bone which eventually duplicates the bone's original shape and strength in 6-12 weeks (Marieb and Hoehn, 2007).

1.2. Clinical Approaches in Bone Repair and Regeneration

Although bone can heal spontaneously and restore function without scarring, it has been recognized that repair is not always satisfactory. The regeneration potential of human bone is inadequate in the case of large bone defects especially those associated with comminuted fractures or bone tumor resection (Carano and Filvaroff, 2003). Rarely, insufficient healing may also occur in much smaller defects; nonunions occur in 1-5% of all cases (Fernandez *et. al.*, 2001). In such cases, a proper filler is required to fill the gap and help restore the structure and the function of bone.

Today, bone transplantations are done at least 10 times more than any organ transplantations (Sutherland and Bostrom, 2005). The ideal bone substitute should satisfy some essential requirements including an osteoconductive matrix that mimics the porosity and the microstructure of the natural tissue, and carry osteoinductive factors and osteogenic cells. Biological and synthetic grafts are used to serve as bone fillers in the clinic.

1.2.1. Biological Grafts

The most commonly used bone substitutes are biological grafts of autogenic, allogenic or xenogenic origin. Cadaver bone and demineralized bone matrix are the other main biological graft sources (Ebraheim *et. al.*, 2001).

An autograft is the tissue transplanted from one part of the body to another in the same individual. Currently, autografts are the preferred biological bone grafts most often used with success rates as high as 80-90% (Nystrom *et. al.*, 2002). They are compatible, do not transmit disease and contain viable osteoblasts that participate in new bone formation which is of utmost importance as the soft callus formation after surgery often depends on the bone formation by the transplanted osteoblasts (Sutherland and Bostrom, 2005). However, disadvantages like the limited availability of autografts and donor site morbidity associated with risks of infection and pain, increased anesthesia duration and significantly increased operative blood loss due to additional harvesting procedure make this method less preferable than it first looks (Younger and Chapman, 1989) and limits the use of autografts.

An allograft is tissue harvested from one person for transplantation into another. This type of grafting is not restricted by availability as much as with the autografts. Although allogenic transplantation techniques have been greatly improved since its inception, rejection, infection and allograft fracture are still among the most commonly encountered complications (Mankin *et. al.*, 1992; Sutherland and Bostrom, 2005). The need for sterilization and detailed testing prior to implantation affects the osteoinductive and osteogenic properties of allografts. Hence, allogenic bone can rarely be used fresh. Generally, they are batch-sterilized

and preserved by freezing below -60°C or by freeze drying which, however, destroys the osteoprogenitor cells, osteoinductive factors and causes decreased compressive strength upon rehydration (Tomford *et. al.*, 1992; Ohlendorf *et. al.*, 1996). Cadaver bone, also a source for allografts, is treated in a similar way. Due to altered properties, allografts can only serve as osteoconductive scaffolds.

Demineralized bone matrix (DBM) is prepared by acid extraction of allograft bone. This results in loss of most of the mineralized component leaving behind collagen and noncollagenous proteins, including growth factors (Khan *et. al.*, 2005). The efficacy of a DBM as a bone graft is dependent on the total amount of BMP retained, their concentration and the ratios of the different BMPs present. DBM is the only allograft with osteoinductive properties, although with a highly variable efficiency. It was shown that there is a significant difference in the capability of DBM of different suppliers in inducing spinal fusion due to differences in allograft processing methods (Peterson *et. al.*, 2004). DBM is currently available in the forms of powder, crushed, chips or as a gel prepared from cortical/cancellous bone by freeze drying and further processing (Figure 1.3).

Xenotransplantation is the transplantation of living cells, tissues or organs from one species to another, such as from pigs to humans. Although xenotransplantation offers a solution to the worldwide shortage of organs for clinical implantation, it raises many medical, legal and ethical issues including potential disease transmission between species. The first bone graft in history was a canine xenograft transplanted in human to repair a cranial defect (van Meekeren, 1668). Bovine bone as a graft material was first introduced in 1957 (Maatz and Bauermeister, 1957), a variety of which is commercially available today as Surgibone® (a sterile, extracellular composite of bovine bone) (Figure 1.4).

Since xenografts are sterilized and processed excessively to prevent cytotoxic/systemic effects, potential antigenicity/immunogenicity and to assure that they are pyrogen-free, they can only function as osteoconductive matrices (Chau and Mobbs, 2009).



Figure 1.3. Different forms of commercial demineralized bone matrix (Company: Exactech) (a) Optecure® gel allograft; (b) slab, (c) spherical, (d) powder forms of Optecure® allograft, (e) Optecure cortical cancellous chips (<http://www.exac.com/products/biologics/optecure-optecure-ccc>).

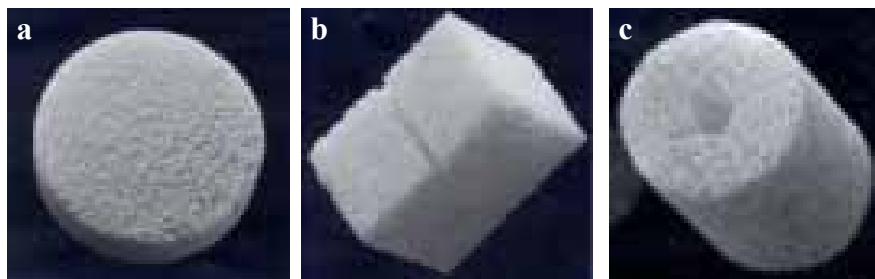


Figure 1.4. Different shapes and sizes of commercial bovine xenograft Surgibone® (a) disk shaped, (b) rectangular prismatic, (c) cylindrical sponges. (www.canmedica.com/Unilab/Surgibone.htm).

1.2.2. Synthetic Grafts

Due to the fact that approximately 6.2 million fractures occur each year in the United States alone and ca. 15% of them require some kind of bone transplantation (Sutherland and Bostrom, 2005), availability of the graft material is a major worldwide health problem. In addition, it is predicted that the percentage of persons over 50 years of age affected by bone diseases will double by 2020 (Navarro *et. al.*, 2008). As the biological grafts have the limitations described above, search for the ideal material with adequate mechanical properties and biocompatibility that can be produced in sufficient quantities continues. Predominantly natural and synthetic polymeric, also ceramic, metallic and composite grafts are in use in the clinic.

These “non-viable” bone substitutes generally lack the ability to fit the defect site structurally and mechanically, and cannot interact properly with the surrounding tissues.

Metallic materials, mostly stainless steels, cobalt-chromium alloys, and titanium alloys are generally used as fixation devices in orthopedic surgery. The excellent corrosion resistance and the ability to become tightly integrated into bone which significantly improves the long-term behavior of the implanted devices, makes titanium and its alloys preferable in orthopedics. Other than fixation devices, titanium meshes are also used as a “cage” to give shape and strength to the transplanted materials. For example, titanium sponge infiltrated with a solution of bovine BMP and noncollagenous ECM proteins was used to produce BMP-Ti composite with which it was shown that direct bone and cartilage formation on the implant surface as well as bone ingrowth was achieved (Kawai *et. al.*, 1993). Similarly, the efficacy of a collagen/calcium phosphate composite wetted with bone marrow aspirate contained within a titanium mesh was shown as a bone graft substitute (Erbe *et. al.*, 2007). Titanium meshes were also used for the treatment of complex mandibular fractures and it was reported that successful union was achieved in 70% of the cases (Schug *et. al.*, 2000).

Approximately 60% of the bone graft substitutes currently available involve ceramics, either alone or in combination with another material (Laurencin

et. al., 2006). Ceramics often require high temperatures for scaffolding and are brittle; therefore they are frequently combined with other materials to form a composite. The use of ceramics, especially calcium phosphates including tricalcium phosphate, synthetic hydroxyapatite (HA), and coralline hydroxyapatite, is favorable because of the fact that the primary inorganic component of bone is hydroxyapatite. In addition, calcium phosphates are osteoconductive, osteointegrative (the newly formed mineralized tissue forms intimate bonds with the implant material) and in some cases, osteoinductive (Ambrosio *et. al.*, 2001). Porous hydroxyapatite bone substitutes that facilitate the penetration of newly formed bone tissue into the graft are commercially available as Neobone® in various forms (Figure 1.5).

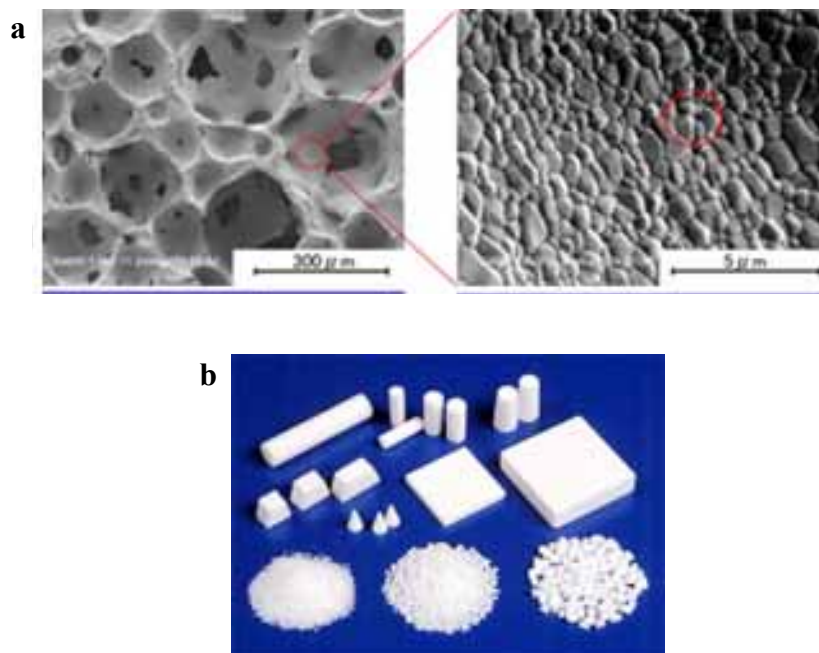


Figure 1.5. Neobone ® ceramic bone substitutes, (a) the microstructure, (b) various forms including cylindrical and rectangular prismatic sponges, powder and crushed forms (<http://www.covalent.co.jp/eng/products/bio/neobone.html>).

Polymers are also widely in use as synthetic bone substitutes. The first generation of polymeric materials used in orthopedics according to Hench's classification (Hench, 1980) were "inert", to reduce the immune response and the foreign body reaction to a minimum, included silicone rubber, PE, acrylic resins, polyurethanes, polypropylene (PP) and PMMA. PE, and more specifically ultra high molecular weight PE (UHMWPE), was used to a great extent due to its unique properties of high abrasion resistance, low friction and high impact strength, excellent toughness and low density, ease of fabrication, biocompatibility and biostability (Fisher and Dowson 1991; Sutula *et al.*, 1995).

The second generation polymeric materials were defined as "bioactive", having the ability to interact with the biological environment to enhance the biological response and the tissue/surface bonding, were developed by the development of biodegradable materials which have the ability to undergo degradation while new tissue regenerates and heals (Navarro *et al.*, 2008). Biodegradable polymers of synthetic and natural origin such as poly(lactide) (PLA) (Kinoshita *et al.*, 1997; Park *et al.*, 2000; Lee *et al.*, 2001), polyglycolide (PGA) (Kellomäki *et al.*, 2000; Ashammakhi *et al.*, 2000) and their copolymers (PLGA) (Goldstein *et al.*, 1999; Lu *et al.*, 2000; Sherwood *et al.*, 2002; Hasirci *et al.*, 2002), poly(ϵ -caprolactone) (PCL) (Corden *et al.*, 2000; Walsh *et al.*, 2001; Cao *et al.*, 2003), polyhydroxybutyrate (PHB) (Lootz *et al.*, 2001; Chen and Wang, 2002) and its copolymers with polyhydroxyvalerate (PHBV) (Kose *et al.*, 2002; Kose *et al.*, 2003), poly(propylene fumarate) (Lewandrowski *et al.*, 2002), chitosan (Lahiji *et al.*, 2000; Lee *et al.*, 2002; Yin *et al.*, 2003), collagen (Tabata, 2001; Freyman *et al.*, 2001; Liu *et al.*, 2003), poly(2-hydroxyethyl methacrylate) (PHEMA) (Filmon *et al.*, 2000; Costa *et al.*, 2003), hyaluronic acid (Bakos *et al.*, 1999; Lisignoli *et al.*, 2002) and other hydrogels were extensively studied during this period in many orthopedic applications such as bone substitution and repair of bone fractures (Cicccone *et al.*, 2001). The surfaces of polymers have also been modified with HA layers to induce their mineralization (Kato *et al.*, 1996; Ma *et al.*, 2002).

The third generation polymers are able to stimulate specific cellular responses at the molecular level (Hench and Polak, 2002). 3-D porous structures

that stimulate the migration, attachment and proliferation of cells, as well as functionalized surfaces with peptide sequences that mimic the ECM components to trigger specific cell responses, are being developed (Hutmacher *et. al.*, 2000; Temenoff and Mikos, 2000; Agrawal and Ray, 2001). Delivery of bioactive agents as well as control of cell behavior through mechanotransduction are some fields of interest. Scaffolds for tissue engineering applications were developed with the advance in this generation of materials.

1.3. An Alternative in Bone Repair: Tissue Engineering

Even after all of the achievements in the materials field, an ideal bone substitute could not be developed. It should carry viable cells (preferably patient's own), scaffold material with desired structural and mechanical properties, and bioactive agents to regulate the behavior of the cells. Tissue engineering could be an ideal solution as a promising alternative strategy to form viable and functional 3-D constructs.

Tissue engineering is an essentially multidisciplinary field, combining various aspects of medicine, materials science, engineering and biology. A commonly applied definition of tissue engineering is that it is "an interdisciplinary field that applies the principles of engineering and life sciences toward the development of biological substitutes that restore, maintain, or improve tissue function or a whole organ" (Langer and Vacanti, 1993). Tissue engineering approach involves the use of biodegradable and biocompatible scaffolds, cells isolated from proper sources, and bioactive agents, in particular growth factors, to stimulate and/or control the behavior of the cells.

The common strategy in bone tissue engineering is to isolate cells, most commonly mesenchymal stem cells or progenitor cells, expand them *in vitro* and seed onto a biocompatible and biodegradable scaffold that meets the structural and mechanical requirements of the defect site. Appropriate growth factors are added to accelerate healing by initiating proliferation and differentiation of local osteoprogenitor cells and thus, bone formation. After *in vitro* maturation and mineralization of this cell seeded construct, preferably in bioreactors, it is implanted

at the target site. In time, the biodegradable scaffold is resorbed while the cells produce their own ECM and replace the implant. Thus, an ideal bone repair environment is created by providing the intrinsic properties of autogenous bone material, which has a porous, 3-D architecture that allows osteoprogenitor cell migration and graft revascularization and the ability to get incorporated into the surrounding host bone to complete the normal bone remodeling process (Freyman *et al.*, 2001).

1.3.1. Cells in Bone Tissue Engineering

Possible sources of cells for tissue engineering include autogenic, allogenic and xenogenic cells. Each category can be subdivided according to whether the cells are in a more or less differentiated stage. In tissue engineering, the ideal source is autologous cells taken from a healthy region of the patient's damaged tissue. However, due to the factors like limited availability of the tissue as well as the difficulty in tissue harvesting for mature cell isolation, other cell sources have been considered. The use of allogenic cells is limited due to possible immunogenic response of the host (Niemeyer *et al.*, 2004). The use of xenogenic cells is often limited to research purposes and application in humans is rare due to possible severe inflammatory and immunological responses that could lead to the rejection by the tissue and the risk of transmission of disease among species (Leyh *et al.*, 2003).

Cells used in bone tissue engineering could be natural or genetically modified cells. Natural cells could be subdivided as *stem cells* which have the capacity of differentiation into different cell types with stimulation as well as high proliferative capacity, and *primary cells* such as osteoblasts and osteocytes. According to the differentiation extent, stem cells could be toti- pluri- or multipotent indicating the ability to differentiate into any kind of cell, any kind except the cells of the placenta or other supporting tissues of the uterus and cells from multiple, but a limited number of lineages, respectively.

The use of embryonic stem cells (ESCs) in tissue engineering applications is promising as they are capable of indefinite undifferentiated

proliferation *in vitro* and can provide an unlimited supply of cells, which can be differentiated into various cell types (Jukes *et. al.*, 2008). However, there is a continuing debate on the use of ESCs and also there are some technical and ethical issues that have to be addressed before ESCs can be used in clinical applications. Multipotent mesenchymal stem cells (MSCs) such as bone marrow derived progenitor cells are the most abundantly used cell source in bone tissue engineering and they can be differentiated into the osteogenic lineage by culturing them in the presence of appropriate osteogenic differentiation supplements.

As the use of mature bone cells (primary cells) does not raise legal issues and there is no risk of immune rejection, they can be considered to be the ideal cell source for bone tissue engineering if only they could be isolated and multiplied properly *in vitro*.

Osteosarcoma cell lines and immortalized cell lines are examples of genetically modified cells used in bone tissue engineering research which are generally used to evaluate basic aspects of *in vitro* cell behavior in non-human settings.

1.3.1.1. Mesenchymal Stem Cells

Since the description of the presence of adherent stromal cells from bone marrow (Friedenstein *et. al.*, 1987), MSCs are of great interest to engineers of mesenchymal tissues, such as bone and cartilage. Bone marrow, adipose tissue, vein wall, peripheral and menstrual blood, foetal and maternal placenta, periodontal ligament, periost and trabecular bone have all been described as sources of MSCs. However, the characteristics such as replication capacity without differentiation and multi-lineage developmental potential have not been fully studied for all these cells.

Bone marrow has been claimed to be the most abundant source of MSCs, and these cells have a high proliferative ability and a great capacity for differentiation (Haynesworth *et. al.*, 1992; Caplan, 1993). As another important advantage, bone marrow is an accessible source of osteogenic cells since it can be collected using a relatively simple aspiration procedure. This method is less invasive than collecting mature osteogenic cells by taking biopsies from calvarium

(Nefussi *et. al.*, 1997; Wada *et. al.*, 1998), periosteum (Miura and O'Driscoll, 1998), or trabecular bone (Robey and Termine, 1985).

The ability of MSCs to differentiate into several cell types is presented in Figure 1.6. Proliferating MSCs enter a lineage after their commitment to that particular pathway. The commitment event involves the action of specific growth factors and/or cytokines. They also play an important role in the lineage progression phase in which the lineage-committed cells progress through several transitory stages. Terminal differentiation involves the termination of proliferation and the biosynthesis of tissue-specific products, usually highly site-specific ECM. Finally, these differentiated cells go through a maturation stage in which they obtain an ability to function in aspects of tissue homeostasis as opposed to high levels of synthetic activity (Haynesworth *et. al.*, 1992; Caplan and Dennis, 2000; Caplan, 2007).

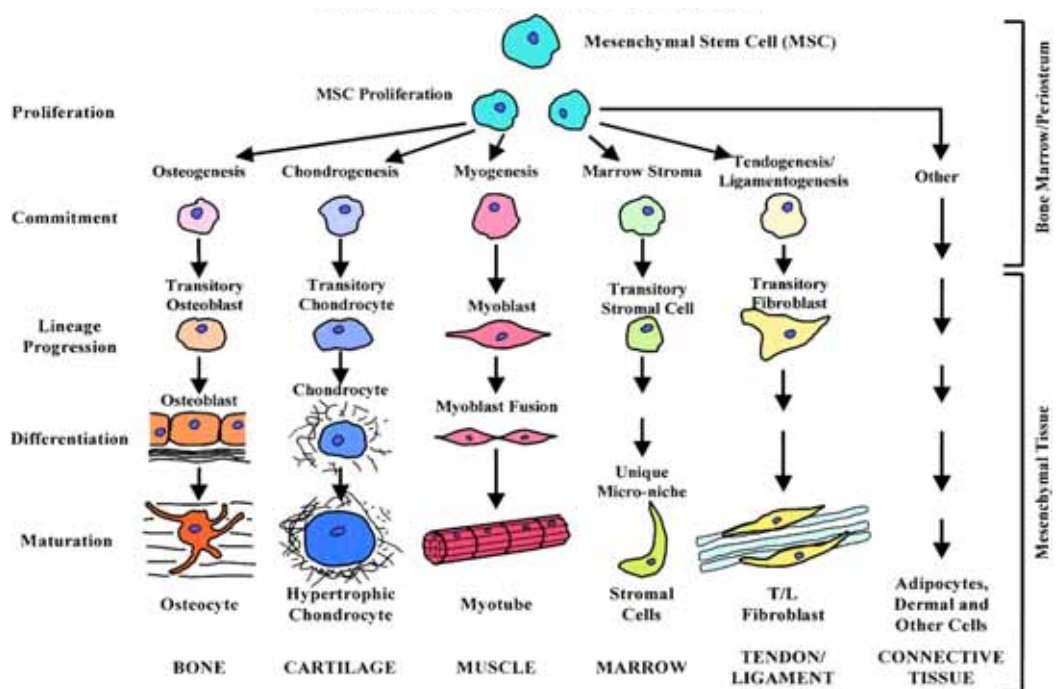


Figure 1.6. The potential of MSCs to differentiate into a variety of mesenchymal tissues, such as bone, cartilage, tendon, muscle, marrow, fat, and dermis (Caplan, 2007).

1.3.2. Scaffolds in Bone Tissue Engineering

Scaffolds play a central role in tissue engineering applications through supporting and guiding regeneration and defining the ultimate shape. Scaffolds need to fulfill the following criteria in order to be used in tissue engineering (Spaans *et. al.*, 2000; Boccaccini *et. al.*, 2002):

- the material must be biocompatible,
- must be biodegradable,
- degradation byproducts should be noncytotoxic,
- should resorb at the same rate as the tissue is repaired,
- mechanical properties must be appropriate to regenerate bone tissue in load-bearing sites,
- must keep its structural integrity during the first stages of the new bone formation,
- should be osteoconductive,
- must have adaptability of shape to defect site,
- must possess a highly interconnected porous network (formed by a combination of macro and micropores) that enable proper tissue ingrowth, vascularization and nutrient delivery. The porous structure should be capable of mimicking the 3-D interconnections between the lacunae that provide intercellular communication.

Although there are alternative views, the consensus of research indicates that the requisite pore size for bone ingrowth into porous implants should be in the range 100 to 500 μm , with the interconnections being larger than 100 μm (Parikh, 2002).

1.3.2.1. Materials Used in Scaffold Production

The materials commonly used in bone tissue engineering mainly include biodegradable polymers of either natural or synthetic origin. In addition to these,

incorporation of calcium phosphate and HA has also been tried to imitate the composite structure of the bone.

1.3.2.1.1. Natural Polymers

Several natural polymers have been successfully used as materials for the production of scaffolds for bone tissue engineering applications. Naturally derived polymers are of special interest as they are natural components of living structures, and have biological and chemical similarities to natural tissues. Proteins such as collagen (Anselme, 2000; Xiao *et al.*, 2003; Kose *et al.*, 2004; Ber *et al.*, 2005) and silk (Altman *et al.*, 2003; Meinel *et al.*, 2005; Fuchs *et al.*, 2009; Zhao *et al.*, 2009), polysaccharides such as alginic acid (Wang *et al.*, 2003; Grellier *et al.*, 2009), starch (Marques *et al.*, 2002; Salgado *et al.*, 2007; Martins *et al.*, 2009) and chitosan (Vandevord *et al.*, 2002; Khor and Lim, 2003; Ho *et al.*, 2005; Qiu *et al.*, 2009) as well as polyesters such as polyhydroxyalkanoates (PHAs) of bacterial origin (Kose *et al.*, 2003; Shishatskaya *et al.*, 2006; Kenar *et al.*, 2008; Wu *et al.*, 2009) have been used in various *in vitro* and *in vivo* studies.

Chitosan has been investigated for a variety of tissue engineering applications as it is structurally similar to naturally occurring glycosaminoglycans (GAGs) and is degradable by enzymes in humans. It is a linear polysaccharide of (1–4)-linked D-glucosamine and N-acetyl-D-glucosamine residues derived from chitin, one of the most abundant organic materials, which is found in arthropod exoskeletons (Drury and Mooney, 2003). Chitosan is soluble in dilute acids which protonate the free amino groups. Once dissolved, chitosan can be gelled by increasing the pH or extruding the solution into a non-solvent. Chitosan has been excessively studied due to its such favorable biological properties as biocompatibility, biodegradability, nontoxicity, physiological inertness, remarkable affinity to proteins, antibacterial, haemostatic, fungistatic, antitumoral and anticholesteremic properties (Nishimura *et al.*, 1984; Tanigawa *et al.*, 1992; Okamoto *et al.*, 1993; Mori *et al.*, 1997; Tokura *et al.*, 1997; Singla and Chawla, 2001; Khor and Lim, 2003). Several studies focused on chitosan–calcium phosphate composites molded into porous structures in bone repair (Zhang and Zhang, 2002;

Martino *et. al.*, 2005). Chitosan was also used in combination with HA in the healing of tibial fractures (Kawakami *et. al.*, 1992).

PHAs are biopolyesters which are generally found accumulated in various microorganisms as an intracellular carbon and energy storage compound, usually under the condition of limiting nutrients in the presence of excess carbon source (Fuller, 1999). Since PHAs are degradable in the human body and the degradation products are not toxic, they are studied as biomaterials to especially replace the synthetic polyesters like polylactide and polyglycolides. The most extensively tested PHA is poly(3-hydroxybutyrate) (P3HB) and its copolymers with 3-hydroxyvalerate, PHBV, found in varying ratios of the two components. Eventhough PHB and PHBV have been reported to induce prolonged acute and chronic inflammatory responses in *in vivo* studies (Akhtar, 1990), other studies showed that these responses subsided eventually. In order to improve the cell attachment and growth and to reduce the *in vivo* inflammatory responses, the surfaces of PHAs have been modified by plasma treatment (oxygen, nitrogen) (Kose *et. al.*, 2003; Wang *et. al.*, 2006), pH treatments (Davies and Tighe, 1995) and by protein coating (Tesema *et. al.*, 2004; Wu *et. al.*, 2004; Kenar *et. al.*, 2006). The use of PHBV to prepare bone tissue engineering matrices has been excessively studied by our research group in various forms including 3-D sponges, micropatterned films and electrospun mats (Kose *et. al.*, 2003; Kenar *et. al.*, 2006; Ndreu *et. al.*, 2008).

1.3.2.1.2. Synthetic Polymers

The advantage of using synthetic polymers over natural ones is that they are more readily available, can be produced in large scale with low cost and their ease of processing. Their main disadvantage is that their degradation products are generally not naturally found in the body and might lead to problems if accumulated.

The most commonly used synthetic polymers in bone tissue engineering applications are poly(α -hydroxyesters) such as PLA, PGA and their copolymers in various ratios (PLGA) (Lu *et. al.*, 2002; Ren *et. al.*, 2005; Yoon *et. al.*, 2007;

Cowan *et. al.*, 2007; Kim *et. al.*, 2008; Kempen *et. al.*, 2008; Jose *et. al.*, 2009; Hacking and Khademhosseini, 2009). Other most widely used synthetic polymers include PCL (Williams *et. al.*, 2005; Zhang *et. al.*, 2009), poly(propylene fumarate) (PPF) (Peter *et. al.*, 2000; Payne *et. al.*, 2002), and poly(ethylene glycol) (PEG) (Deschamps, 2000; Drury and Mooney, 2003).

PLGA is an FDA approved material for use in medical devices. Depending on the ratio of lactide to glycolide in the copolymer, PLGA with different properties are obtained. All PLGAs are amorphous and show a glass transition temperature (T_g) in the range of 40-60°C. Unlike the homopolymers of PLA and PGA which show poor solubilities, PLGA can be readily dissolved by a wide range of common, especially chlorinated solvents. PLGA is hydrolyzed through its ester linkages in the presence of water. It has been shown that the time required for degradation of PLGA is very much dependent on the monomer ratio (and therefore, crystallinity) used in its production: the higher the content of glycolide units, the shorter is the time required for degradation. The copolymer with 50:50 ratio (PLGA 50:50) exhibits the fastest degradation (Hasirci and Yucel, 2007). The use of PLGA for scaffold preparation has been particularly widespread as it already had a range of medical applications (e.g. in degradable sutures, stents, wound dressings) and have FDA approval in those devices. However, its hydrophobicity can be disadvantageous in tissue regeneration applications, due to poor wetting and lack of cellular attachment and interaction, therefore, surface treatment and functionalization is generally required to enhance the attachment efficiency of cells (Park *et. al.*, 2007; Shen *et. al.*, 2008; Chen *et. al.*, 2009). In several *in vitro* and *in vivo* studies, successful application of PLGA scaffolds either pure or blended with other synthetic or natural polymers (Oh *et. al.*, 2006; Li *et. al.*, 2006; Yang *et. al.*, 2007; Kim *et. al.*, 2008; Ngiam *et. al.*, 2009; Jose *et. al.*, 2009) in the forms of sponges, electrospun mats and rapid prototyped structures was shown.

PCL is a completely biodegradable, thermoplastic polyester. It has thermal stability in molten state, and has such favorable properties as low glass transition temperature (-60°C), low melting temperature (60°C), and high decomposition temperature (350°C) (Hoque *et. al.*, 2005). PCL degrades much

slower than PLGA due to its high hydrophobicity and crystallinity (Pitt, 1990), therefore, was found to be suitable for use in long term, load bearing applications. PCL was successfully used as a scaffold material in various forms including computer designed porous scaffolds, sponges, nanofibrous scaffolds and injectable gels (Schantz *et al.*, 2005; La Gatta *et al.*, 2005; Rai *et al.*, 2005; Li *et al.*, 2005; Shor *et al.*, 2007; Venugopal *et al.*, 2007; Guarino and Ambrosio, 2008; Porter *et al.*, 2009). PCL has also been used in combination with other materials; a number of studies using PCL biocomposites and copolymers with both natural and synthetic polymers such as HA, chitosan, starch and PLA have been reported (Hoque *et al.*, 2005; Verma *et al.*, 2006; Santos *et al.*, 2007; She *et al.*, 2007; Guarino *et al.*, 2008). Similar to PLGA, surface modifications have been performed such as O₂ plasma treatment (Oyane *et al.*, 2005a; Yildirim *et al.*, 2008), NaOH application to introduce carboxylate groups on its surface (Oyane *et al.*, 2005b), grafting several molecules including collagen, gelatin and silk fibroin (Chen *et al.*, 2004; Ma *et al.*, 2005; Duan *et al.*, 2007) to improve the cell attachment onto PCL surfaces.

1.3.2.2. Scaffold Production Techniques

The maintenance of cellular activities and interconversions of the connective tissue cells (fibroblasts, chondroblasts and osteoblasts) are highly dependent on their shape and anchorage which controls their gene expression (Benya and Schaffer, 1982). The architecture of a scaffold defines the geometry of cell adhesion sites and thus determines their adhesion, spreading and orientation. For this reason, along with the need for the adaptability to the defect site, architecture of the scaffolds is of utmost importance in the control of cell behavior.

Porosity is one of the most important properties of a 3-D scaffold which facilitates its population by the cells and enables nutrient and oxygen transfer, and aid bone ingrowth and vascularization. Several techniques have been employed to produce porous 3-D structures, the easiest and probably the most commonly used one is solvent casting/particulate leaching to produce 3-D sponges that have pore interconnectivity and controlled pore size. Sponges made of PHBV and collagen are some examples of their successful application in bone tissue engineering (Kose *et al.*

al., 2003; Kose *et. al.*, 2004). Fiber bonding (Gomes *et. al.*, 2006), electrospinning (Ndreu *et. al.*, 2008), membrane lamination (Mikos *et. al.*, 1993), melt molding (Se *et. al.*, 2006) and gas foaming (Almirall *et. al.*, 2004) are some of the other techniques employed in scaffold production. Electrospinning is a recent widely used technique with both natural (Cao *et. al.*, 2009) and synthetic polymers (Yu *et. al.*, 2009), and with their copolymers (Santos *et. al.*, 2008; Yang *et. al.*, 2009) to produce fibrous scaffolds of nano and micro size. Thin fiber layers (mats) obtained by electrospinning are generally used as multilamellar 3-D structures. However, all of these techniques lack the ability to produce structures with predefined form and properties. Instead, their reproducibility is poor, pore shapes are irregular and pore interconnectivity is insufficient. Rapid prototyping is a recent technique in scaffold fabrication that overcomes this problem.

1.3.2.2.1. Rapid Prototyping

Rapid prototyping (RP) is a common name for a number of advanced manufacturing techniques that are based on reading data from the computer-aided design (CAD) drawings and manufacture 3-D objects layer-by-layer according to the virtual design (Hutmacher *et. al.*, 2004). RP was first used in the early 1980s and since then a large variety of applications including the fabrication of automotive engine parts and small telecommunication industry components have been performed (Peltola *et. al.*, 2008). In 1990s, RP techniques were adapted into the medical and biomedical fields to design and manufacture custom-made prosthesis for individual patients, primarily craniomaxillofacial implants (Webb, 2000; Bibb *et. al.*, 2000).

RP technique can create a scaffold directly from the CT or MRI scans of the damaged region which has a strictly defined porosity in a specific 3-D shape to fit into an irregular defect site to provide a structurally and mechanically perfect fit (Yeong *et. al.*, 2004) (Figure 1.7). It is a typical bottom-up approach, where 3-D objects are produced through repetitive deposition of material layers by computer-controlled equipment based on the cross-sectional data obtained from slicing a CAD model of the object (Lam *et. al.*, 2002).

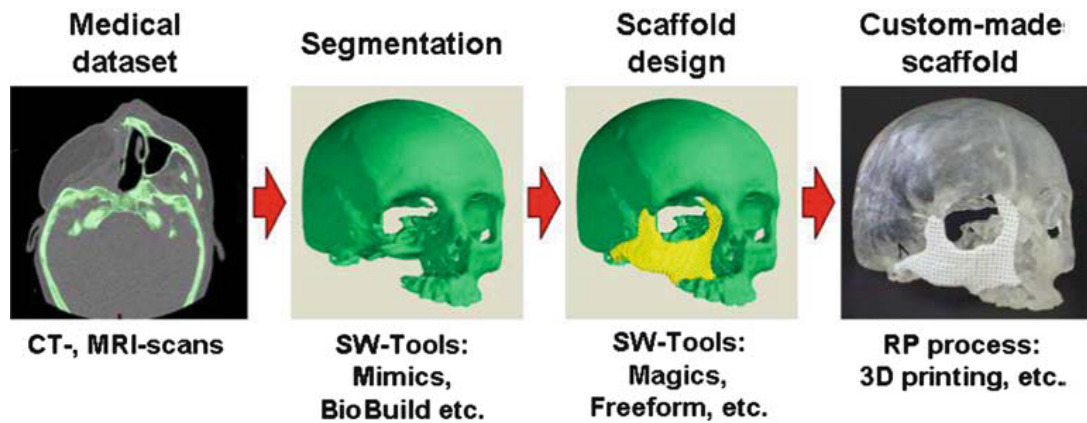


Figure 1.7. A typical rapid prototyping chain for manufacturing custom-made implants. (Schieker *et. al.*, 2006).

Recent developments in solid free-form fabrication techniques and the polymers used have made it possible to produce tailor-made tissue engineering scaffolds. Besides having precise control over porosity, pore size, stiffness and permeability; the RP scaffolds are usually designed to have full interconnectivity of the pore structure (Moroni *et. al.*, 2006). With the capability to create scaffolds with defined structure and architecture, RP technique is a good method to investigate the effect of scaffold properties such as geometry on cell behavior for further optimization of the scaffold design.

There are several approaches to RP of scaffolds which can be classified in three basic types: liquid-based, solid-based, and powder-based RP systems. Liquid-based technologies include stereolithography and two-photon polymerization, whereas fused deposition modeling is a solid-based system. Selective laser sintering (SLS) and 3-D printing fall in the category of powder-based methods. RP scaffolds have been fabricated by a variety of these methods including SLS (Chua *et. al.*, 2004; Williams *et. al.*, 2005; Wiria *et. al.*, 2007), fused deposition modeling (FDM) (Choong *et. al.*, 2004; Chen *et. al.*, 2005; Chim *et. al.*, 2006), 3-D fiber deposition (Moroni *et. al.*, 2007; Fedorovich *et. al.*, 2008) and 3-D

plotting (Geng *et. al.*, 2005; Oliveira *et. al.*, 2007). Among the available fabrication techniques, 3-D plotting is the most convenient method due to its milder operation conditions, absence of left over polymer powder within the scaffold and the ability to produce scaffolds without any binders. Thus, 3-D plotting appears to be an appropriate method for producing scaffolds for bone tissue engineering.

PCL has been widely used as material for the production of RP scaffolds due to its favorable properties such as ease of processing and high decomposition temperature. PCL scaffolds have been created with a variety of RP techniques including FDM (Rohner *et. al.*, 2003), shape deposition modeling (Marra *et. al.*, 1999), SLS (Williams *et. al.*, 2005), low-temperature deposition (Xiong *et. al.*, 2002) and multi-nozzle free-form deposition (Sun *et. al.*, 2004a; Sun *et. al.*, 2004b). In these systems the cells adhered and started growing on the PCL scaffolds and the applicability of the produced scaffolds were thus demonstrated *in vitro* and *in vivo*.

Although synthetic polymers are widely used for RP of scaffolds, current efforts include the use of natural polymers such as chitosan, agarose, PEG and collagen (Landers *et. al.*, 2002; Geng *et. al.*, 2005; Maher *et. al.*, 2009; Norotte *et. al.*, 2009) to produce hydrogels with predefined structure. Even, direct printing of single cells and cell aggregates was studied to achieve scaffold-free viable constructs (Mironov *et. al.*, 2003; Demirci and Montesano, 2007).

1.3.2.2.2. Wet Spinning

Fibrous scaffolds have gained great attention over the recent years as they have appropriate porosity for cell penetration, nutrient exchange and tissue ingrowth. Polymeric fibers can be manufactured using three main techniques: melt spinning, dry spinning, and wet spinning. In melt spinning, a molten polymer with a suitable viscosity is extruded at high pressure and constant rate through a spinneret to form continuous strands of polymeric fibers (Buttafoco *et. al.*, 2004). In the dry spinning process, a polymer solution is extruded instead of molten polymer (Lazzeri *et. al.*, 2005). In wet spinning, polymer solution is extruded into a non-solvent and polymeric fibers are obtained in the coagulation bath (Nelson *et. al.*, 2003; Funakoshi *et. al.*, 2005; Chung *et. al.*, 2007). Recently, electrospinning which uses

electrical potential to produce fine fibers from a polymer solution, is attracting more attention as nano-and micro-scale fibers with uniform size could be obtained (Huang *et. al.*, 2001; Matthews *et. al.*, 2002; Ndreu *et. al.*, 2008). The combination of wet spinning and electrospinning techniques was shown to be promising in mimicking the macro and micro structure of the natural ECM (Tuzlakoglu *et. al.*, 2005; Santos *et. al.*, 2008).

Fibrous scaffolds produced by wet spinning from synthetic polymers like polyurethanes (Guelcher, 2008), PLGA and PLLA (Nelson *et. al.*, 2003; Ellis and Chaudhuri, 2007), PCL (Williamson and Coombes, 2004) and natural polymers such as chitosan (Funakoshi *et. al.*, 2005; Tuzlakoglu *et. al.*, 2004) and cellulose acetate (Ye *et. al.*, 2005) are some examples of successful application of the procedure to prepare scaffolds for bone tissue engineering.

1.3.3. Growth Factors in Bone Tissue Engineering

Growth factors serve as signaling molecules and are secreted by many cell types. They promote and/or prevent cell adhesion, proliferation, migration and differentiation by up or down-regulating the synthesis of proteins, other growth factors and receptors. They act in a concentration and time dependent manner, often requiring minute quantities to elicit biological activity, and their effectiveness depend on a variety of factors including cell location within a tissue and the state of the cell cycle.

Growth factors are among the most essential elements of successful tissue engineering applications, and are able to induce the natural bone regeneration cascade which was shown to include several signaling molecules that regulate cellular activities. The growth factors responsible in bone healing and regeneration are members of the TGF- β superfamily, especially the BMPs, IGF, FGF, PDGF and VEGF (Allori *et. al.*, 2008). The use of either one or a combination of these growth factors is important for cellular adhesion, proliferation, migration and differentiation.

The TGF- β proteins are a superfamily including BMPs, inhibins, and activin. The most osteogenic members of the family, BMPs, are discussed in section

1.3.3.1. TGF- β s are ubiquitously expressed, although the two largest reservoirs are bone and platelets (Bonewald and Mundy, 1989). They are expressed by many cells during bone healing, and their distribution varies according to phase. For example, TGF- β 1 was shown to be localized to the inflammatory cells within the fracture hematoma after acute injury. During the activation phase, osteoblasts, mesenchymal cells and connective tissues adjacent to the fracture site express it intensely. After a 4-week period of external fixation, TGF- β 1 expression was found to be limited to osteoblasts within the remodeling bone (Mehrra *et al.*, 1999). Functionally, TGF- β 1 has multiple functions such as attracting osteoprogenitor cells (Hughes *et al.*, 1992), inhibiting osteoclasts to allow ossification during the early phases (Chenu *et al.*, 1988; Pfeilschifter *et al.*, 1988) then it activates osteoclasts in the later phases (Centrella *et al.*, 1994) to take part in bone remodeling. In addition, TGF- β s are important regulators of the production of collagen and noncollagenous ECM proteins (Centrella *et al.*, 1992; Hiltunen *et al.*, 1993).

Both *in vivo* and *in vitro* data suggest that IGF-1 stimulates or facilitates osteoprogenitor cell mitosis and differentiation, thereby increasing the number of functionally mature osteoblasts (Spencer *et al.*, 1991). IGF-1 expression also appears to be time dependent as an initial increase in serum IGF-1 levels during the activation period (released from the surrounding soft tissues) is followed by an increase in skeletal IGF-1 levels in both the distracted callus and surrounding bone (Lammens *et al.*, 1998; Eingartner *et al.*, 1999; Liu *et al.*, 1999). 3 weeks after fracture, low-level expression of IGF-1 was revealed (Tavakoli *et al.*, 1999) which suggested that IGF-1 may play an important role during early fracture healing.

FGFs act in concert with heparin sulfate-containing proteoglycans to modulate cell migration, angiogenesis, bone development and repair (Seetharam *et al.*, 1995; Nishimura *et al.*, 1999). FGF-2 is the most abundant ligand and it has been shown to stimulate the proliferation of osteoblasts and enhance bone formation *in vitro* and *in vivo* (Kimoto *et al.*, 1998). FGF-2 expression is elevated in fracture healing, and exogenously applied FGF-2 accelerates osteogenesis in critical-size bone defects and fracture sites (Kawaguchi *et al.*, 1994). FGF-2 also induces angiogenesis (Allori *et al.*, 2008).

EGF has been shown *in vitro* to be able to induce proliferation of MSCs (Tamama *et. al.*, 2006). It has been shown to stimulate bone resorption (Raisz *et. al.*, 1980) and upregulate production of the matrix metalloproteinases (van der Zee *et. al.*, 1998) thus promoting remodeling.

PDGF has a significant role in angiogenesis and is involved in cellular migration and proliferation. It is secreted systemically by platelets and localized in the stromal cells of the bone marrow (Abboud, 1993). PDGF was found to be expressed predominantly during the early inflammatory stages of the healing process and was found to stimulate the proliferation of MSCs (Rasubala *et. al.*, 2003). This early expression enhances the laying of fibrous structure for vascularization and subsequent bone deposition (Zhang *et. al.*, 1998).

VEGFs are involved in both angiogenesis and vasculogenesis by increasing endothelial cell and endothelial progenitor cell chemotaxis and mitogenesis (Allori *et. al.*, 2008). Osteoblasts and osteoclasts secrete VEGF which promotes osteoblast differentiation although it does not have a direct osteogenic effect (Tombran and Barnstable, 2004; Deckers *et. al.*, 2000). VEGF may also serve to complement and potentiate the osteogenic function of several other growth factors (Eckardt *et. al.*, 2005).

1.3.3.1. Bone Morphogenetic Proteins

BMPs are the most osteoinductive growth factors presently described (Cowan *et. al.*, 2005). They promote the formation of cartilage and bone by inducing MSCs toward chondroblastic and osteoblastic differentiation, and also causing them to proliferate *in vivo* (Urist, 1965; Wang *et. al.*, 1990). Several of them, BMP-2 to BMP-18, were identified in humans. Out of these BMP-2, 4, 6, 7, and 9 are known to induce complete bone morphogenesis and are considered to be the most osteogenic ones (Bessa *et. al.*, 2008) where BMP-2 and -7 possess strong ability to induce bone formation and are the only ones that recently received FDA approval for use within collagen carriers in the applications for spinal fusion and sinus lift (White *et. al.*, 2007; McKay *et. al.*, 2007).

Several BMP molecules participate in a cascade that regulates fracture healing process by following different paths (Saito *et. al.*, 2005; Bandyopadhyay *et. al.*, 2006). It was shown in mice that in the absence of both BMP-2 and BMP-4, there was a severe decrease in the development of bone tissue, even though chondrogenic differentiation was taking place (Bandyopadhyay *et. al.*, 2006). In other *in vivo* studies, BMPs naturally secreted by the tissues were shown to appear sequentially to influence different aspects of skeletal development (Hogan, 1996). In particular, BMP-2 was reported to be an early factor peaking at day 1 after fracture while BMP-14 peaks at day 7 during cartilage formation and BMP-3, 4, 7 and 8 are expressed mainly after 2 weeks (Cho *et. al.*, 2002).

In bone formation, at low concentrations BMPs promote chemotaxis and proliferation, whereas at high concentrations they favor differentiation and bone formation (Zimmerman *et. al.*, 1996; Urist, 1997). *In vitro* studies have shown that even femtomolar concentrations of BMP can initiate chemotaxis of cell types such as monocytes and mature osteoblasts. BMP doses in the nanogram range have shown osteogenic effects in *in vitro* experiments (Mayer *et. al.*, 1996). Studies also revealed that, extremes of BMP release (high initial dose with rapid degradation or prolonged low-level release) do not enhance bone induction in animals as they diffuse easily in bodily fluids due to their water solubility (Cowan *et. al.*, 2005; Allori *et. al.*, 2008).

Due to the time-dependent action of BMPs, delivering them in combination, particularly in a sequential manner by controlling their release time and duration, may have great advantage over the conventional strategies for bone tissue engineering applications. A control over the dose of the BMP applied is of utmost importance and selecting a suitable carrier that allows for control of BMP concentration present is ideal for maximizing their osteogenic potential.

1.4. Controlled Growth Factor Delivery in Tissue Engineering

As described previously, the common strategy in tissue engineering is to seed the cells on appropriate scaffolds and allow this construct to mature *in vitro* prior to implantation. However, in such systems there is no further interference by

the researcher over the growth rate and differentiation of the seeded cells; and, similarly, after the implantation no control on the host cells. Since cell growth and differentiation as well as construct mineralization are the main properties to obtain implantable tissue engineered constructs; more accurate control over these properties is desirable. Under *in vivo* conditions, these events are controlled by the growth factors in the environment as described in section 1.3.3 and it is known that the dose and duration of these factors are strictly controlled by the body.

The conventional strategy in growth factor administration for clinical orthopedic applications is to apply the agent in the form of large doses by either single or repeated injections. However, in such cases a considerable proportion of the agent is lost through leakage from the site, by biodistribution and/or by denaturation (Lee and Shin, 2007).

Encapsulation of growth factors in protective carrier structures, therefore, is of utmost importance in the protection of the bioactivity of the agent and to sustain the local concentration over a given period of time at the target site. Addition of these factors inside a tissue engineering scaffold would enhance the effectiveness of the scaffold and with the optimization of the parameters such as the release rate and concentration, a control on new bone formation is possible. Hence, it can be stated that bone tissue engineering should incorporate controlled delivery of the required biologically active agents within the scaffold itself just like in the natural ECM, thus creating multi-functional constructs. These multi-functional constructs would serve as the filler at the target site and also combine osteoconduction and osteoinduction (Li and Wozney, 2001). The carrier system would thus function as an artificial ECM and also serve to stabilize entrapped or encapsulated growth factors. This is often challenging because processes used to prepare protein delivery constructs may denature or deactivate the protein. Therefore, methods that do not require harsh conditions, strong solvents or high temperatures, are often desirable.

A variety of polymeric delivery systems have been designed to meet the design criteria for growth factor delivery including nano/microspheres, porous scaffolds and injectable gels. The factors themselves may also be directly incorporated into the polymer. Alternatively, plasmid DNA encoding the factor may

be immobilized within the polymer allowing the local production of the factor by cells that take up and express this DNA following implantation of the system at the desired site. Finally, the polymer system may be used to transplant cells that secrete the desired factor (Chen and Mooney, 2003).

After the realization of their great potential to induce bone regeneration (Urist, 1965), numerous delivery strategies have been developed for the sustained release of BMPs especially over the last decade. Both nano and micro sized delivery vehicles mainly made of synthetic materials (Lee *et al.*, 1994; Schrier *et al.*, 2001; Kempen *et al.*, 2008; Jeon *et al.*, 2008), natural polymers (Tabata *et al.*, 1998; Wang *et al.*, 2003; Chen *et al.*, 2007; Bessa *et al.*, 2008; Patel *et al.*, 2008a) and HA-based particles (Matsumoto *et al.*, 2004; Akazawa *et al.*, 2006) have been reported. PLGA microspheres were used to deliver BMP-2 for over a 70 day period and increased alkaline phosphatase (ALP) activity was observed both *in vitro* and *in vivo* rat model (Kempen *et al.*, 2008). Several other models that have been developed by using BMP-delivering micro and nanoparticles of PLGA showed enhanced bone production when implanted in rat hind limb muscle pocket (Jeon *et al.*, 2008), rat femur (Lee *et al.*, 1994), and calvarial defects in rabbits (Schrier *et al.*, 2001). rhBMP-7 encapsulated within PLGA nanoparticles which were then loaded into nanoporous poly(L-lactic acid) PLLA scaffolds induced bone healing (Wei *et al.*, 2007). Gelatin microparticles were used in a mouse model for rhBMP-2 delivery and a lower burst release was observed when compared to PLGA particles (Patel *et al.*, 2008a). Particles made of other natural polymers such as collagen (Wang *et al.*, 2003), chitosan-alginate (Bessa *et al.*, 2008) and dextran (Chen *et al.*, 2007) were also successfully used in the delivery of BMPs. HA particles were produced at different temperatures and the absorbability of BMP molecules on these particles were shown (Matsumoto *et al.*, 2004).

1.4.1. Impact of Nanotechnology on Controlled Delivery

Advances in nanotechnology and their application to the biomedical field led to significant developments in the area of drug delivery. The promise of utilization of nanotechnology in drug delivery systems is the possibility of

intracellular delivery of agents such as DNA (Kumar *et. al.*, 2004), antisense RNA and anticancer drugs (Park *et. al.*, 2005), as well as increased penetration through barriers such as blood-brain barrier (Olivier, 2005) and tight junctions, therefore permitting the accumulation of an agent at the previously “unreachable” target site. Nanoparticles of all sorts can penetrate through capillaries; their uptake by the cells and movement through the dense extracellular matrix is evidently easier than with microparticles. Enhanced targeting that might be achieved by nanoparticles would decrease the amount of drug used.

Even though the definitions vary for some, solid, colloidal substances varying in size from 10 nm to 1000 nm are defined as nanoparticles (Brigger *et. al.*, 2002). An active agent is coupled with the nanoparticle through entrapment, adsorption, attachment, encapsulation or directly dissolving the agent within the nanoparticle structure. Solid or hollow nanospheres, porous or solid nanoparticles can be formed depending on the method of preparation. The most common controlled release system forms are micro and nanospheres, micro and nanocapsules and liposomes which can be scaled-down to nanometer range by modified manufacturing methods. Nanospheres are solid particles in which the active agent is physically and uniformly dispersed, whereas nanocapsules are hollow particles where the content is encapsulated by a membrane (Sahoo and Labhasetwar, 2003). Micelles and dendrimers are other important vehicles currently receiving great deal of attention as drug delivery carriers.

The biodegradable and biocompatible polymers PLGA and PHBV have both been successfully used earlier as nanoparticulate carriers of bioactive agents (Kempen *et. al.*, 2008; Wei *et. al.*, 2007; Jaklenec *et. al.*, 2008; Kang *et. al.*, 2008; Kim *et. al.*, 2006; Baran *et. al.*, 2002). Different release rates obtained with these particles were due to the differences in their hydrophilicity, crystallinity and degradation rates. These parameters have been earlier used in controlling release rates (Burgess and Hickey, 1994). Additional parameters are molecular weight (MW) and the various device characteristics such as particle size and loading (Lemaire *et. al.*, 2003; Zolnik *et. al.*, 2006; Cui *et. al.*, 2005). PLGA degrades significantly more rapidly in vivo compared to PHBV (99% vs. 43% in 6 months) although having similar chemical structures (Kök and Hasırcı, 2003). When all the

other properties are comparable (MW, crystallinity), then it is expected that PLGA would degrade faster.

1.4.2. Multiple Growth Factor Delivery from Tissue Engineering Constructs

The most recent approach to growth factor delivery for tissue engineering is a combined scaffold/controlled delivery system construct that involves the delivery of several growth factors from the same scaffold. Although copying from the nature could have been quite effective in bone healing, there is not much literature on creation of a simulated system by mimicking the sequence, the dose and duration of growth factors. The few studies in the literature include BMP-2 and TGF- β 3 delivery from alginate hydrogels transplanted in mice, in which it was observed that the individual application of growth factors resulted in negligible bone formation where their combined delivery led to significant healing (Simmons *et. al.*, 2004). Simultaneous delivery of VEGF and BMP-2 from gelatin microparticles entrapped in porous degradable scaffolds had a positive effect on repair of a rat cranial defect (Patel *et. al.*, 2008b). The effect of combined and sequential delivery of IGF-1 and BMP-2 with two-layered, heterogeneously loaded, and crosslinked gelatin coatings *in vitro* was reported (Raiche and Puleo, 2004). The early delivery of BMP-2 followed by IGF-1 after 5 days resulted in the largest, and the earliest, elevation of ALP activity and mineralized matrix formation compared to the single use of the growth factors. Other studies involving the use of multiple growth factors included combinations of BMP-7/IGF-1 or BMP-7/interleukin-6 (IL-6) revealed increased ALP activity and bone nodule formation in osteoblastic cell cultures (Yeh *et. al.*, 2002). Combined delivery of IGF-1 and TGF- β 1 from biodegradable implant coatings has been shown to improve maximum load and torsional stiffness of the new bone that formed (Raschke *et. al.*, 2002). The positive effect of co-administration of BMP-2 and BMP-7 from complexed microspheres embedded in porous PLGA matrix on osteogenic differentiation was shown (Basmanav *et. al.*, 2008).

As it was discussed in Section 1.3.3.1, BMPs, the most osteoinductive growth factors, function in coordination during the bone formation and fracture

healing processes which starts from the initial inflammatory phase up to the construction of the mineralized tissue in a time and dose dependent manner. It is known that BMP-2 and BMP-7 (the FDA approved members of the BMP family) act sequentially during bone formation and regeneration. BMP-2 peaks immediately after fracture where BMP-7 peaks at ca. day 14. Therefore, it was hypothesized that delivering combinations of these growth factors in a sequential manner by mimicking their natural timing would be a promising approach to induce bone healing.

1.5. Aim, Approach and Novelty of the Study

The aim of this study was to prepare multi-functional tissue engineered constructs composed of polymeric scaffolds seeded with bone marrow MSCs carrying a sequential BMP-2/BMP-7 delivery system in order to mimic the bone healing process in nature. The approach was to encapsulate BMP-2 and BMP-7 in different polymeric nanocapsules (PLGA and PHBV) with different degradation rates and properties and, therefore, with different drug release rates to achieve the release of BMP-2 followed by the release of BMP-7. Initially, these nanoparticulate delivery systems were characterized and then the effect of single, simultaneous and sequential delivery of BMP-2 and BMP-7 from the nanoparticles was studied *in vitro* with bone marrow MSCs. The positive effect of using these two growth factors in a sequential manner by roughly mimicking their natural bioavailability timing was shown with maximized osteogenic activity results. BMP-2 loaded PLGA nanocapsules were subcutaneously implanted into Wistar rats and their biocompatibility as well as the positive effect of BMP-2 release on the formation of osteoclast-like cells was shown. Then, this nanoparticulate sequential delivery system was incorporated into two different types of polymeric systems, natural (chitosan) produced by wet spinning and synthetic (PCL) produced by 3-D plotting and wet spinning. Incorporation of nanocapsules into 3-D chitosan scaffolds was achieved by two different methods: incorporation within and onto chitosan fibers. Incorporation into 3-D PCL scaffolds was achieved by coating the nanocapsules in an alginate layer onto the fibers of the scaffolds. With both scaffold systems,

incorporation of nanocapsule populations capable of delivering BMP-2 and BMP-7 in single, simultaneous and sequential fashion was done. As with free nanocapsules, the positive effect of sequential delivery on the osteogenic differentiation of MSCs was shown with both scaffold systems.

Novelty of the study: Tissue engineering is developing into a new direction which includes the development of multi-functional tissue engineering scaffolds capable of delivering the required bioactive agents to induce and control the cellular activities both *in vitro* and *in vivo*. The current few attempts in the literature generally rely on mixing the polymer solution with the growth factor during the preparation phase, therefore, forming scaffolds that carry the factor within the polymer matrix. However, there is no control on the release rate in these cases as the release of the agent is dependent on the degradation of the scaffold itself or on its solubility. In some other studies, growth factors were loaded into microparticles, which were then incorporated into the scaffolds and thus affected the structure and properties of the scaffold. In the present study, two important osteogenic growth factors, BMP-2 and BMP-7, were encapsulated in biodegradable and biocompatible capsules of nano-size which were then incorporated into 3-D scaffolds without affecting the porosity and/or the structural properties of the main scaffold. The 3-D scaffolds were, therefore, functionalized by the addition of the sequential BMP-2/BMP-7 delivery system. The effect of co-administration of BMP-2/BMP-7 in a sequential fashion was illustrated with enhanced MSC differentiation results. By this way, the prepared constructs had the capability of mimicking natural processes occurring during bone regeneration.

CHAPTER 2

MATERIALS AND METHODS

2.1. Materials

PLGA (50:50) (Resomer® RG503H) (i.v. 0.32-0.44 dL/g, 0.1% in chloroform, 25°C) was purchased from Boehringer-Ingelheim (Germany). PHBV (HV content 8% w/w), low molecular weight chitosan (deacetylation degree 90.85%, i.v. 185 cps for 1% in 1% acetic acid), dexamethasone, β -glycerophosphate disodium salt, L-ascorbic acid were bought from Sigma-Aldrich (Germany). Poly(ethyleneoxide) (PEO) (Polyox™ WSR 301, MW $4 \cdot 10^6$) was obtained from Dow Chemical Company (USA). PCL (MW $3.7 \cdot 10^4$) was purchased from Solvay Caprolactones (CAPA 6404; UK). Bovine serum albumin (BSA) and polyvinyl alcohol (PVA) (MW $1.5 \cdot 10^4$) were obtained from Fluka (USA). Recombinant human BMP-2 from InductOs® (12 mg kit for implant; Wyeth Pharmaceuticals, USA) and recombinant human BMP-7 from Prospec Tany Technogene (Israel) were used. For the determination of BMP-2 and BMP-7, Quantikine BMP-2 immunoassay from R&D Systems (USA) and human BMP-7 Elisa kit from Ray Biotech (USA), respectively, were used. Dulbecco's Modified Eagle Medium (DMEM, high glucose) and fetal bovine serum (FBS) were obtained from Hyclone (USA). NucleoCounter reagents were supplied by Chemometec (Denmark) and Alamar Blue cell proliferation assay was from Biosource (USA). For the assessment of cell differentiation, alkaline phosphatase kit (Randox, USA) was used.

2.2. Methods

2.2.1. Preparation of Scaffolds for Bone Tissue Engineering

2.2.1.1. Production of Chitosan Fiber Mesh Scaffolds by Wet Spinning

Wet spun scaffolds of chitosan were prepared from pure chitosan and its blends with PEO according to Tuzlakoglu *et. al.* (2004) as shown Figure 2.1. Chitosan or chitosan:PEO (2:1) were dissolved in aqueous acetic acid to yield 4% chitosan and 2% PEO solutions. Solutions (0.6 mL of chitosan or chitosan:PEO, 2:1) were then injected at a rate of 5 mL/h through a needle with a diameter of 0.5 mm by using a syringe pump (World Precision Instruments, UK) into a coagulation bath of Na₂SO₄ (0.5 M):NaOH (1 M):distilled water = 3:1:6 (v/v). After chitosan fibers were kept in the coagulation bath overnight, they were exhaustively washed with distilled water, followed by dehydration with 50% methanol (1 h) and 100% methanol (3 h). The fibers were then placed in a plastic cylindrical mould with a diameter of 1.2 cm and a height of 0.8 cm and were dried at 60°C for 4 h. Dried scaffolds were 0.6 cm in diameter and 0.4 cm in height.

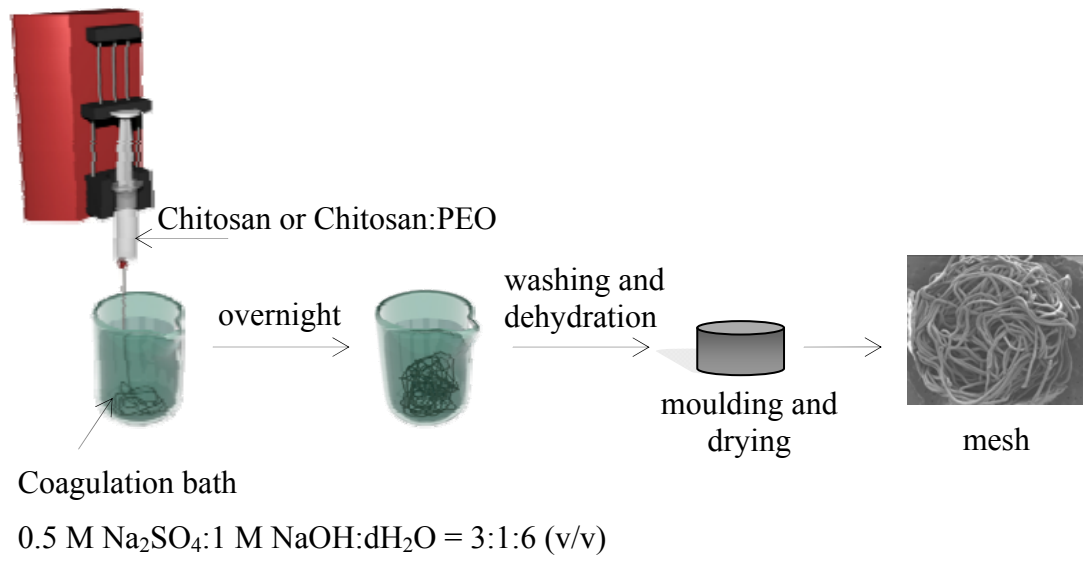


Figure 2.1. Scheme of wet spun chitosan and chitosan/PEO mesh production.

Chitosan was blended with PEO to improve the mechanical and structural properties of the chitosan scaffold. Chitosan concentration, PEO ratio and acetic acid concentration of the aqueous solvent were varied as presented in Table 2.1 to obtain the scaffold with optimum properties.

Table 2.1. Composition of chitosan scaffold preparation media.

Sample Code	Concentrations in the Aqueous Solvent		
	CHI (%, w/v)	PEO (%, w/v)	HAc (%, v/v)
CHI4-HAc2	4	-	2
CHI6-HAc2	6	-	2
CHI4-PEO2-HAc2	4	2	2
CHI4-PEO2-HAc5	4	2	5

CHI: Chitosan, Hac: Acetic Acid, PEO: Polyethyleneoxide.

2.2.1.2. Production of Poly(ϵ -caprolactone) (PCL) Scaffolds

3-D PCL scaffolds were fabricated by using two methods presented below. These were 3-D plotting, a rapid prototyping technique, and wet spinning.

2.2.1.2.1. PCL Scaffold Fabrication by 3-D Plotting

Oriented PCL scaffolds were fabricated using a Bioplotter® (Envisiontec GmbH, Germany) (Figure 2.2). Before the plotting procedure, PCL cartridges were prepared by manually compressing ca. 5 g of polymer in plastic tubes while heating to 100°C until the polymer slightly melts. After cooling, the formed PCL cartridges were removed from the holder, placed in the stainless steel syringe of the equipment (needle length 28.1 mm, needle inner diameter 0.5 mm) and heated to 140°C in the heated cartridge unit. When the polymer melted, CO₂ pressure (5 mm Hg) was applied to the syringe through a pressurized cap. Rectangular block models (20 mm x 20 mm) were uploaded on the Bioplotter CAD/CAM software (Figure 2.3) and the 3-D scaffold was plotted up to 10 layers,

through the extrusion of polymer as fibers. Each layer was 20 mm x 20 mm with a thickness of 0.25 mm (Figures 2.4 and 2.5) yielding a final 10 layered scaffold of 20 x 20 x 2.5 mm.

Scaffolds with different architectures were produced by changing the respective orientation of the deposited fibers using the CAD/CAM software. PCL scaffolds were produced to have four different standard architectures, named as: basic (B), basic-offset (BO), crossed (C) and crossed-offset (CO) (Figure 2.5). The B architecture is produced by the consecutive deposition of the layers, where each layer (N) is plotted orthogonally to the layer below (N-1), and is plotted in the same relative position of layer N-2 (Figure 2.5 a, b). The BO architecture is similar to B, but layer N is plotted with in an offset distance relative to layer N-2 (Figure 2.5 c, d). The C architecture is produced by the consecutive deposition of 2-D layers, in which layer N is plotted diagonally to layer N-1, and is plotted in the same relative position of layer N-4 (Figure 2.5 e, f). The CO architecture is similar to C, but layer N is plotted with in an offset distance relative to layer N-4 (Figure 2.5 g, h). Finally the scaffolds were cut using a circular die with 5 mm of diameter.

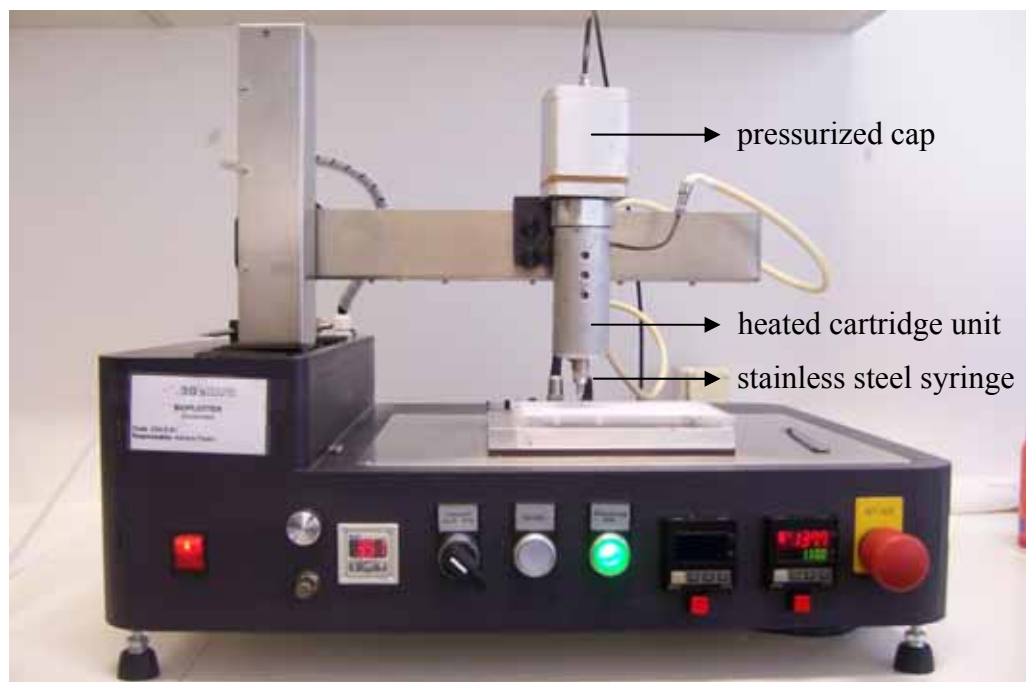


Figure 2.2. Bioplotter equipment and its components that was used to fabricate oriented PCL scaffolds.



Figure 2.3. A representative example of Bioplotter CAD/CAM software working window by which the scaffold production parameters were set for the fabrication of basic PCL scaffold (Needle length: 28.1 mm, Needle diameter: 0.5 mm, Dispenser temperature: 140°C, Layer thickness: 0.25 mm, Basic structure, Offset X: 0, Offset Y: 0).

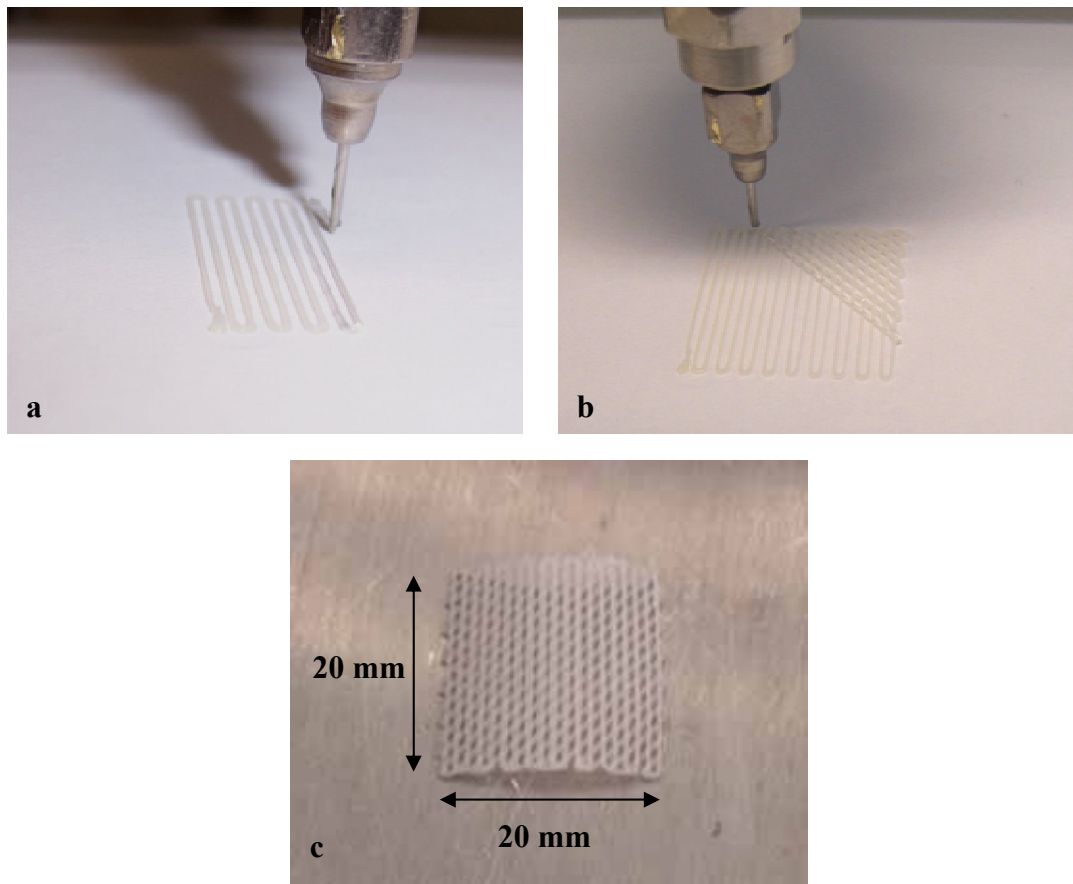


Figure 2.4. Production of the first two layers of crossed PCL scaffold. (a) production of the first layer, (b) production of the second layer on the first layer, (c) two-layered scaffold (length 20 mm, height 20 mm and thickness 0.5 mm).

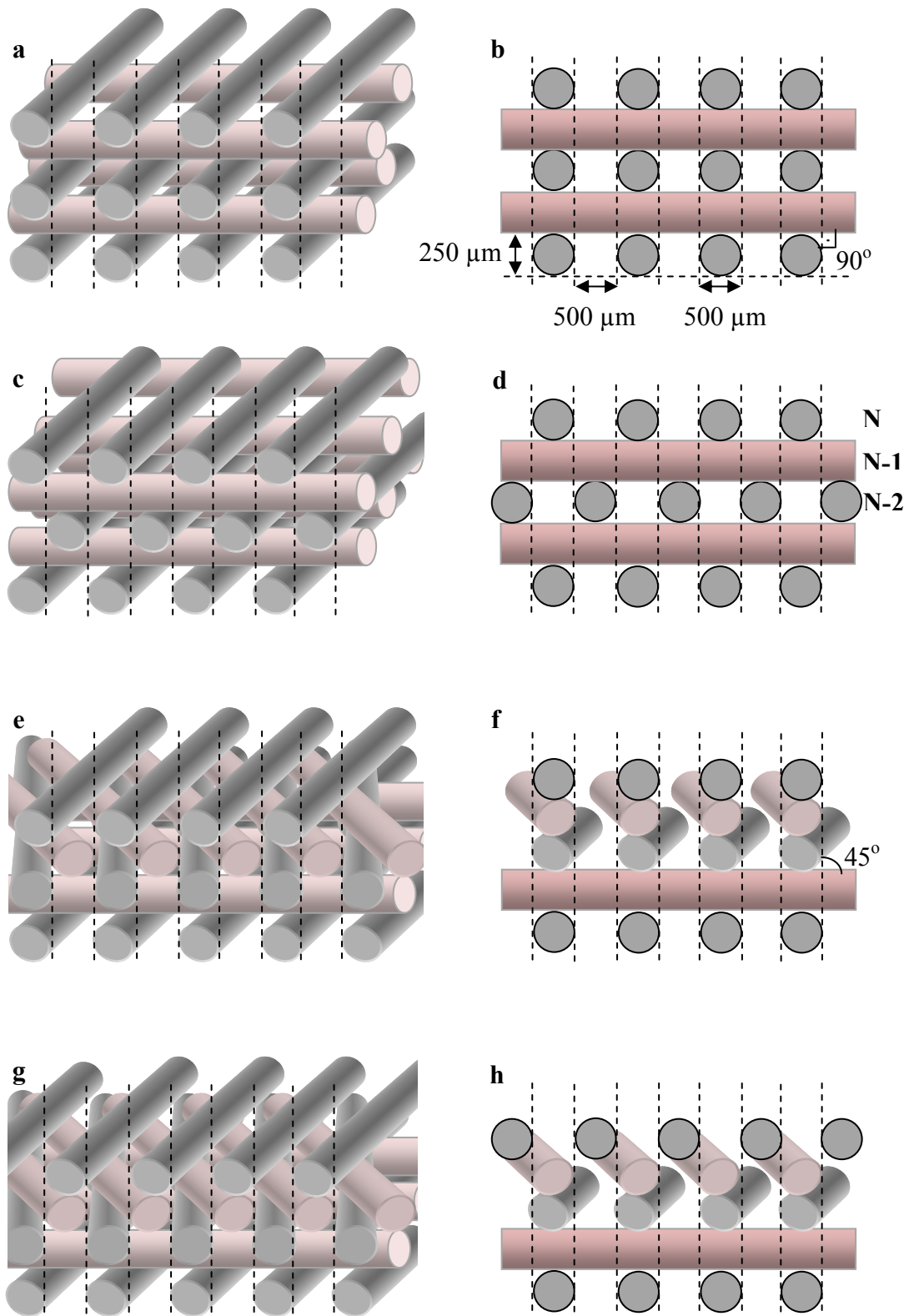


Figure 2.5. The design of oriented PCL scaffolds loaded on Bioplotter software. 3-D and cross sectional views of basic, B (a, b), basic-offset, BO (c, d), crossed, C (e, f), crossed-offset, CO (g, h).

2.2.1.2.2. PCL Scaffold Fabrication by Wet Spinning

PCL scaffolds with randomly oriented fibers were prepared by wet spinning (Figure 2.6). The polymer was dissolved in chloroform at a concentration of 90% (w/v). The polymer paste was then loaded into a syringe of the syringe pump (World Precision Instruments, UK). The solution was injected through a needle with an inner diameter of 0.5 mm into cold methanol at a rate of 6 mL/h and randomly oriented fibers formed upon manual movement of the coagulation bath. In order to prevent fusion of the fibers in the 3-D scaffold, initially individual layers of ca. 0.8 mm thickness were produced from 0.2 mL of the polymer paste. After the layers were washed with distilled water and dried overnight at room temperature for complete removal of the solvent, 3 of these layers were combined by moistening them with hexane:chloroform (4:1 v/v) and then by manually pressing the 3 layers together.

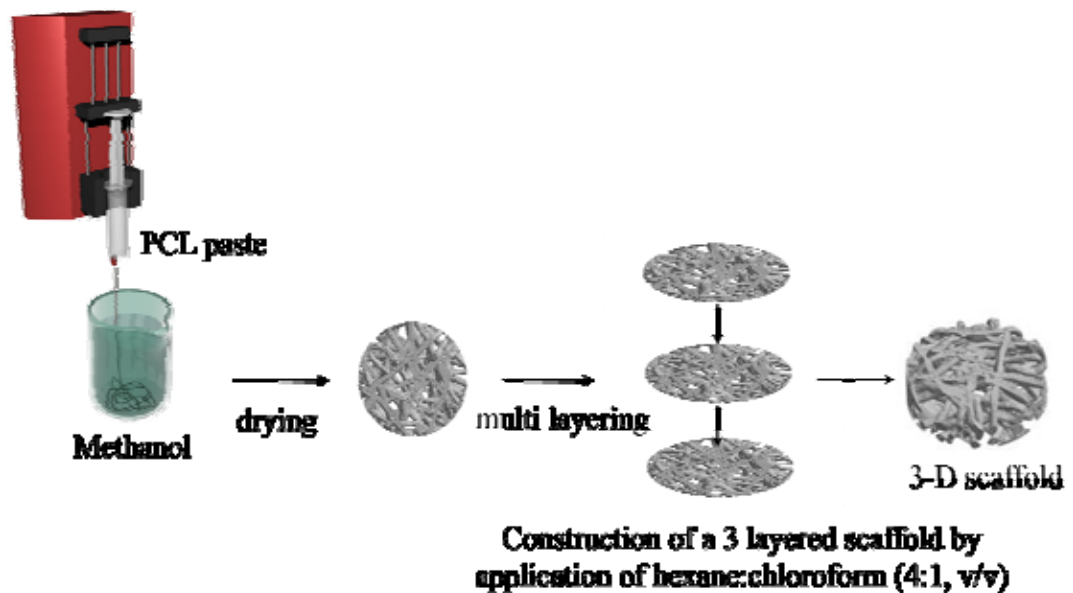


Figure 2.6. PCL mesh production by combining 3 layers of PCL fibers.

2.2.2. Preparation of Nanocapsules for Growth Factor Delivery

PLGA and PHBV nanocapsules carrying the model protein BSA and the growth factors (BMP-2 and BMP-7) were prepared by the double emulsion technique according to the scheme in Figure 2.7. Briefly, an aqueous solution of the bioactive species (2 mg BSA or 1 μ g BMPs in 0.1 mL dH₂O) was emulsified in a PLGA or PHBV solution in dichloromethane (0.6 mL) (30, 60, 120 mg polymer, to yield 5, 10, 20% w/v) by probe sonication at an output of 50 W for 15 s (Ultrasonic homogenizer, 4710 series, Cole-Parmer Instruments, USA). This first emulsion (w₁/o) was added into an aqueous solution of PVA (2 mL, 4% w/v) to form the w₁/o/w₂ system. The double emulsion was then added into more PVA solution (50 mL, 0.3% w/v) and then the organic solvent was evaporated by vigorous stirring overnight.

Nanocapsules were collected by centrifugation (Sigma 3K30, Germany) (15000 rpm, 10 min), washed with Tris-HCl (pH 7.4) and finally, resuspended in the buffer and lyophilized (Labconco Freezone 6, USA) after freezing at -20°C overnight. BSA loaded nanoparticles were stored in 4°C before *in situ* release experiments whereas BMP loaded nanocapsules were stored at -20°C and UV sterilized prior to *in vitro* studies.

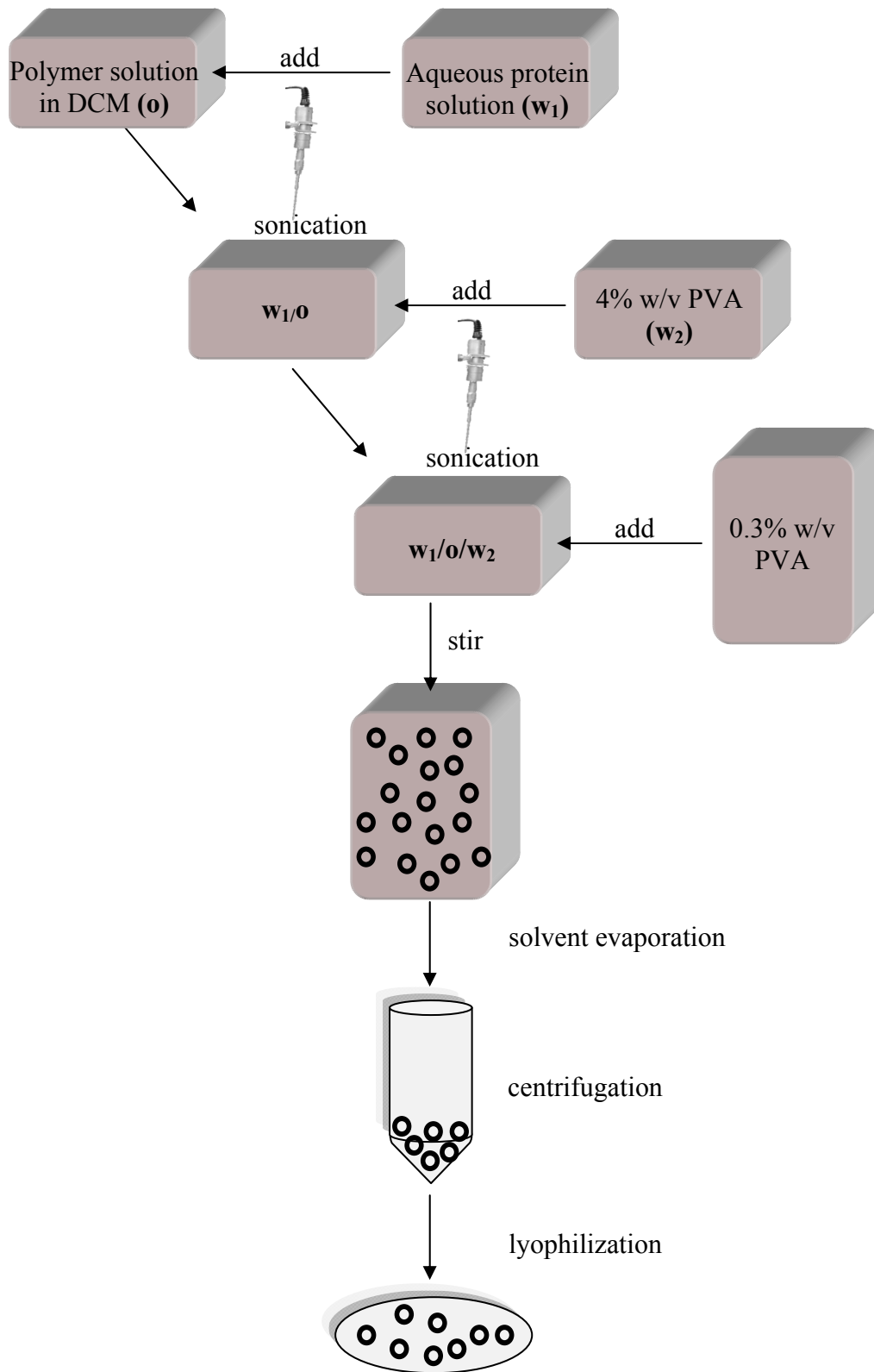


Figure 2.7. Preparation of polymeric (PLGA, PHBV) nanocarriers of BMPs by $w_1/o/w_2$ double emulsion method.

2.2.3. Incorporation of Nanocapsules into/onto the Carriers

Incorporation of PLGA and PHBV nanocapsules into fibrous chitosan scaffolds was carried out in two ways: within the fibers (NP-IN) and on the fibers (NP-ON) of the scaffolds. NP-ON loading was done for the incorporation of PLGA and PHBV nanocapsules onto PCL scaffolds.

2.2.3.1. Incorporation of Nanocapsules into Chitosan Scaffolds (NP-IN)

Chitosan fibers containing nanocapsules within their structure (NP-IN) were prepared by following the procedure presented in section 2.2.1.1. BSA or BMP loaded PLGA and PHBV nanocapsules (section 2.2.2) were incorporated into the polymer solution before injection of into the coagulation bath. Briefly, 2 mg PLGA and 10 mg PHBV nanocapsules carrying either BSA or BMPs were mixed with 0.6 mL of chitosan solution in aqueous acetic acid and this was injected into the coagulation bath. The rest of the procedure was the same as in section 2.2.1.1.

After the incorporation of the BMP loaded nanocapsules into the fibers, the constructs were ethylene oxide (EtO) sterilized (Steri-Vac gas sterilizer 5XL, T= 37°C, t= 4 h 45 min; at Hacettepe University Hospital, Department of Orthopedics and Traumatology) prior to experiments. 40 ng BMP per scaffold was used for all conditions (single, simultaneous and sequential delivery of BMP-2 and BMP-7). The amount of PLGA and PHBV nanocapsules carrying 40 ng of BMP-2 and BMP-7, respectively, were calculated from the encapsulation efficiencies. This calculation led to the use of 2 mg PLGA and 10 mg PHBV nanocapsules per scaffold. For both NP-IN and NP-ON (section 2.2.3.2) cases, four different release regimes were studied: (1) *single delivery of BMP-2*, (2) *single delivery of BMP-7*, (3) *simultaneous delivery of BMP-2 and BMP-7* and (4) *sequential delivery of BMP-2 and BMP-7*. Single delivery was achieved by BMP-2 and BMP-7 encapsulation within PLGA and PHBV nanocapsules, respectively, and by their separate incorporation to the constructs. For the simultaneous delivery case, both BMP-2 and BMP-7 were encapsulated in PLGA nanocapsules, therefore, performing the rapid release of both BMPs from the constructs. The sequential delivery, on the other hand, was achieved

by encapsulation of BMP-2 in PLGA and BMP-7 in PHBV nanocapsules and thus achieving two different release rates.

The effect of BMP-2 dose on proliferation and differentiation of rat bone marrow mesenchymal stem cells (MSCs) was studied by loading PLGA nanocapsules carrying 20, 40 and 80 ng BMP per scaffold. This was achieved by loading the appropriate amount of BMP-loaded nanocapsules into the chitosan fibers.

2.2.3.2. Incorporation of Nanocapsules onto Chitosan Scaffolds (NP-ON)

The second method applied for incorporation of nanoparticulate sequential delivery system onto chitosan scaffolds was NP-ON approach. This was achieved by introducing 100 μ L of 20 mg/mL PLGA and 100 mg/mL PHBV nanocapsule suspensions onto the top and the bottom of the chitosan scaffolds, followed by the application of a series of vacuum-pressure cycles to achieve proper penetration and distribution. The scaffolds were then dried overnight in a vacuum oven at room temperature.

After the BMP loaded nanocapsules were incorporated into the scaffolds, they were EtO sterilized ($T= 37^{\circ}\text{C}$, $t= 4\text{ h }45\text{ min}$) prior to *in vitro* experiments. The effect of BMP-2 dose on proliferation and differentiation of rat bone marrow MSCs was studied by incorporating 20, 40 and 80 ng BMP-2 loaded nanocapsules per scaffold.

2.2.3.3. Incorporation of Nanocapsules onto PCL Scaffolds

PLGA and PHBV nanocapsules were introduced to the surfaces of the fibers of the PCL scaffolds by a “post-seeding” method. The surfaces of the fibers constituting the scaffolds, produced with 3-D plotting and wet spinning, were treated with oxygen plasma at 50 W for 1 min (Advanced Plasma Systems Inc., USA) prior to nanocapsule incorporation. Oxygen plasma was applied in order to diminish the difference in the surface properties between the oriented and random

PCL scaffolds which was originated from the production methods involving heat treatment or extrusion of a paste.

In the mean time, dry nanocapsules were suspended in 1% (w/v) alginic acid solution at a concentration of 20 mg/mL for PLGA and 100 mg/mL for PHBV nanocapsules. After O₂ plasma treatment of the fibers, 100 µL of the nanocapsule suspension was placed onto one side (top or bottom) of the scaffold (diameter 5 mm, height 2.5 mm) and was allowed to dry at room temperature. After drying, another 100 µL of suspension was applied onto the other side of the scaffold. In total, 40 ng of BMP loaded nanoparticles were incorporated per scaffold for all delivery conditions (single, simultaneous or sequential delivery of BMP-2 and BMP-7). The scaffolds were finally dipped into ethanol to shrink the alginic acid on the fiber surfaces prior to 1 h incubation in 5% (w/v) CaCl₂ to crosslink the alginic acid and to immobilize the particles on the scaffold. The construct was then allowed to dry at room temperature. The constructs were EtO sterilized (T= 37°C, t= 4 h 45 min) prior to *in vitro* experiments.

2.2.4. Characterization

2.2.4.1. Scanning Electron Microscopy (SEM)

To prepare the samples for SEM, 50 µL of aqueous PLGA and PHBV nanocapsule suspensions were added onto the carbon tapes that were attached onto the stubs prior to SEM examination and the samples were allowed to dry at room temperature. Chitosan and PCL scaffolds, were lyophilized before attaching to the carbon tapes.

Cell seeded scaffolds, described in section 2.2.6, were fixed after 21 days of incubation with glutaraldehyde (2.5% in cacodylate buffer, pH 7.4) for 2 h and then washed with cacodylate buffer several times and lyophilized after freezing at -20°C overnight before for SEM examination. The structure of PLGA and PHBV nanocapsules, chitosan and PCL scaffolds, nanoparticle incorporated constructs (chitosan and PCL) and the cell attachment on the fiber surfaces of both types of

scaffolds after 21 days of incubation were studied by SEM after sputter coating with gold (Quanta 400F Field Emission SEM, the Netherlands).

2.2.4.2. Particle Size Distribution Analysis

Size distribution of PLGA and PHBV nanocapsules was determined by using the Zeta Potential and Mobility Measurement System (Malvern Nano ZS90, UK).

2.2.4.3. Assessment of *in situ* Degradation

2.2.4.3.1. Degradation of PLGA and PHBV Nanocapsules

For the assessment of the extent of *in situ* degradation, 5 mg of BSA loaded PLGA or PHBV nanocapsules were placed in sterile phosphate buffered saline (PBS, 1 mL, 10 mM, pH 7.4) in duplicate and incubated at 37°C on an orbital shaker. On days 3, 10, 15 and 21, samples were centrifuged (Sigma 3K30, Germany), washed twice with distilled water and lyophilized before SEM examination. The pH of the supernatant was determined (CyberScan 510 pH, Eutech Instruments, USA) in order to determine the extent of acidic product formation during degradation of the polymeric nanocapsules.

2.2.4.3.2. Swelling and Degradation of Chitosan Scaffolds

The change in physical properties (fiber thickness, sample weight and surface properties) of the chitosan scaffolds was investigated at 37°C in triplicate by placing the scaffolds in 3 mL of sterile PBS (10 mM, pH 7.4) for 6 weeks. At various time points (1, 2, 3 and 6 weeks) weight measurements were carried out with 0.001 g sensitivity, and SEM were obtained to study the weight loss (erosion) and the change in surface properties of the scaffolds.

At each time point, samples were removed from the medium, lyophilized and weighed in order to determine the weight loss based on erosion or

degradation of the scaffold structure. The weighed sample was then placed back into the medium and incubation was continued.

After 6 weeks in the medium, the dimensions of the scaffolds were measured by a micrometer (with 1 μm sensitivity). The change in individual fiber thickness was determined from at least three fluorescence micrographs (Leica TCS SPE, Germany) of the fibers.

2.2.4.3.3. Degradation of PCL Scaffolds

Degradation was studied using the “Basic” (B) PCL scaffold. The sample was placed in 3 mL of sterile PBS and incubated at 37°C on an orbital shaker for 6 weeks. At various time points (1, 2, 3 and 6 weeks) pH of the medium was measured to determine the extent of acidic by-product formation due to degradation of PCL.

Samples were removed from the medium, lyophilized and weighed in order to examine the weight loss due to erosion of the scaffolds. The weighed samples were then placed back into the medium and incubation was continued. At 3 and 6 weeks of the incubation, samples were washed with distilled water and then lyophilized before examination with SEM. All experiments were carried out in triplicates.

2.2.4.4. Microcomputed Tomography (μ -CT)

Porosity and its distribution in the 3-D chitosan and PCL scaffolds were assessed by using microcomputed tomography (μ -CT 20, Scanco Medicals, Switzerland). Scanner settings were 40 keV and 248 μA . Entire scaffolds were scanned in 200 slices 7 μm thick. 3 samples were analyzed for each scaffold architecture (chitosan and PCL). CT Analyzer and CT Vol Realistic 3-D Visualization (SkyScan, Belgium) softwares were used for image processing in CT reconstructions and in creation and visualization of the 3-D representations.

2.2.4.5. Dynamic Mechanical Analysis (DMA)

Dynamic mechanical analysis of the unseeded PCL samples before nanoparticle incorporation was carried out using a Perkin Elmer DMA7e (USA). An oscillating compressive force was applied to the dry samples at 37°C and the resulting displacement of the sample was measured, from which the stiffness of the sample and the sample modulus were calculated. The real (storage) modulus, E' , and the imaginary (loss) modulus, E'' , components of the complex modulus, E^* (where $E^*=E'+iE''$), were recorded against frequency that varied between 0.1 and 70 Hz.

2.2.5. *In situ* Release Studies

2.2.5.1. BSA Release from Nanocapsules in Free Form and in Scaffolds

Encapsulation efficiencies and release kinetics of the PLGA and PHBV nanocapsules were studied by using bovine serum albumin (BSA) as the model protein. Released protein was determined with Coomassie Plus Bradford Assay (Pierce, USA) by using the micro protocol of the assay.

BSA release from PLGA and PHBV nanocapsules was studied by placing nanocapsules (5 mg) in PBS (1 mL, pH 7.4) in Eppendorf tubes and incubating at 37°C. At various time points (3 h and 1, 2, 4, 6, 8, 10, 15, 21, 28, 36 and 45 days) sample was centrifuged, and the released protein amount in the supernatant was determined using the Bradford assay. Briefly, 150 μ L of the sample was put into the 96 well plate and 150 μ L of Bradford reagent was added onto these wells. The protein in the sample binds to the Coomassie dye, which results in a spectral shift from the reddish/brown (λ_{max} 465 nm) to blue (λ_{max} 610 nm). After 10 min at room temperature, the absorbance at 595 nm, at which difference between the two forms of the dye is greatest, was determined using a plate reader (Molecular Devices, USA). The absorbance was correlated with the protein concentration by a calibration curve (Appendix A).

The precipitate was resuspended in fresh 1 mL PBS solution and incubation was continued.

Encapsulation efficiency of PLGA and PHBV nanocapsules was determined by dissolving the nanocapsules in dichloromethane. For this, 5 mg of PLGA or PHBV nanoparticles were placed in glass test tubes and then 2 mL of dichloromethane was added, and medium was vortexed until a clear solution was obtained. Then the protein of the nanocapsules was extracted several times with water by adding 2 mL of dH₂O onto the dichloromethane and vortexing. The water phase was then removed and the amount of protein in the water phase was quantified using the assay described above.

Release from the nanoparticles introduced to chitosan and PCL constructs was performed by using BSA to represent BMPs. BSA loaded 2 mg PLGA and/or 10 mg PHBV nanocapsule incorporated scaffolds were put into the 24 well plates, 1 mL of sterile PBS was added into each well and incubated at 37°C on orbital shaker. At various time points (1, 3, 5, 10, 15 and 25 days), the medium was removed and protein amount was determined spectrophotometrically by using Coomassie Plus Assay as described above. Then, 1 mL of fresh, sterile PBS was added to the wells and incubation was continued. These experiments were carried out in triplicate.

2.2.5.2. BMP Release from Free Nanocapsules

After optimization of the loading efficiency and release behavior using BSA, BMP-2 and BMP-7 were encapsulated in PLGA and PHBV nanocapsules and their release kinetics were determined with corresponding ELISA kits. For this purpose, 2 mg of BMP-2 loaded PLGA or BMP-7 loaded PHBV nanocapsules were placed in 1 mL sterile PBS in Eppendorf tubes and incubated at 37°C. At various time points (1, 3, 10, 15 and 21 days) sample was centrifuged, supernatant was removed and fresh, sterile PBS (1 mL) was added. The released BMP was determined using the corresponding ELISA kits for BMP-2 and BMP-7.

BMP-2 was determined with the sandwich enzyme immunoassay technique. Into a microplate precoated with a monoclonal antibody specific for BMP-2 standards (to prepare a calibration curve) and samples were placed (50 μ L). BMP-2 in the sample was bound by the immobilized antibody and after washing away any unbound compounds, an enzyme-linked monoclonal antibody specific for BMP-2 was added to the wells. Following a wash to remove any unbound antibody-enzyme reagent, a substrate solution was added to the wells and the intensity of color that developed was in proportion to the amount of BMP-2 bound in the initial step. This was measured by the plate reader (Molecular Devices, USA).

BMP-7 released from PHBV nanocapsules was determined by the BMP-7 Elisa kit working with the same principle described above.

2.2.6. *In vitro* Studies

2.2.6.1. Isolation of Bone Marrow Mesenchymal Stem Cells

Bone marrow mesenchymal stem cells (MSCs) (osteoprogenitor cells) were isolated from 6 weeks old, approximately 150 g, male Sprague-Dawley rats. The rats were euthanized by placing them in a covered glass vessel containing ether soaked gauze pads. Their femurs and tibia were excised and washed with DMEM containing 1000 U/mL penicillin and 1000 μ g/mL streptomycin under aseptic conditions. The marrow in the midshaft was flushed out with primary media (PM) (DMEM containing 20% fetal bovine serum (FBS), 100 U/mL penicillin and 100 μ g/mL streptomycin) and collected in a 15 mL sterile centrifuge tube. Then, the cells were centrifuged at 500 g for 5 min and the resulting cell pellet was resuspended in primary medium and plated in T-75 flasks (cells from one femur per flask) (Kose *et. al.*, 2004). These primary cultures were incubated for 2 days.

2.2.6.2. Bone Marrow MSC Culture

After 2 days of incubation, hematopoietic and other unattached cells were removed from the flasks by repeated washes with PBS (10 mM, pH 7.4) and the primary medium of the flasks was renewed every other day until confluency. These primary cultures were detached from the flasks and frozen in FBS containing 10% DMSO for storage in liquid nitrogen until use.

Following thawing, cells were incubated until confluency prior to seeding. All cell culture experiments were conducted under standard culture conditions (37°C and 5% CO₂) in a CO₂ incubator. Cell seeding and further incubation was done in complete media (CM) consisting of DMEM supplemented with 10% FBS, 10 mM β-glycerophosphate, 50 μg/mL L-ascorbic acid, 10 nM dexamethasone, 100 U/mL penicillin, 100 μg/mL streptomycin against bacterial contaminations and 1 μg/mL amphotericin B against fungi and yeast contaminations. Dexamethasone was used to promote osteoblastic differentiation (phenotype expression) of the bone marrow mesenchymal cells. It accelerates upregulation of postproliferative osteoblast genes resulting in induction of ALP activity and increase in number of bone nodules (Coelho *et. al.*, 2000). L-Ascorbic acid influences the differentiation of the protoblasts and plays an important role in the production of the collagenous bone ECM by increasing expression of collagen in a dose dependent manner (Stein and Lian, 1993). β-Glycerophosphate serves as a source of phosphate ions and is strictly required for the formation of a mineralized ECM by the osteoblasts.

2.2.6.3. Cell Seeding

Confluent cells were detached from the flask surface by treatment with 0.25% trypsin for 5 min at 37°C. After detachment, trypsin was deactivated with FBS and cells were collected by centrifugation. Number of viable cells was determined with a Nucleocounter (Chemometec, Denmark). The calculated volume of cell suspension (ca. 50 μL) containing $5 \cdot 10^4$ viable cells was seeded onto TCPS or scaffolds according to the experimental design.

2.2.6.3.1. Cell Seeding for Free Nanocapsules

Cells ($5 \cdot 10^4$) were seeded on tissue culture polystyrene (TCPS) and 3 h post-seeding, BMP loaded nanocapsules which were UV sterilized and suspended in the growth medium were added to the wells containing the cells. Nanocapsules carrying 40 ng BMP was introduced to individual wells (2 mg PLGA and 10 mg PHBV nanocapsules per well). In the simultaneous and sequential cases, 40 ng of each BMP type was used, whereas in the single BMP cases only 40 ng of the specific BMP was introduced. To change the medium, liquid was removed from the wells, centrifuged and the collected nanocapsules were resuspended in fresh medium and then put onto the cells.

2.2.6.3.2. Cell Seeding on Chitosan and PCL Scaffolds

EtO sterilized chitosan and PCL scaffolds and nanoparticle incorporated constructs were seeded with rat bone marrow MSCs at a seeding density of $5 \cdot 10^4$ cells per scaffold. During seeding, the scaffolds and growth factor incorporated constructs were placed onto sterile Teflon disks in order to prevent cell attachment onto TCPS surface. Cell seeding was done in ca. 50 μ L of cell suspension (according to the viable cell number in the cell suspension upon trypsinization) and 2 h incubation in CO₂ incubator was done prior to medium addition to ensure cell attachment onto the scaffolds. At the end of 2 h incubation period, the volume of the medium in the wells was completed to 1 mL under sterile conditions. Incubation was performed at 37°C and 5% CO₂ in CM. 40 ng BMP/scaffold was used for all conditions unless otherwise is stated.

2.2.6.4. Determination of Cell Proliferation

Viable cell number during *in vitro* incubations was assessed using Alamar Blue assay. At each time point, the medium in the wells was discarded and the wells were washed with sterile PBS to remove any remaining medium. Then Alamar Blue solution (10%, 1 mL) in colorless DMEM was added to the wells and

incubated at 37°C and 5% CO₂ for 1 h. After 1 h, 200 µL of the test solution was transferred to a 96 well plate and absorbance was determined at 570 and 595 nm using the plate reader. The test medium in the wells was then discarded, washed with sterile PBS, fresh CM was added to the wells and the incubation was continued. All experiments were carried out in triplicates.

Alamar Blue assay incorporates a colorimetric growth indicator based on detection of metabolic activity. Specifically, the system incorporates an oxidation-reduction (redox) indicator that changes color in response to chemical reduction of growth medium resulting from the metabolic activity of the cells. Reduction related to metabolic activity (related to cell number) causes the redox indicator to change from oxidized (blue) form to reduced (red) form.

The redox indicator incorporated in the Alamar Blue assay was demonstrated by the manufacturer to be minimally toxic to living cells as shown by analysis of the possible interaction of the reagent with the cellular respiration. The relative redox potential of the various components of the biological respiration chain was compared to that of the Alamar Blue. It was shown that the flow of electrons was interrupted in the presence of other commonly used artificial electron-acceptors such as tetrazolium salt (MTT). Whenever a substrate is oxidized in the presence of MTT, the released electrons are not transported through the usual sequence of cytochromes but are trapped, which shuts down the respiratory chain. Alamar Blue, on the other hand, is intermediate and may substitute for molecular oxygen for any of the oxidoreductases which routinely utilize molecular oxygen as electron acceptor.

The absorbance values were recorded at 570 nm and 595 nm which gives the absorption spectra of the reduced and oxidized forms of Alamar Blue, respectively. Since there is considerable overlap in these spectra, the following equation is used for the calculation of percent reduction of Alamar Blue:

$$\% \text{ Reduction} = \frac{(\epsilon_{\text{OX}})_{\lambda_2} * A_{\lambda_1} - (\epsilon_{\text{OX}})_{\lambda_1} * A_{\lambda_2}}{(\epsilon_{\text{RED}})_{\lambda_1} * A'_{\lambda_2} - (\epsilon_{\text{RED}})_{\lambda_2} * A'_{\lambda_1}} * 100$$

where;

ϵ_{OX} = molar extinction coefficient of Alamar Blue oxidized form (Blue)

ϵ_{RED} = molar extinction coefficient of Alamar Blue reduced form (Red)

A = absorbance of test wells

A' = absorbance of negative control wells

λ_1 = 570 nm

λ_2 = 595 nm

To correlate the % reduction with the viable cell number, a calibration curve of known cell numbers vs % reduction was constructed (Appendix B).

2.2.6.5. ALP Assay for the Assessment of MSC Differentiation

Alkaline phosphatase (ALP) activity was used as the indicator of MSC differentiation into osteoblastic cells and was determined by using Randox ALP kit. The absorbance of p-nitrophenol formed from p-nitrophenyl phosphate was determined at 405 nm and the amount of enzyme was calculated as described by the manufacturer. Experiments were carried out in triplicates.

Briefly, TCPS or scaffolds seeded with cells were washed with PBS (10 mM, pH 7.4) and scaffolds were transferred into Tris buffer (10 mM, pH 7.5, 0.1% Triton X-100). Cells on TCPS were lysed with the same buffer and were transferred into sterile centrifuge tubes. Then the samples were freeze-thawed three times and sonicated for 5 min at 25 Watts on ice in order to achieve complete cell lysis and release of alkaline phosphatase and the samples were centrifuged at 2000 rpm for 10 min to settle the cell debris. An aliquot of 100 μL of each sample was added to 150 μL of p-nitrophenyl phosphate solution (10 mmol/L) at room temperature in the well of a 96-well plate. p-nitrophenyl phosphate was converted to p-nitrophenol by alkaline phosphatase and its absorbance was measured at 405 nm between 0 and 12 min at 2 min intervals by the plate reader. The slope of the absorbance vs time plot

was used to express the alkaline phosphatase activity per minute. Calibration curve of p-nitrophenol at 37°C was used to determine the enzyme activity in units of nmole substrate converted to product per minute.

2.2.6.6. Determination of Cell Phenotype

At the end of 21 days of incubation, cell seeded PCL scaffolds were rinsed with PBS (pH 7.4) in order to remove the media and fixed with 4% p-formaldehyde in PBS for 30 min at room temperature. The samples were then treated with Triton X-100 (0.1%) for 5 min to permeabilize the cell membranes. After washing with PBS, samples were incubated at 37°C for 30 min in BSA-PBS (1%) solution before staining to prevent non-specific binding. After washing with 0.1% BSA in PBS, the scaffolds were stained with FITC-labeled phalloidin (1:100 dilution of the stock) for actin filaments. After several washings with PBS to remove the unbound stain, the samples were studied with the confocal laser scanning microscope (CLSM) (Leica TCS SPE, Germany) with a 488 nm laser for FITC-phalloidin.

2.2.7. *In vivo* Studies

2.2.7.1. *In vivo* Evaluation of BMP-2 Loaded PLGA Nanocapsules

Evaluation of BMP-2 loaded PLGA nanocapsules *in vivo* was done in order to assess the suitability of the nanoparticulate sequential delivery system for use in clinical applications. This part of the study was carried out by Dr. Shahram Ghanaati in the laboratories of Prof. Dr. James Kirkpatrick (REPAIR Lab, Institute of Pathology, Johannes Gutenberg University, Mainz, Germany) within the scope of EU FP6 NoE Project Expertissues.

24 female, five weeks old Wistar rats were divided into two groups of 12 animals each. From each group, 3 animals were used for each of the following time points: 3, 10, 30 and 40 days. Group 1 was treated with BMP-2 loaded nanocapsules. Group 2 was the sham group. Using the subcutaneous implantation

model, 0.2 mg of PLGA nanocapsules was implanted in a preformed subcutaneous pocket of the subscapular region (Figure 2.8).

At each time point, the surrounding peri-implant tissue was explanted and fixed in 4% formaldehyde for 24 hours for histological, histochemical and electron microscopical analysis.

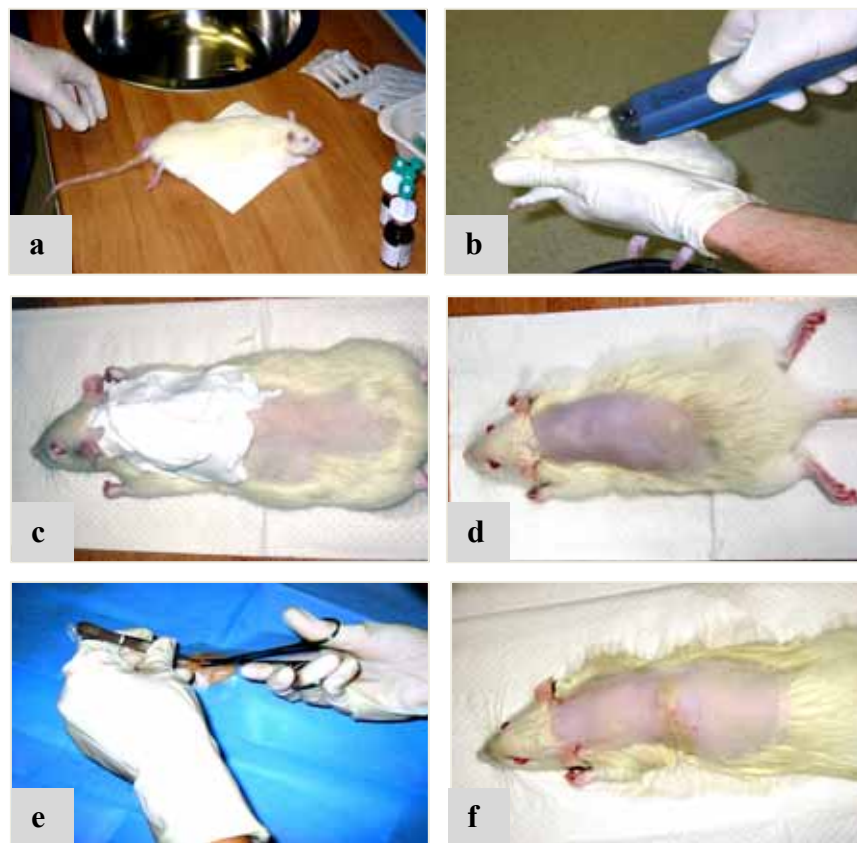


Figure 2.8. Subcutaneous implantation of BMP-2 loaded PLGA nanocapsules to Wistar rats. (a) Pre-op, (b, c, d) shaving, cleaning and disinfection of the subscapular region, (e) subcutaneous implantation, (f) post-op.

2.2.7.2. *In vivo* Evaluation of BMP-2/BMP-7 Releasing Tissue Engineered PCL Constructs

The *in vivo* performance of tissue engineered PCL constructs was studied by using a rat pelvis model. Implantations were done by Dr. Bülent Önal under the supervision of Prof. Dr. Semih Keskil at GUDAM (Gazi Üniversitesi Laboratuvar Hayvanları Yetiştirme ve Deneysel Araştırmalar Merkezi, Ankara).

There were two major aims in this study: (1) investigating the performance of the MSC seeded, tissue engineered construct capable of sequential delivery of BMP-2 and BMP-7 on the healing of bone defects, and (2) investigating the effect of PCL fiber orientation on the healing of bone defects.

27 female four weeks old Sprague-Dawley rats were randomly divided into 9 groups of 3 animals each. Two scaffolds were implanted to each animal; one sample (3 mm in diameter and 2 mm in height) on each side of the superior iliac crest of pelvis (Figures 2.9 and 2.10) according to the ethical committee approval provided by Gazi University (Appendix C). In total, each sample group had 6 implantations as presented in Table 2.2.

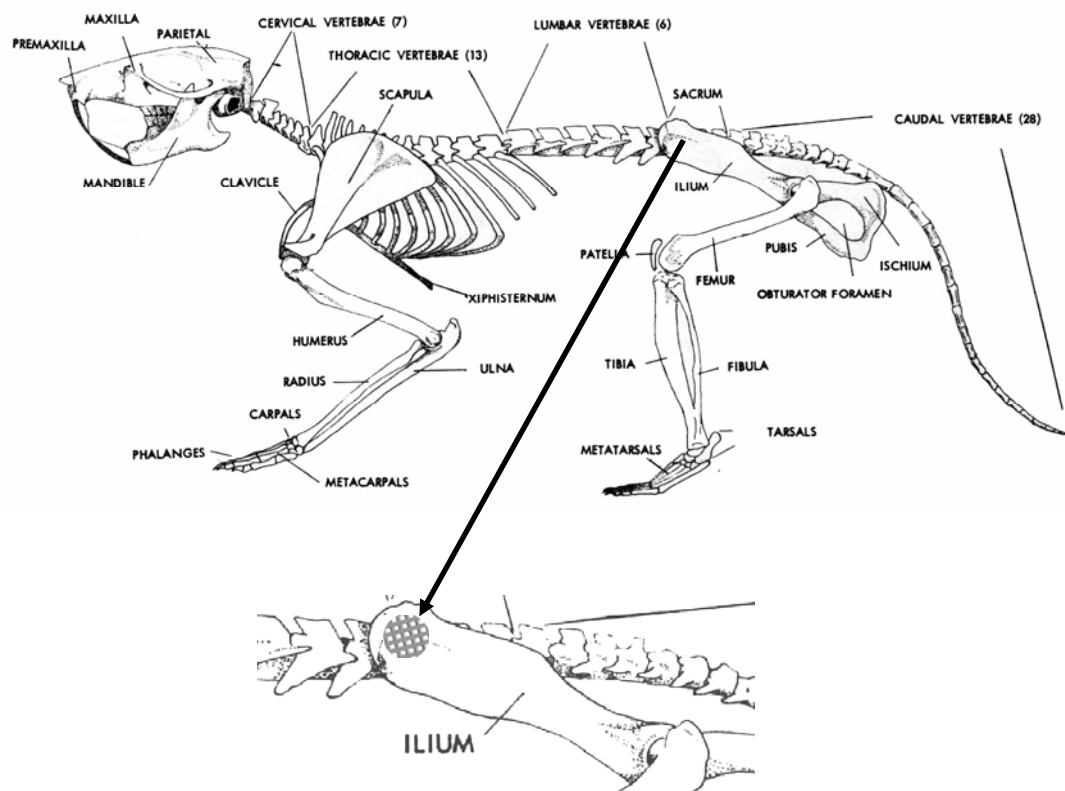


Figure 2.9. The scheme of implantation into the iliac crest.

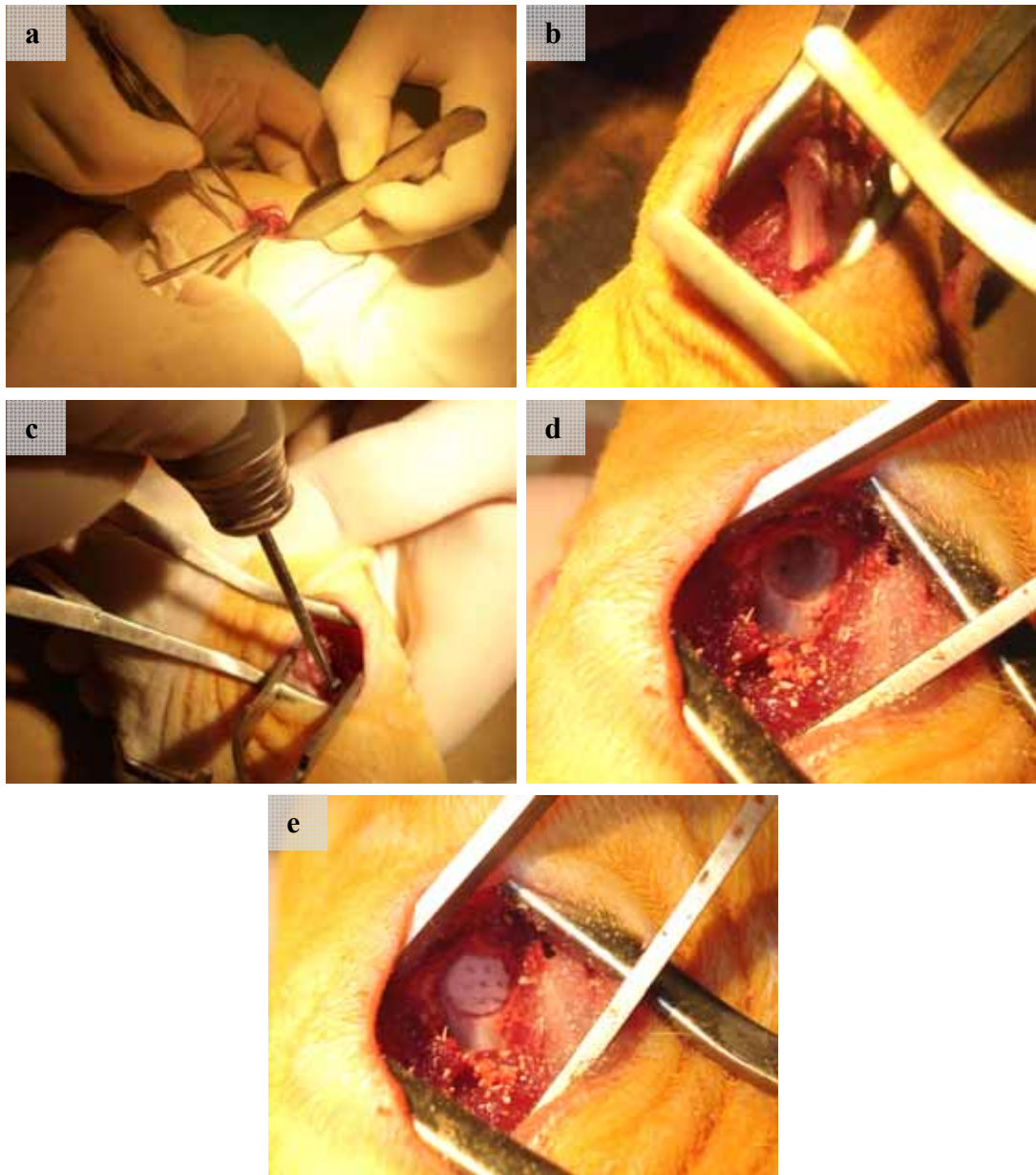


Figure 2.10. Implantation of scaffold C into the pelvis of a Sprague-Dawley rat. (a) Incision, (b) iliac crest, (c) creation of the bone defect, (d) bone defect, (e) insertion of the scaffold into the defect site.

Table 2.2. Experimental groups of *in vivo* evaluation of BMP releasing PCL scaffolds.

SAMPLE	SAMPLE CODE
Empty defect (negative control)	Sham
BMP-2 loaded PLGA and BMP-7 loaded PHBV nanocapsules (free nanocapsules)	NC
B-scaffold with basic architecture (no nanocapsules)	B
B-scaffold incorporating BMP-2 loaded PLGA and BMP-7 loaded PHBV nanocapsules	B+NC
B-scaffold seeded with rat bone marrow MSCs (seeded 1 week before implantation)	B+MSC
B-scaffold seeded with MSCs (seeded 1 week before implantation) incorporating BMP-2 loaded PLGA and BMP-7 loaded PHBV nanocapsules	B+NC+MSC
BO-scaffold with basic-offset architecture	BO
C- scaffold with crossed architecture	C
CO-scaffold with crossed-offset architecture	CO

The animals were sacrificed at 6 weeks after implantation and immediately after sacrifice, computer tomographic assessment (performed by Prof. Dr. Sadi Gündoğdu, Ufuk University, Department of Radiology) was performed in order to investigate the difference of the extent of bone regeneration and healing among the experimental groups. After the radiological analysis, the animals were fixed with 4% formaldehyde for 7 days. Following dissection of the pelvic area, the bone samples were decalcified with 5% formic acid at 37°C for 5 days prior to sectioning for histological analysis (performed by Assit. Prof. Dr. Güldal Yılmaz, Gazi University, Department of Pathology) to investigate the (1) quality of the bone-scaffold interface; (2) tissue response within the pores of the scaffold; and (3) quantity of bone formation within the defect.

2.2.8. Statistical Analysis

MSC proliferation and differentiation assays were carried out in triplicates. Data were analyzed with statistically significant values defined as $p < 0.05$ based on one-way analysis of variance (ANOVA) followed by Tukey's test for determination of the significance of difference between different groups ($p \leq 0.05$).

CHAPTER 3

RESULTS AND DISCUSSION

3.1. Preparation of Nanoparticulate Sequential Delivery System

3.1.1. Particle Structure and Size

In order to construct a sequential growth factor delivery system, two different populations of nanoparticles were prepared; one to provide a fast and the other a relatively slower release of the content. Due to the fact that PLGA degrades significantly more rapidly compared to PHBV (99% vs. 43% in 6 months), although having similar chemical structures (Kök and Hasırcı, 2003), when all the other properties are comparable (MW, crystallinity) it is expected that PLGA would degrade faster. Therefore, in this study the rapid release component of the sequential delivery system was constructed from PLGA particles, and from PHBV particles the slower release component was prepared.

Production of PLGA and PHBV capsules were carried out by using 5, 10 and 20% (w/v) polymer solutions. The use of 5% polymer solutions did not lead to the formation of spherical capsules possibly due to the very low viscosity.

Proper capsular structures were obtained by using higher concentrations of both polymers. It was observed from the SEM micrographs that increasing the concentration of the polymer improved the nanoparticle shape and increased the capsule diameter (Figure 3.1). An increase in polymer concentration from 10 to 20% led to an increase in capsule diameter by almost 5-fold (from ca. 300 nm to 1500 nm) for PLGA capsules and ca. 10-fold (from ca. 400 nm to 4000 nm) for

PHBV capsules. The capsules produced by using 10% PLGA and PHBV were in the submicron range, where 20% capsules were larger. It was also observed that the walls of 10% PLGA particles were quite thick (ca. 200 nm) (Figure 3.1a inset).

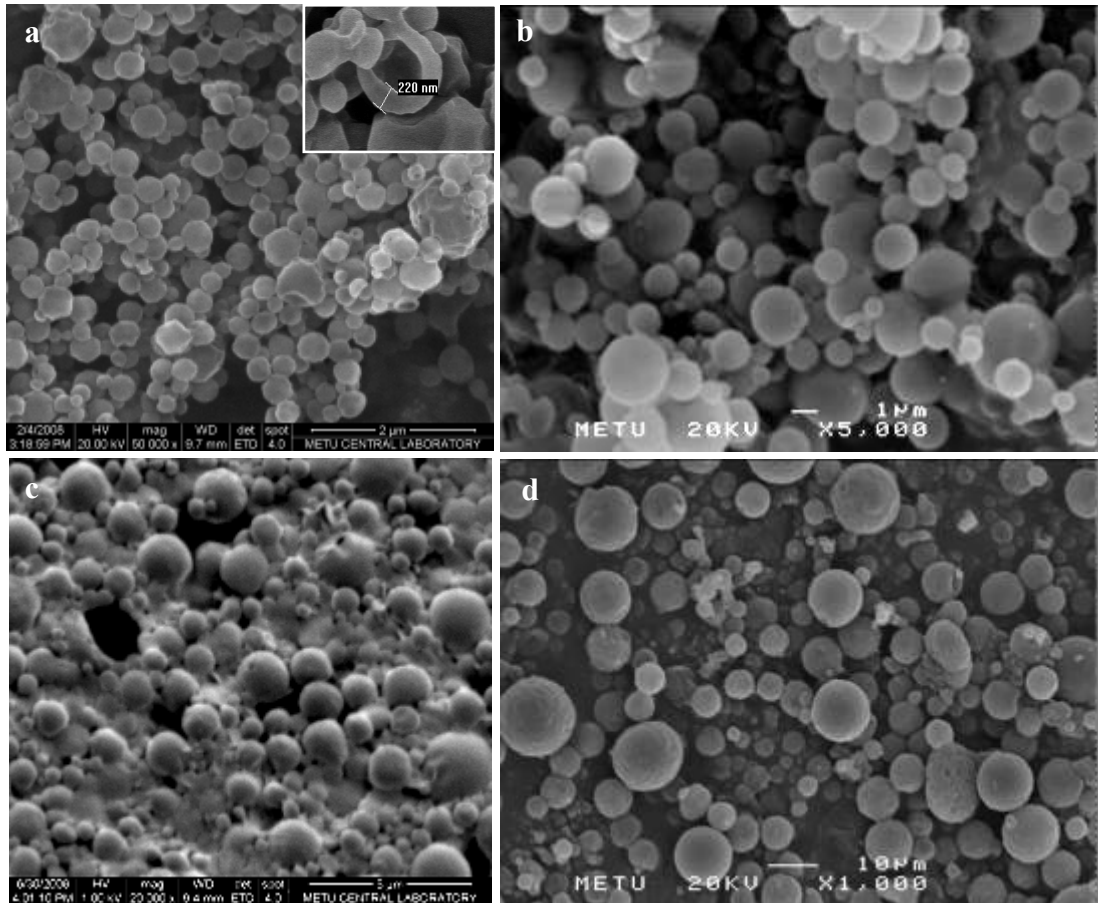


Figure 3.1. BSA loaded capsules (a) PLGA: 10% (x50,000; inset shows wall thickness of 220 nm), (b) PLGA: 20% (x5,000), (c) PHBV: 10% (x20,000), (d) PHBV: 20% (x1,000).

The particle size distribution of the submicron range particles, 10% PLGA and 10% PHBV, were determined. PLGA capsules were found to have an average diameter of 327 nm, with the particle size in the range 190-615 nm. PHBV capsules had a larger mean diameter of 438 nm and a particle size range of 255-712 nm (Figure 3.2). These indicated that both capsules were in the nanometer range.

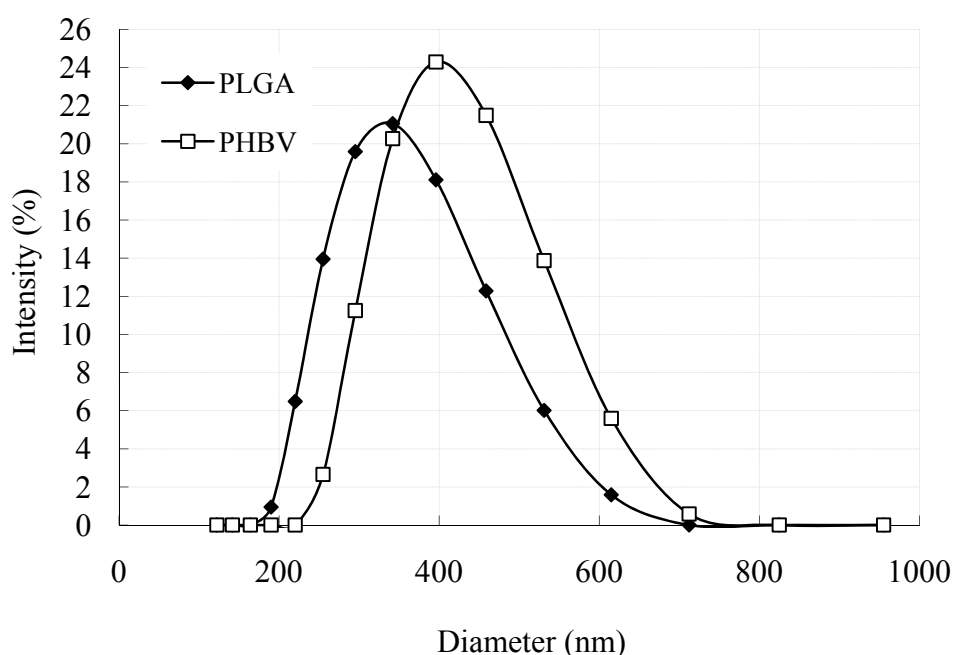


Figure 3.2. Particle size distribution of 10% PLGA and 10% PHBV capsules.

3.1.2. Degradation of Loaded PLGA and PHBV Nanocapsules

Since the delivery of the bioactive agent from the carrier depends partially on the degradation of the nanocapsules, their degradation was investigated *in situ*. As an indicator of degradation, the change of the pH of the degradation medium (PBS) during 21 days of incubation was recorded (Figure 3.3). A decrease

in the medium pH was observed with time for both particle types, probably as a result of the hydrolytic degradation of the polymers producing acidic degradation products including lactic acid, glycolic acid, 3-hydroxybutyric acid and 3-hydroxyvaleric acid. The rate of decrease of the medium pH was higher initially in the beginning of the incubation period (first 3 days) for PLGA nanocapsules, as expected from the higher degradation rate of PLGA.

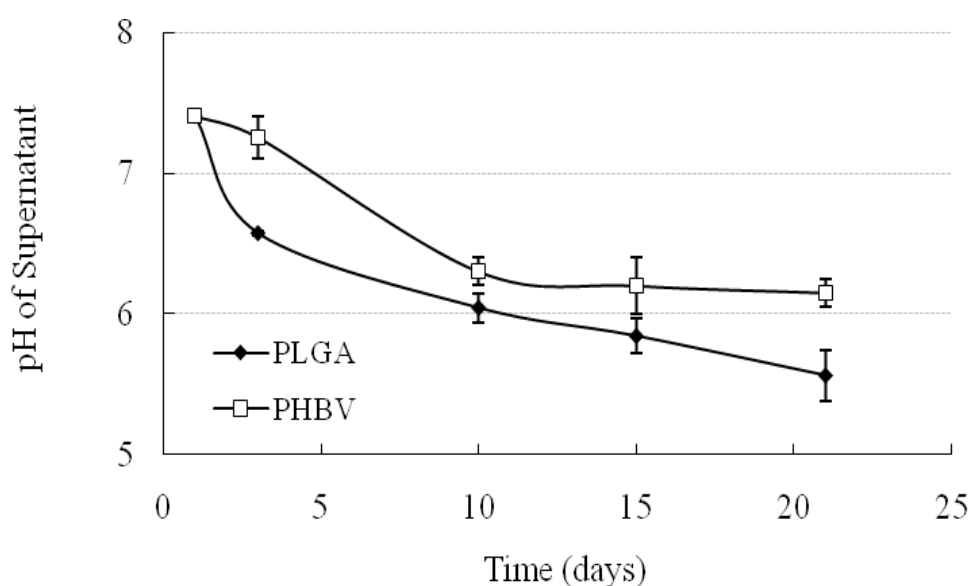


Figure 3.3. pH change of the medium during incubation of PLGA and PHBV nanocapsules.

The *in situ* degradation of the PLGA and PHBV nanocapsules was also followed by SEM. The loss in capsule integrity was more evident with PLGA capsules than with PHBV counterparts during the 21 days of incubation (Figure 3.4), providing the appropriateness of the choice of PLGA nanocapsules as the early stage release component of the sequential delivery system.

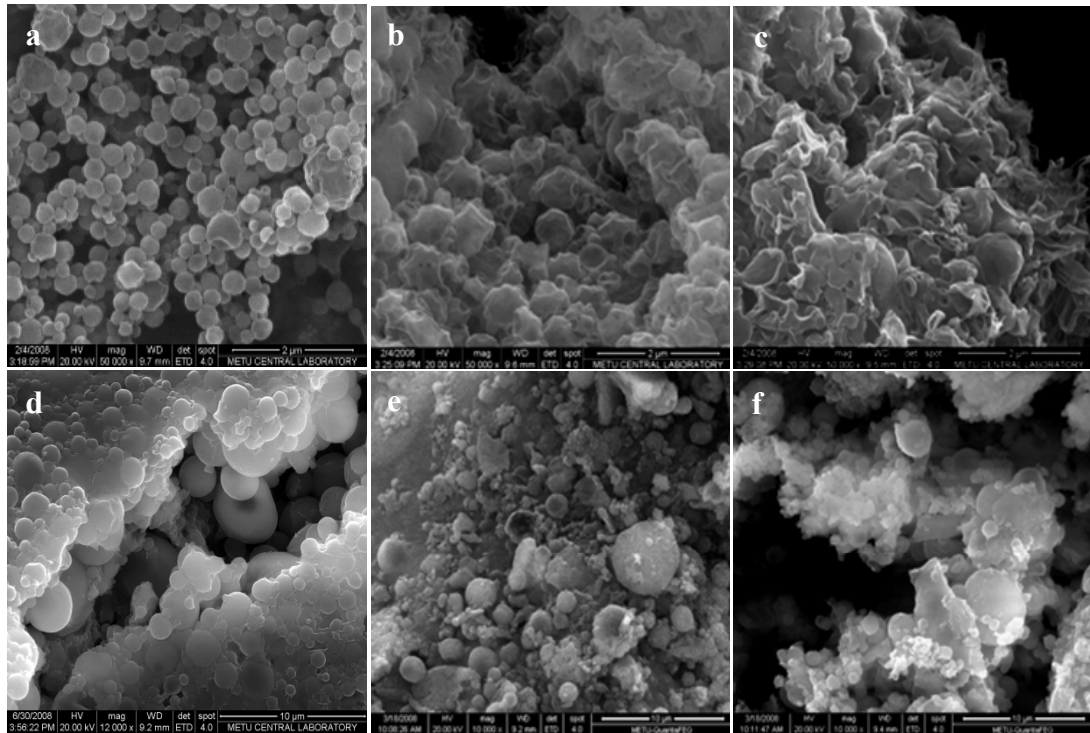


Figure 3.4. Degradation of BSA loaded nanocapsules at 37°C in sterile PBS (pH 7.4) (a) PLGA, day 0 (x50,000), (b) PLGA, day 15 (x50,000), (c) PLGA, day 21 (x50,000), (d) PHBV, day 0 (x10,000), (e) PHBV, day 15 (x10,000), (f) PHBV, day 21 (x10,000).

3.1.3. Encapsulation Efficiency and Release Kinetics

Encapsulation efficiency and release rate of 5, 10 and 20% (w/v) PLGA and PHBV capsules were investigated initially by using BSA as a model protein for BMPs and later with BMP-2 and BMP-7. With both PLGA and PHBV capsules, it was observed that 10% polymer concentration is optimal to achieve maximum encapsulation of BSA (Table 3.1). Encapsulation efficiency of PLGA capsules was almost 5 fold higher than their PHBV counterparts (84.75 ± 1.47 vs. 16.72 ± 1.06). The percent encapsulation values of the model protein with both PLGA and PHBV nanocapsules are in agreement with the literature; 78-81% of BMP-7 in PLGA

nanospheres (Wei *et. al.*, 2007) and 24% of L-asparaginase in PHBV nanocapsules (Baran *et. al.*, 2002).

Table 3.1. BSA encapsulation efficiency of PLGA and PHBV nanocapsules

Polymer Concentration (%, w/v)	Encapsulation Efficiency	
	PLGA	PHBV
5	74.30±2.33	12.55±0.12
10	84.75±1.47	16.72±1.06
20	70.66±1.34	12.06±0.53

The release results of the model protein BSA from PLGA and PHBV capsules are presented in Figures 3.5a and b, and Table 3.2. With both capsule populations, both the size and the release rate increased with increasing polymer concentration. This increase in release rate could be due to thinner capsule walls. The kinetics of release was investigated by fitting the data to rate equations and the best fit was obtained with the Higuchi model ($Mt/M_0 = k.t^{1/2}$) (Higuchi, 1961) (Table 3.2) which involves the plotting of amount of content released per surface area versus square root of time (Mt/M_0 vs $t^{1/2}$). The Higuchi rate constants, k , (the slope of the Mt/M_0 vs $t^{1/2}$ plot) calculated from the earlier part of the release profiles showed that with increase in polymer concentration the release rate also increases.

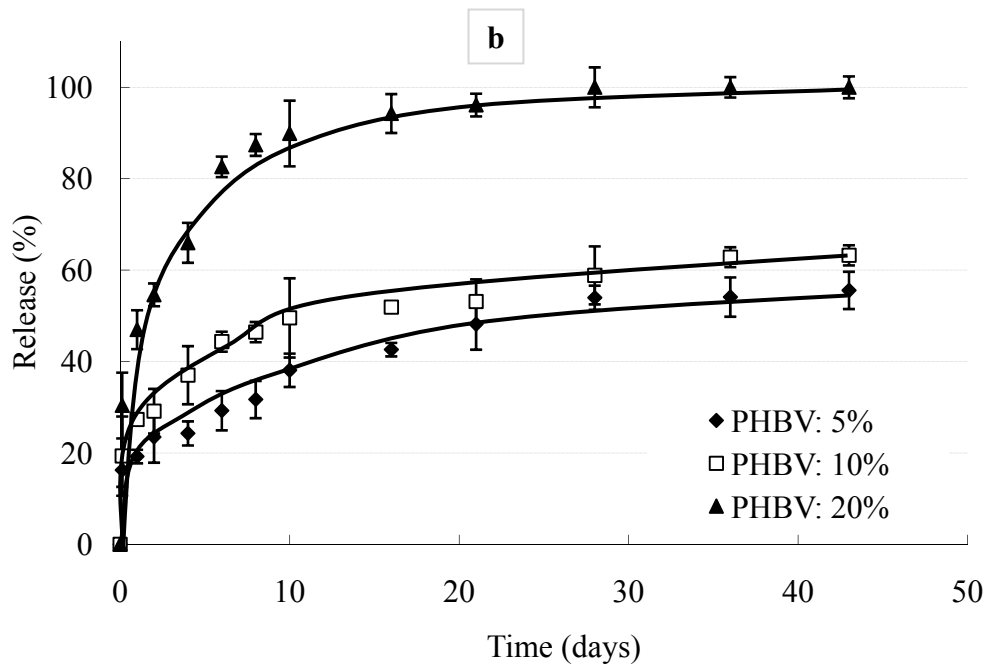
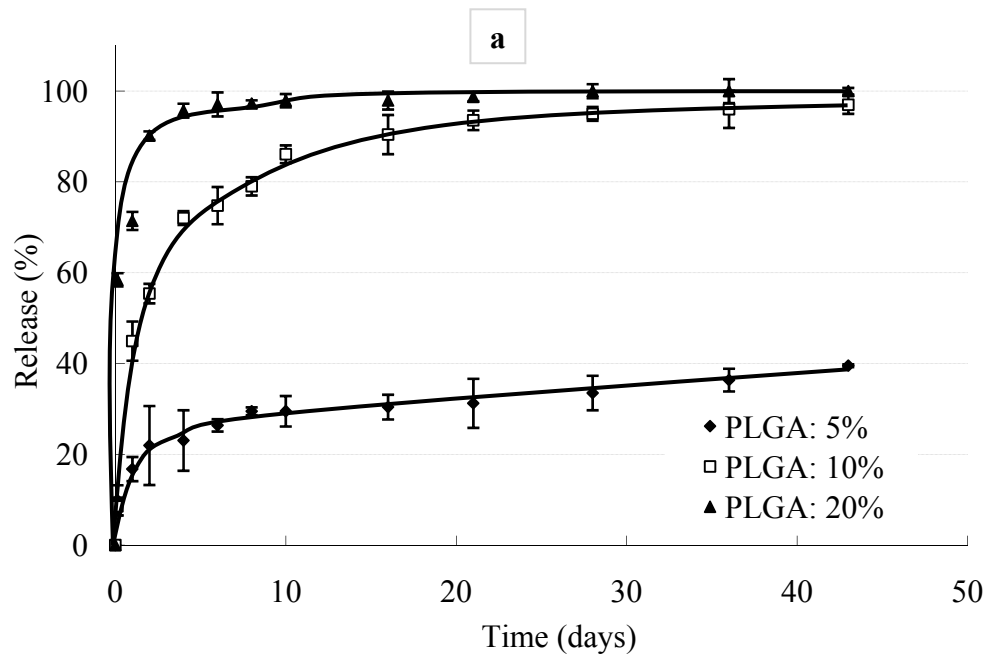


Figure 3.5. BSA release from (a) PLGA capsules, (b) PHBV capsules with varying initial polymer concentrations.

Table 3.2. Kinetic analysis of BSA, BMP-2 and BMP-7 release from PLGA and PHBV nanocapsules according to Higuchi Model.

Polymer Type and Initial Polymer Concentration (w/v)	Capsule Content	k_H	r^2
PLGA, 5%	BSA	0.0306	0.9454
PLGA, 10%	BSA	0.0908	0.9842
PLGA, 20%	BSA	0.0924	0.9141
PHBV, 5%	BSA	0.0754	0.9834
PHBV, 10%	BSA	0.0789	0.9869
PHBV, 20%	BSA	0.1081	0.9289
PLGA, 10%	BMP-2	0.0987	0.9525
PHBV, 10%	BMP-7	0.0636	0.9941

After considering the release rates, encapsulation efficiency and size distribution of the particles, the 10% (w/v) PLGA capsules were selected as the rapid release element and the 10% (w/v) PHBV capsules as the slower release element of the sequential delivery system.

BMP-2 release profile was similar to that with BSA, but slightly faster. On the other hand, BMP-7 release rate was slower than that with BSA (Figures 3.6 and 3.7 and Table 3.2). It was observed that combined together they would form the sequential delivery system for the two growth factors.

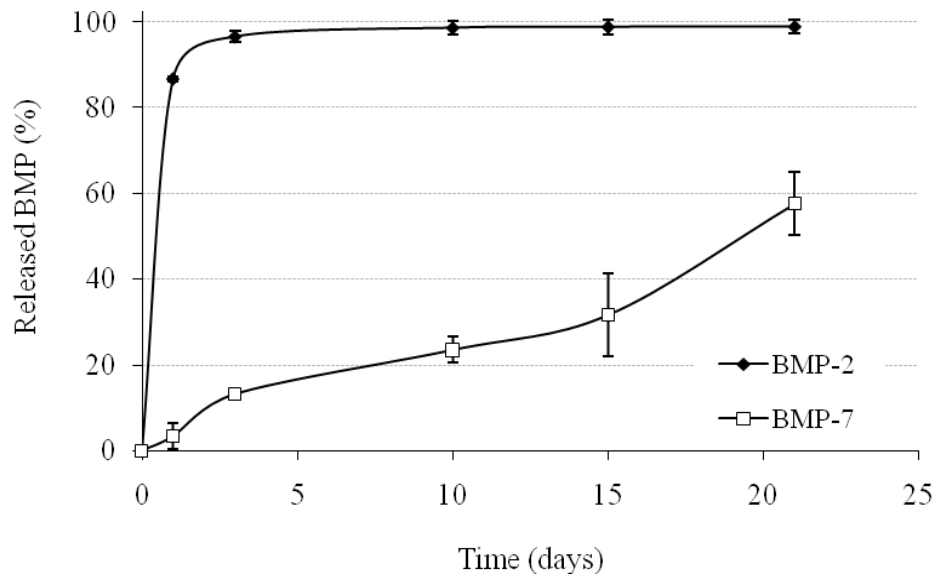


Figure 3.6. BMP release from polymeric nanocapsules (BMP-2 from 10% PLGA nanocapsules, BMP-7 from 10% PHBV nanocapsules).

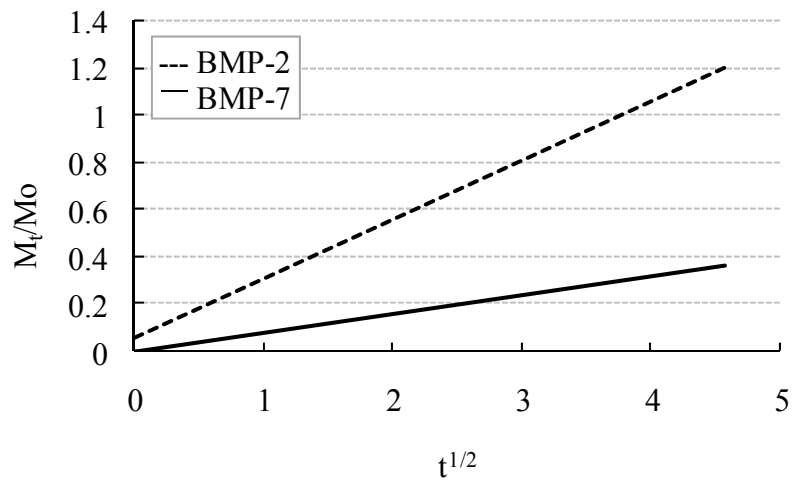


Figure 3.7. The kinetic analysis of BMP release according to Higuchi Model (BMP-2 from 10% PLGA nanocapsules, BMP-7 from 10% PHBV nanocapsules).

3.1.4. Influence of Sequential BMP-2/BMP-7 Delivery on MSC Proliferation and Differentiation

After the preparation and characterization of the sequential delivery system, the BMP loaded nanoparticles were tested by using MSCs of rat bone marrow origin in order to assess their suitability for use in bone tissue engineering applications.

The conditions tested were: (1) BMP-2 delivery from BMP-2 loaded PLGA nanocapsules, (2) BMP-7 delivery from BMP-7 loaded PHBV nanocapsules, (3) simultaneous BMP-2 and BMP-7 delivery from BMP-2 loaded PLGA nanocapsules and BMP-7 loaded PLGA nanocapsules (early release of both BMPs), (4) sequential BMP-2 and BMP-7 delivery from BMP-2 loaded PLGA nanocapsules and BMP-7 loaded PHBV nanocapsules (BMP-2 followed by BMP-7). The changes observed in cell proliferation and differentiation through different administration routes of BMPs indicated that PLGA and/or PHBV nanocapsules released the growth factors in a bioactive form for an extended period.

Alamar Blue test was used to determine the cell numbers (Figure 3.8). The change in cell numbers were statistically significant ($p < 0.001$) between days 7, 14 and 21 for single delivery of BMP-7, simultaneous and sequential delivery of BMP-2 and BMP-7. For single delivery of BMP-2, statistically, cell proliferation was not significant ($p > 0.05$) between 7, 14 and 21 days; however, there appears to be a distinct increase in proliferation with time. Generally, it was observed that the presence of growth factors improved cell proliferation. The increasing order of effectiveness was BMP-2 < BMP-7 < BMP-2/BMP-7 sequential delivery < BMP-2/BMP-7 simultaneous delivery for days 7, 14 and 21.

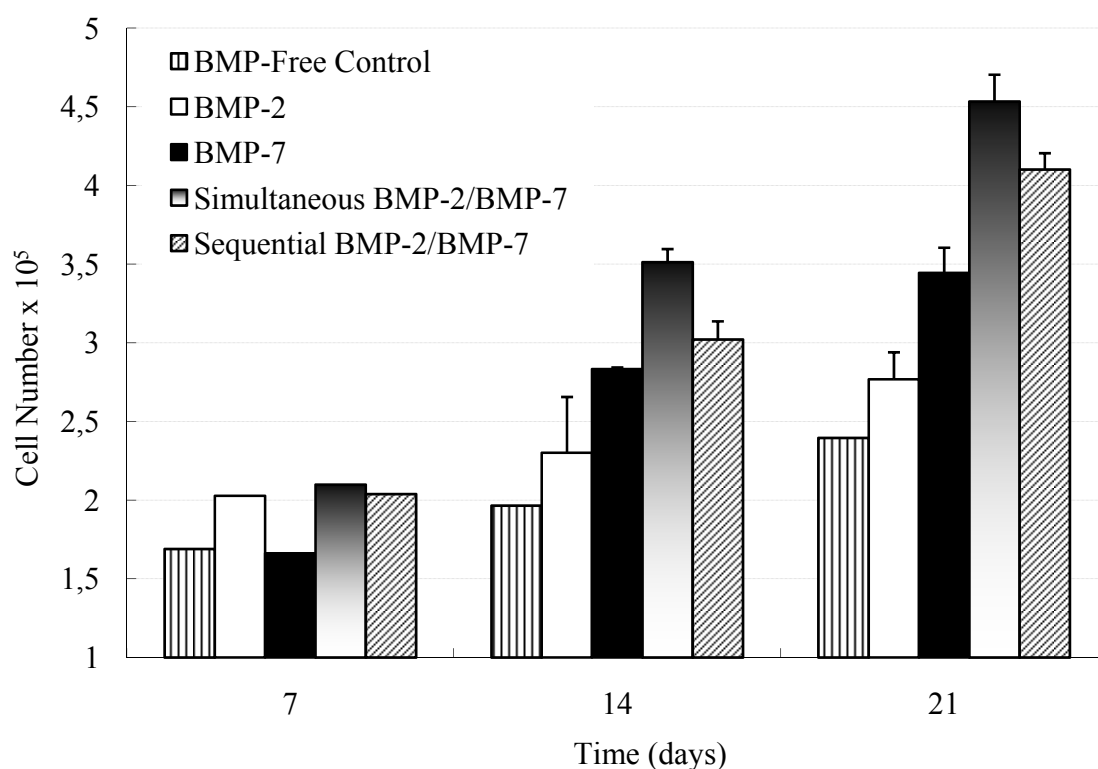


Figure 3.8. Effect of BMP-2 and BMP-7 on MSC proliferation.

In Figure 3.9, it is observed that BMP-2 was more effective in inducing differentiation than BMP-7, and sequential delivery was better than the simultaneous. In the literature, it is reported that proliferation and differentiation follow and counteract each other (Stein and Lian, 1993). Here, we observed the same trend. Cell proliferation observed with simultaneous delivery of BMP-2/BMP-7 was higher than with the sequential case, and a higher differentiation was observed with sequential delivery. Similar comparison can be made for the single growth factor carrying samples. Simultaneous application of BMP-2 and BMP-7 by encapsulating them both into PLGA nanocapsules (BMP-2/BMP-7 simultaneous) enabled the release of the contents in the very first days of the incubation, led to increased cell proliferation. Sequential delivery of these two bone growth factors, on the other hand, led to the highest ALP activity. If the ALP production efficiency

is plotted as activity per cell, the BMP-2 value is observed to be the highest. However, we are concerned with bone healing and the highest total amount of ALP with the given population is more important than that per cell. The highest value obtained with sequential delivery indicates the importance of mimicking the natural conditions where BMP-2 was shown to appear in the first days after fracture while BMP-7 peaks mainly after two weeks (Cho *et. al.*, 2002). The increase of ALP activity was statistically significant ($p < 0.001$) between days 7, 14 and 21 for every delivery condition tested. This improvement was achieved through the sequential delivery system developed.

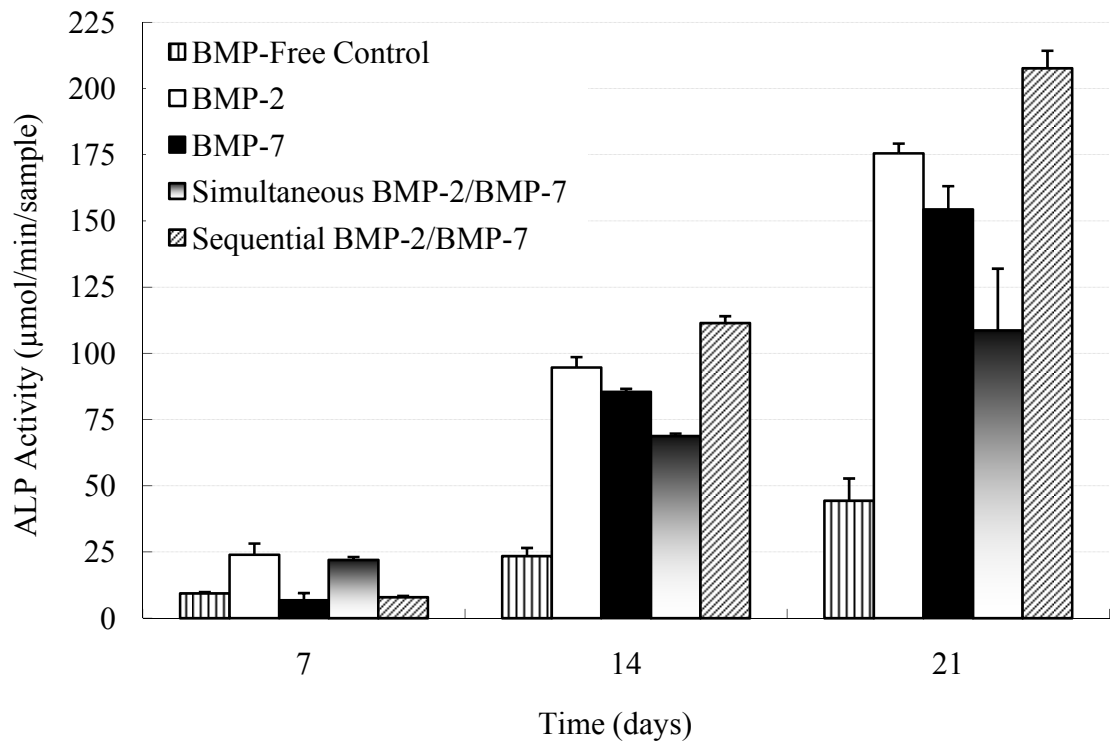


Figure 3.9. Effect of single, simultaneous and sequential delivery of BMP-2 and BMP-7 on MSC differentiation into osteoblastic cells.

3.2. Growth Factor Delivery from Chitosan Scaffolds

3.2.1. Chitosan Fiber Mesh Scaffold Production

3-D fibrous chitosan scaffolds were produced by wet spinning. The effect of polymer (chitosan) concentration, composition (chitosan, PEO) and the solvent (acetic acid) concentration on the properties of fibers were studied.

Initially, the effect of concentration of pure chitosan on the structure of the fibers produced was investigated by using 4% (CHI4-HAc2) and 6% (CHI6-HAc2) chitosan solutions. Chitosan solutions less concentrated than 4% did not lead to the formation of fibrous structures. It was observed that 4% chitosan solution had an optimal viscosity to produce fibers and also led to smoother surfaces than with 6% (Figure 3.10). With 8% chitosan it was not possible to form proper fibrous structure.

After the selection of 4% as the optimal concentration to prepare smooth fibers, the preparation medium was further modified by blending chitosan with PEO in order to improve the structural properties. Chitosan (4%) was blended with PEO in 2:1 ratio, creating chitosan (4%)/PEO (2%) fibers (CHI4-PEO2-HAc2) (Figure 3.11). It was observed that introduction of PEO resulted in improved stability of the scaffold. However, addition of PEO more concentrated than 2% created solutions that were too viscous to be spun into proper fibers. The effect of PEO presence could be observed by comparing Figures 3.10b and Figure 3.11b in which chitosan (4%) and chitosan (4%)/PEO (2%) fibers produced in 2% acetic acid are presented. PEO did not alter the smoothness of the fiber surfaces; however, this resulted in increased fiber thickness, as expected from the increased total polymer concentration (ca. 100 μm vs ca. 125 μm).

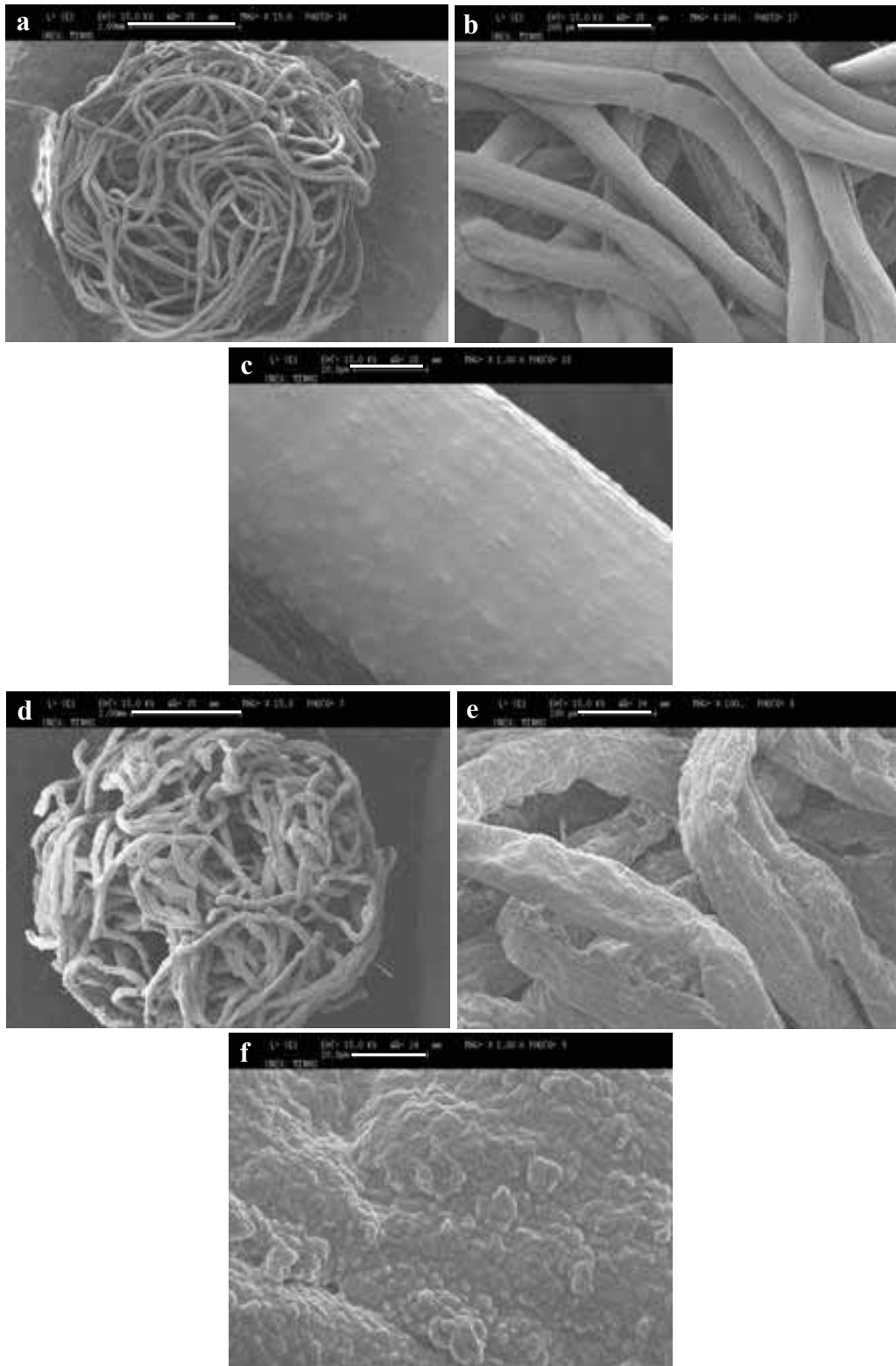


Figure 3.10. CHI4-HAc2 fiber mesh scaffold, (a) x15, (b) x100, (c) x1,000; CHI6-HAc2 fiber mesh scaffold, (d) x15, (e) x100, (f) x1,000. Bar represents (a, d) 2 mm, (b, e) 200 μm , (c, f) 20 μm .

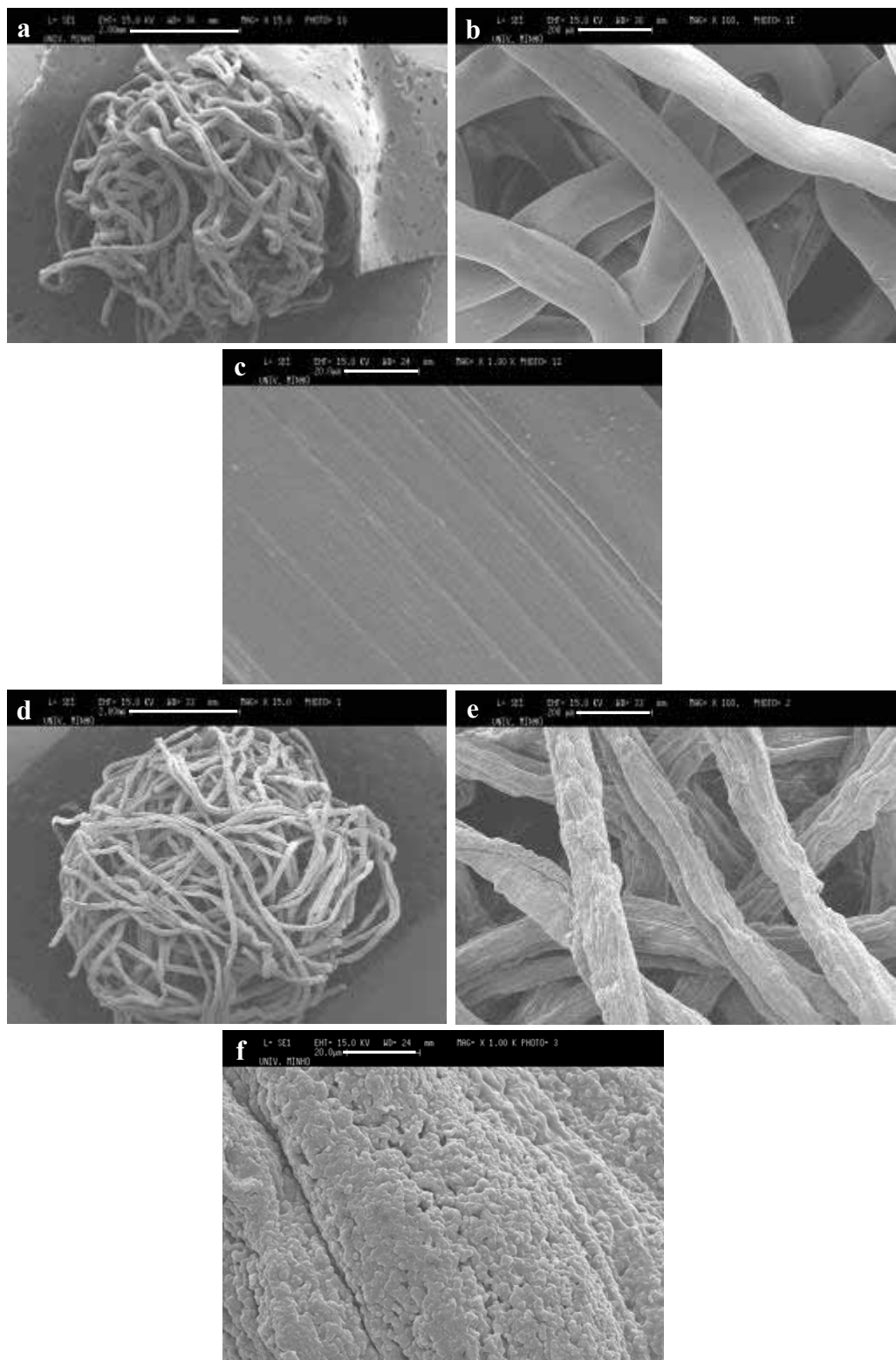


Figure 3.11. CHI4-PEO2-HAc2 fiber mesh scaffold, (a) x15, (b) x100, (c) x1,000; CHI4-PEO2-HAc5 fiber mesh scaffold, (d) x15, (e) x100, (f) x1,000. Bar represents (a, d) 2 mm, (b, e) 200 μm , (c, f) 20 μm .

Meanwhile, the effect of concentration of solvent on surface topography of the chitosan (4%) / PEO (2%) fibers was studied by using 2% and 5% (v/v) acetic acid as the solvent. It was observed that the more dilute acetic acid solution leads to smoother surfaces (Figure 3.11).

After studying the effect of various conditions, two scaffolds, one with smooth and another with rough fiber surface, were selected for the following investigation as the surface properties are known to make a difference in cell-material interactions through altered surface chemistry and roughness. Scaffolds of CHI4-HAc2 with a smooth fiber surface, and CHI4-PEO2-HAc5 with a rough surface were used to incorporate the delivery systems.

3.2.2. Characterization of the Scaffolds

The porosity and its distribution throughout the thickness of the chitosan scaffolds were investigated by μ -CT. The 3-D representations of the scaffolds obtained with μ -CT showed the presence of complete interconnectivity of the pores throughout the structure (Figure 3.12).

Analysis revealed that the porosity of the scaffolds was not influenced significantly by the chitosan and chitosan/PEO concentration and composition used. The porosity values for CHI4-HAc2 and CHI4-PEO2-HAc5 scaffolds were 85.4 ± 3.5 % and 86.7 ± 4.8 %, respectively. The almost uniform porosity throughout the thickness of CHI4-HAc2 scaffold is presented in Figure 3.13.

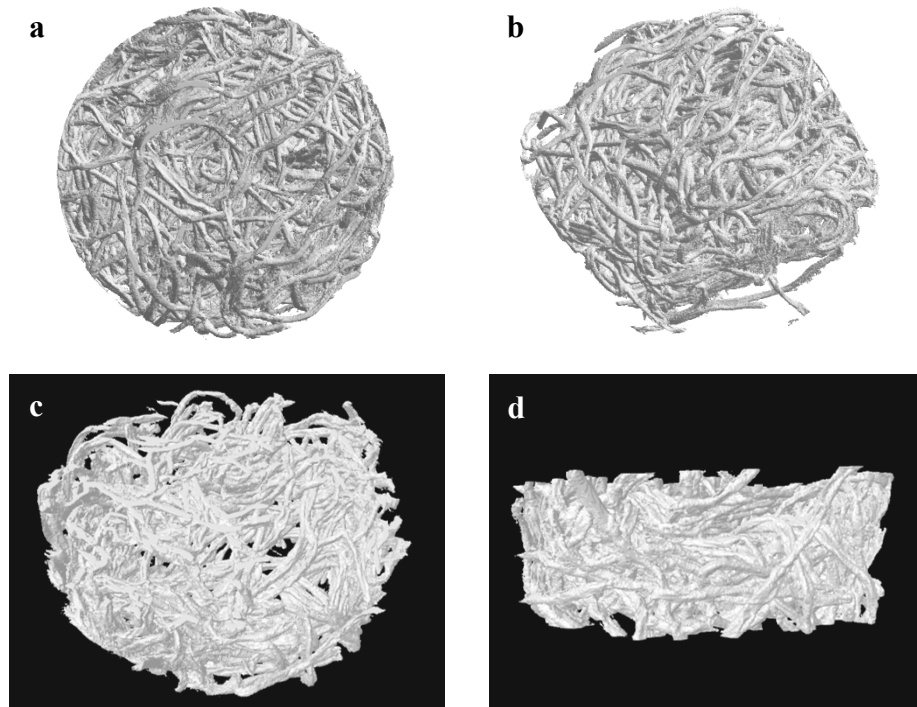


Figure 3.12. 3-D representations of chitosan scaffolds obtained through μ -CT. (a, b) CHI4-HAc2, (c, d) CHI4-PEO2-HAc5.

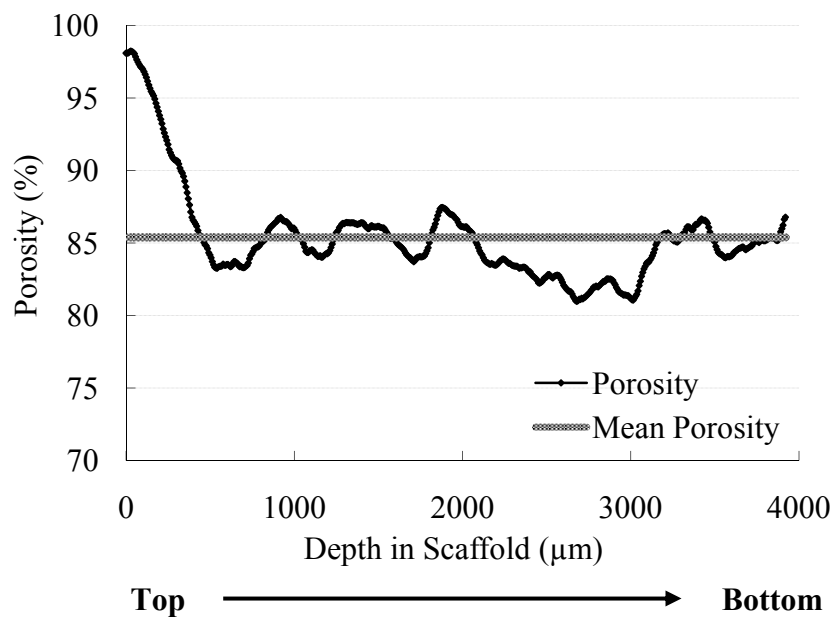


Figure 3.13. Porosity distribution throughout the thickness of CHI4-HAc2 scaffold.

It was also observed from the porosity distribution profile that the pores were completely interconnected throughout the whole structure. Moreover, the profile showed that the porosity from top to bottom of the scaffold did not change significantly. The top of the scaffold had a high porosity (ca. 98%) which reduces to ca. 85% towards the bottom. This is especially a very important asset because most scaffolds produced by other methods do not have complete connectivity and the porosity decreases significantly from the surface towards the core leading to insufficient cell population and oxygen/nutrient concentrations in the core.

The change in the physical properties of CHI4-HAc2 and CHI4-PEO2-HAc5 scaffolds were investigated in wet state (PBS, pH 7.4) at 37°C and 5% CO₂ conditions. After 21 days of incubation in the medium, the dimensions and the weight of the fibers were altered significantly (Table 3.3). Both scaffolds absorbed water and swelled as soon as they were put into the medium and became 500-600% (w/w) heavier. The increase in individual fiber thickness was also significant; around 55% for both scaffolds. The diameter and height of both scaffolds were also increased, being in the range of 20% for both of them.

Table 3.3. Changes in chitosan scaffold properties after incubation in sterile PBS (pH 7.4) for 21 days.

	CHI4-HAc2	CHI4-PEO2-HAc5
Fiber Thickness (%)	53	59
Scaffold Diameter (%)	18	29
Scaffold Height (%)	25	29
Scaffold Weight (%)	600	500

Gravimetric analysis revealed that after 3 weeks of incubation in sterile PBS, there was no change in the weight of chitosan scaffolds. SEM observation was done to examine the changes in surface properties for both scaffolds after 3 weeks of incubation *in situ*. Micrographs of CHI4-HAc2 scaffolds revealed that there was almost no change in the fiber appearance at the end of the incubation (Figure 3.14 a), however, PEO had dissolved out of CHI4-PEO2-HAc5 scaffold leading to increased surface roughness (Figure 3.14 b) compared to day 0 micrographs presented in Figure 3.10 and Figure 3.11, respectively.

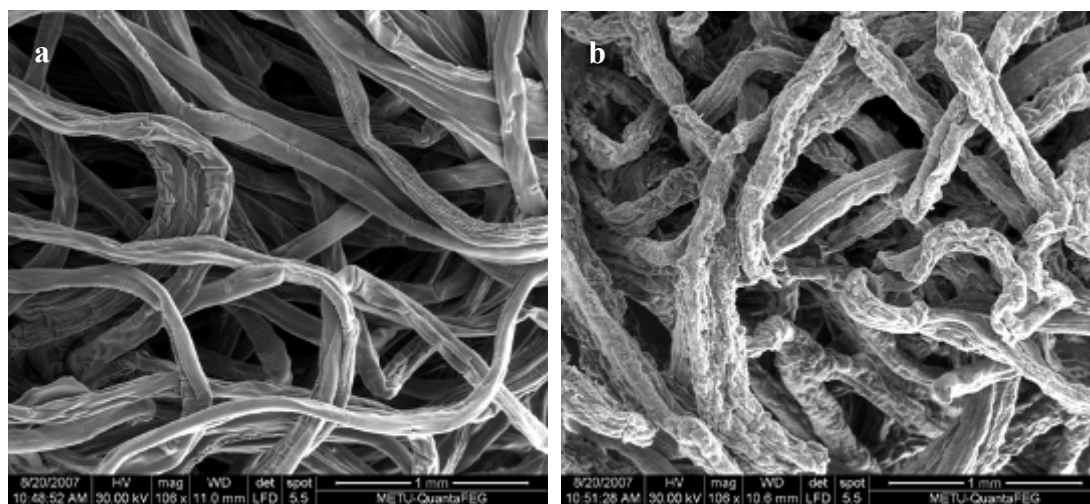


Figure 3.14. Fiber structure after 21 days of incubation in PBS. (a) CHI4-HAc2, (b) CHI4-PEO2-HAc5 scaffolds.

3.2.3. MSC Culture on Chitosan Scaffolds

Suitability of chitosan scaffolds for use in bone tissue engineering applications was studied using rat bone marrow MSCs. It was observed that although cell numbers were almost the same after 21 days, initial cell adhesion and proliferation rate during the first week was higher on CHI4-HAc2 scaffold than on CHI4-PEO2-HAc5 (Figure 3.15).

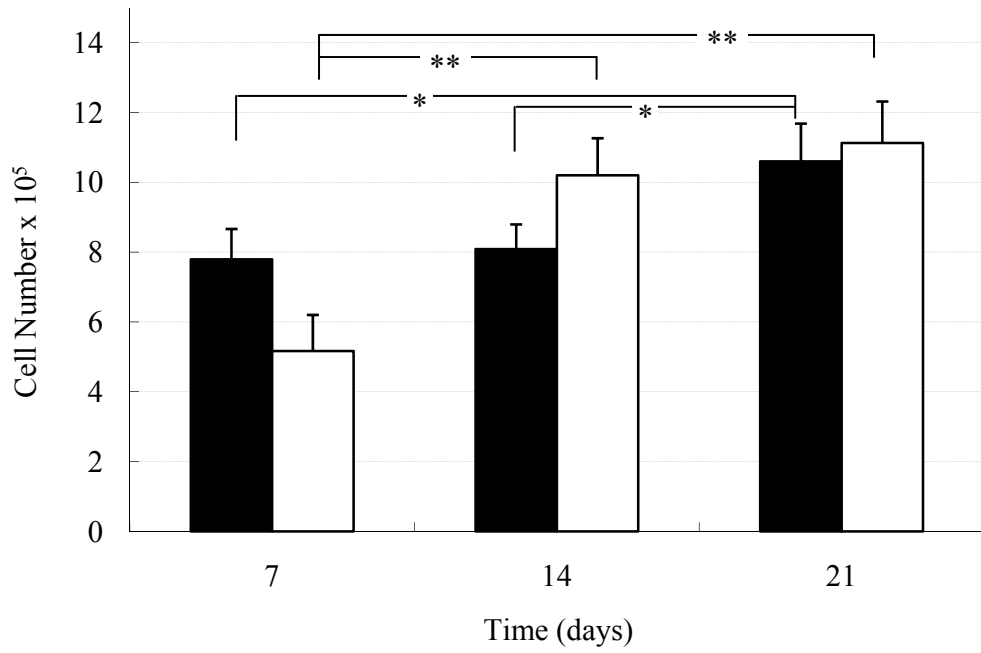


Figure 3.15. MSC proliferation on CHI4-HAc2 (■) and CHI4-PEO2-HAc5 (□) scaffolds (n=3, *p<0.05, **p<0.001).

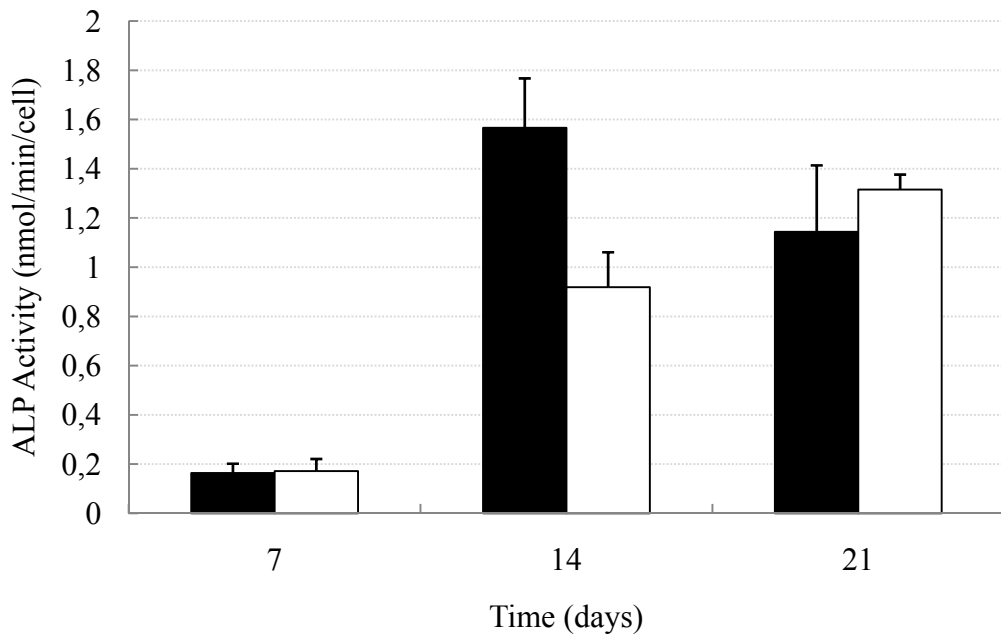


Figure 3.16. Specific ALP activity of MSC on CHI4-HAc2 (■) and CHI4-PEO2-HAc5 (□) scaffolds.

In the period of cell proliferation between 7-14 days, the cell number increase was much lower for CHI4-HAc2 than it was for CHI4-PEO2-HAc5. The specific ALP activities are presented in Figure 3.16. In the first 7 days the ALP activity is very low as expected. In the 7-14 period the increase in ALP activity, the indicator for MSC differentiation, was higher for CHI4-HAc2 when compared to CHI4-PEO2-HAc5 scaffold and the difference was statistically significant at all time points ($p < 0.01$) (Figure 3.16). The increase in cell number was statistically significant after the first week of incubation for CHI4-HAc2 scaffold ($p < 0.05$) and started a decrease after day 14 due to increased differentiation. Cell proliferation and ALP activity were shown to increase gradually during 21 days of incubation for the PEO containing blend scaffolds.

SEM analysis revealed that the cells attached and spread well on both scaffolds after 21 days of culturing (Figure 3.17). It is seen that the smooth chitosan fibers become rougher in cell presence after 21 days and the shapes of the cells indicate a proper spread. On CHI4-PEO2-HAc5 fibers the roughness is maintained and the cell spread is also very good.

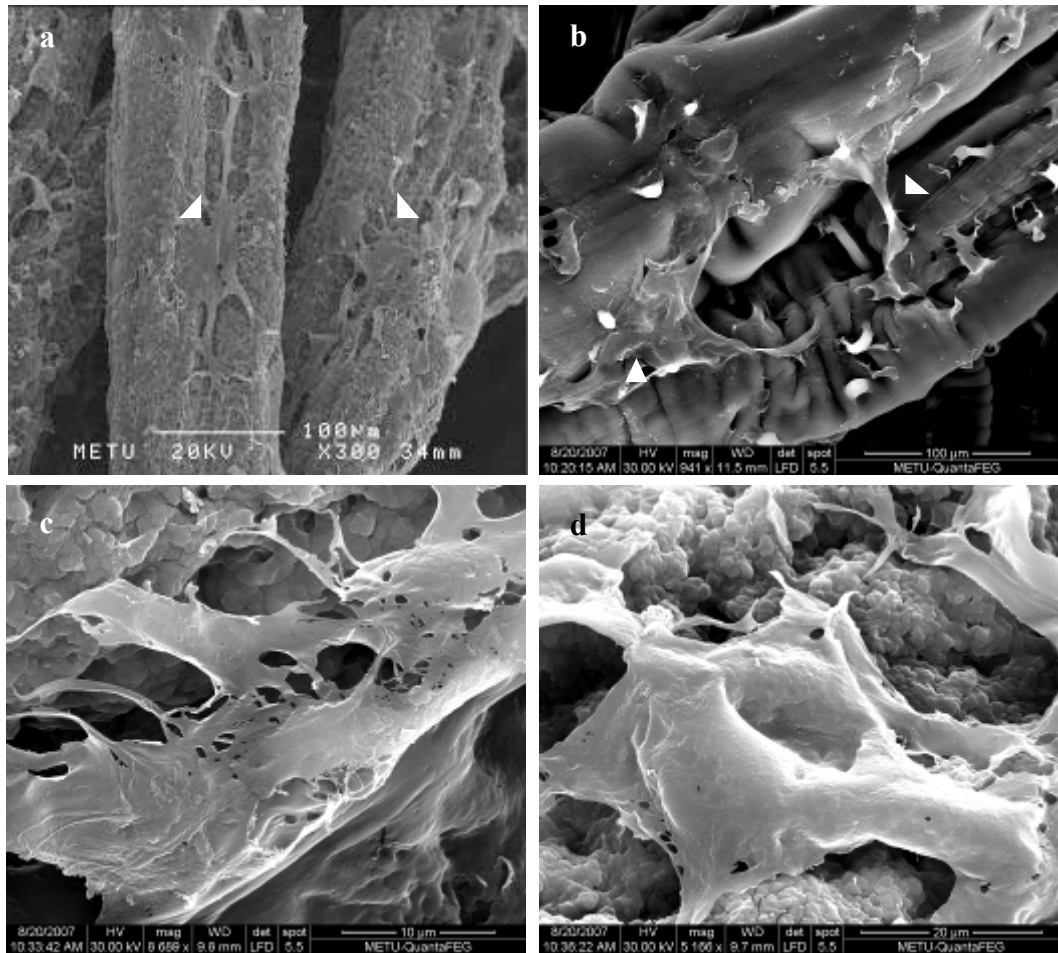


Figure 3.17. MSC attachment and spreading on (a, b) CHI4-HAc2 (arrow head show cells); (c, d) CHI4-PEO2-HAc5 scaffolds after 21 days of incubation.

3.2.4. Incorporation of the BMP Loaded Nanocapsules into the Chitosan Scaffolds

In order to incorporate the PLGA and PHBV nanocapsules into chitosan scaffolds, two different approaches were used: they were either introduced within the chitosan fibers (NP-IN) or incorporated onto the fibers (NP-ON).

NP-IN were prepared by mixing the nanocapsules with chitosan and chitosan/PEO solutions and then spun to produce fibers containing the nanocapsules within their structure. Nanocapsules incorporated into CHI4-HAc2 fibers were clearly visible due to increased roughness as the unloaded fiber surfaces were smooth. Detection was difficult in the case of CHI4-PEO2-HAc5 fibers, because the unloaded fibers had also rough surfaces (Figure 3.18).

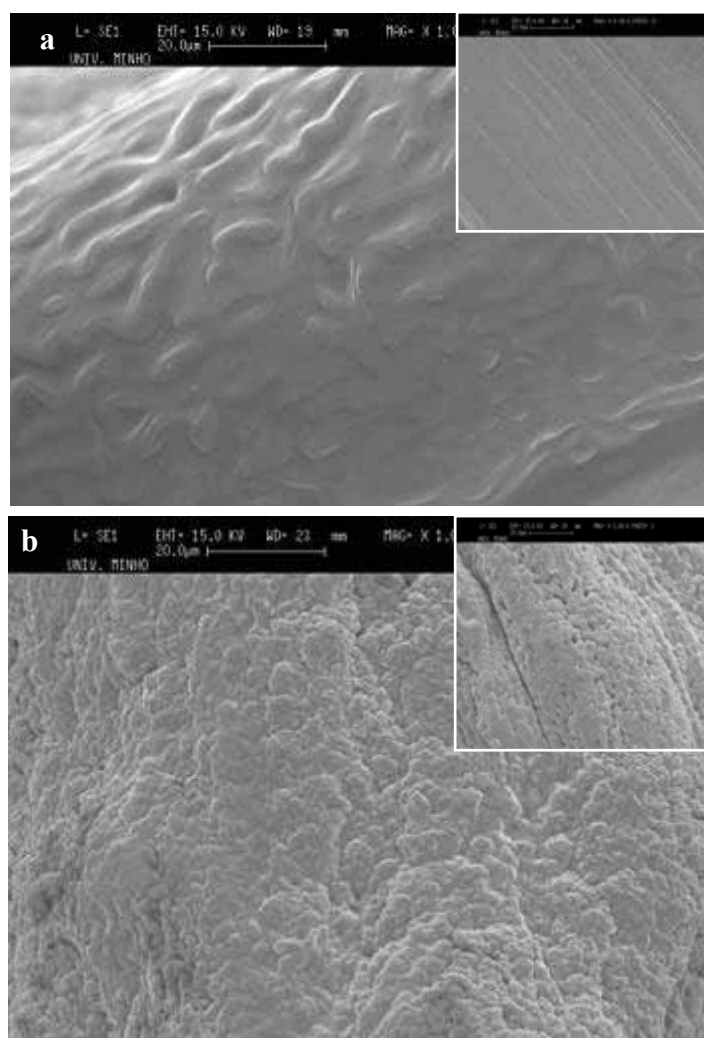


Figure 3.18. PLGA nanocapsules incorporated (NP-IN) in (a) CHI4-HAc2 fiber, (b) CHI4-PEO2-HAc5 fiber (x1,000 in all micrographs including insets). Insets are unloaded counterparts.

In the second method, both type of capsules were “seeded” onto the CHI4-HAc2 scaffolds after the preparation of both the fibers and the nanocapsules leading to the attachment of the capsules onto the fiber surfaces (Figure 3.19a, b). Here, the nanoparticles appear to have adhered properly onto the fibers for a prolonged duration. The presence of PLGA and PHBV nanocapsules on the CHI4-HAc2 fiber surfaces (NP-ON) after 21 days of culturing in PM (37°C, 5% CO₂) was observed (Figure 3.19c, d).

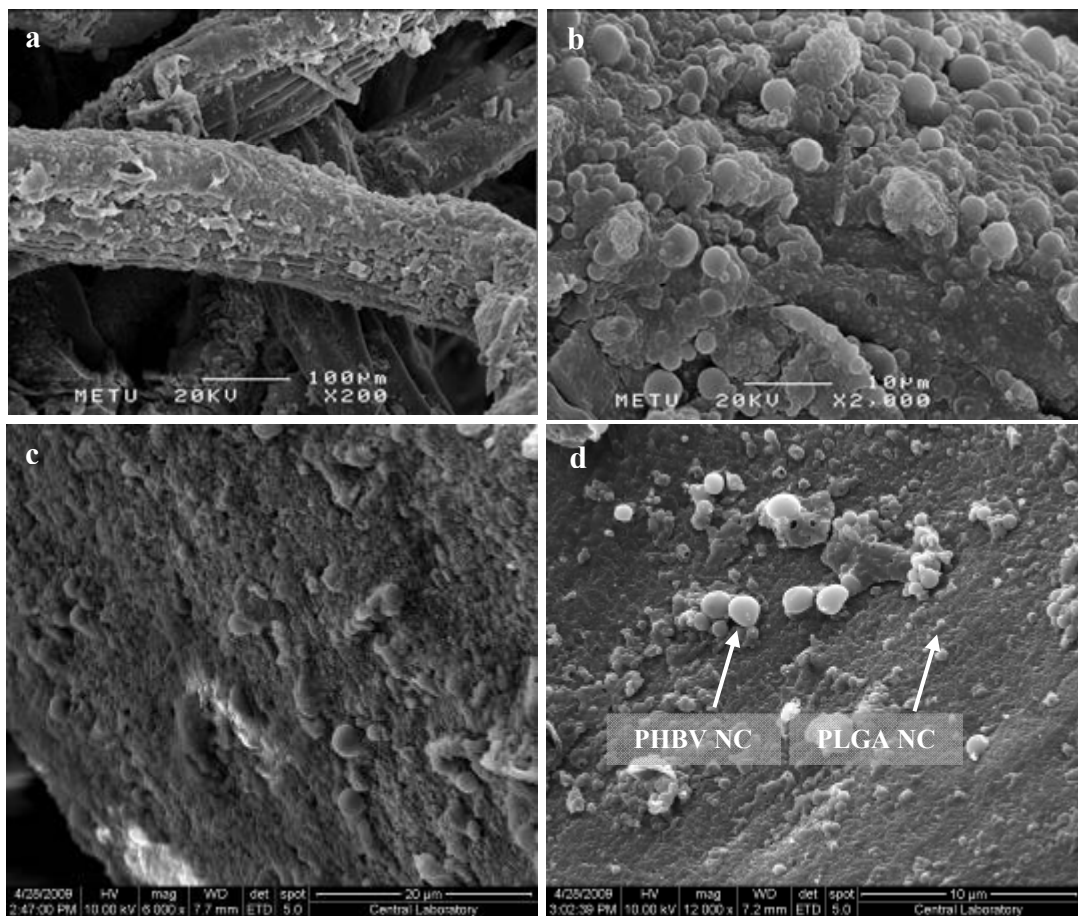


Figure 3.19. PLGA and PHBV nanocapsules on CHI4-HAc2 scaffold (NP-ON), (a) x200 (t=0), (b) x2,000 (t=0), (c) x6,000 (t=21 day), (d) x12,000 (t=21 day).

3.2.5. The Release Behavior

The release of BSA, a protein used as a model to study the release kinetics, from the nanoparticle incorporated (NP-ON and NP-IN) constructs (CHI4-HAc2) was studied and compared with that of free nanocapsules. It was observed that although not influencing the overall release pattern, incorporation into the scaffolds (NP-ON and NP-IN) suppressed the burst release in addition to slowing down the release for the rest of the period for both PLGA and PHBV nanocapsules (Figure 3.20).

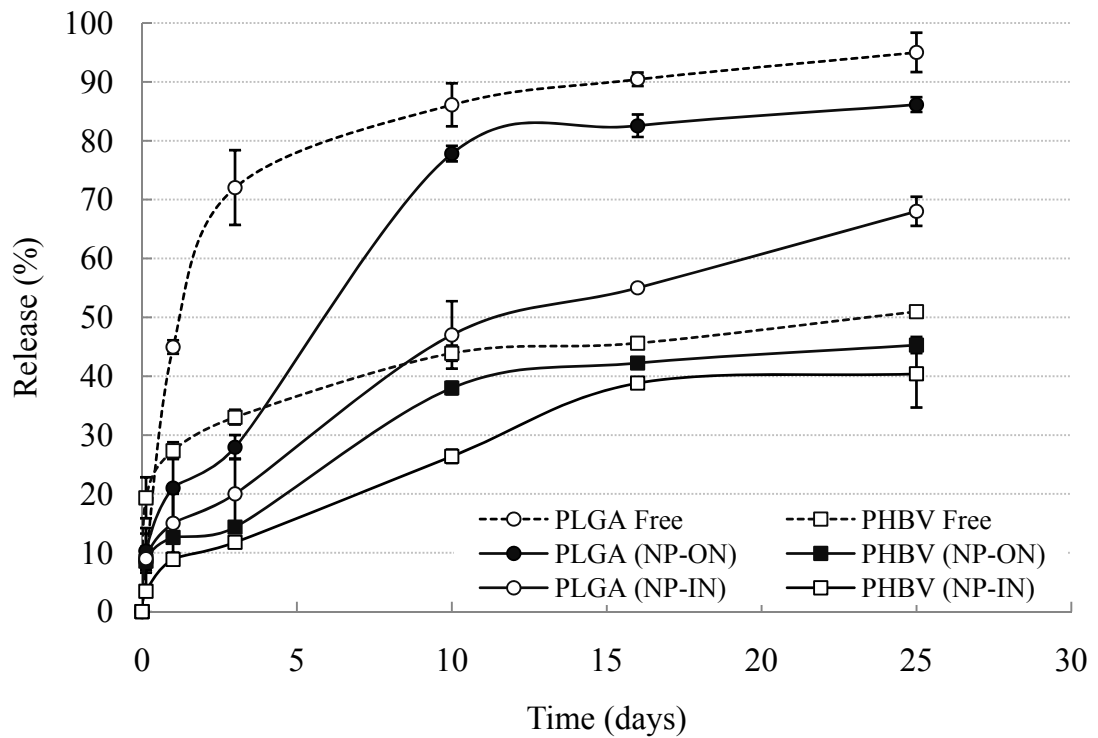


Figure 3.20. Release of BSA from free and incorporated particles.

The main difference in the release rates for both nanocapsules was observed during the first 3 days of the incubation where suppression in release rates was observed. As described previously, PLGA nanocapsules, either free or incorporated in the scaffold structure, released their contents faster than PHBV counterparts which is why they were selected to serve as the early stage release component of the sequential delivery system. While the protein encapsulated in PLGA nanocapsules was almost completely released, both the free and the incorporated PHBV nanocapsules did not release their total content in the 21 days of the test. On the other hand, PLGA and PHBV particles incorporated in the CHI4-HAc2 scaffolds (NP-IN) presented a much slower release rate, even slower than with NP-ON. It was observed that at the end of the incubation period of 25 days only 70% and 40% of the content in PLGA and PHBV nanocapsules, respectively, was released from the NP-IN construct. The release of the content apparently is affected by the location of the drug carrying nanoparticles. When they are on the fibers, there is only the diffusional restriction due to the tortuosity of the path of the protein due to the fibers of the scaffold, but when in the fiber, there is an additional barrier, the fiber structure.

3.2.6. Effect of BMP-2 Dose on the Proliferation and Differentiation of MSCs

The effect of BMP-2 dose on MSC proliferation and differentiation was studied by incorporating varying amounts of BMP-2 loaded PLGA nanocapsules per CHI-HAc2 scaffold that contained 20, 40 and 80 ng BMP-2. Both incorporation methods (NP-ON and NP-IN) were used with each of the BMP concentrations and the results were compared with that of the unloaded fiber mesh scaffolds.

It was observed that the presence of BMP-2 suppressed cell proliferation and this suppression was more significant with increasing BMP-2 concentration (Figure 3.21). Cell proliferation was statistically significant at all time points except between 7-14 days for NP-IN 40, NP-IN 80 ng and NP-ON 40 ng (details given on the figure).

When cell proliferation was suppressed, higher ALP activities were obtained with both NP-IN and NP-ON cases (Figure 3.22) due to the stimulation of

differentiation in the presence of BMP-2. ALP activity was increased with increasing BMP-2 concentration. The difference in the ALP activity was statistically significant at all time points for all conditions ($p < 0.001$). In Figure 3.22, the increase in ALP activity in the presence of BMP-2 was apparent regardless of the delivery condition, however, the increase was more significant between 20 and 40 ng than it was between 40 and 80 ng. Especially for the NP-IN case, the increase in ALP activity in the case of 80 ng BMP-2 in comparison to 40 ng was almost insignificant. Therefore, 40 ng of BMPs was chosen for use in further studies, also considering the prohibitive cost of the growth factors.

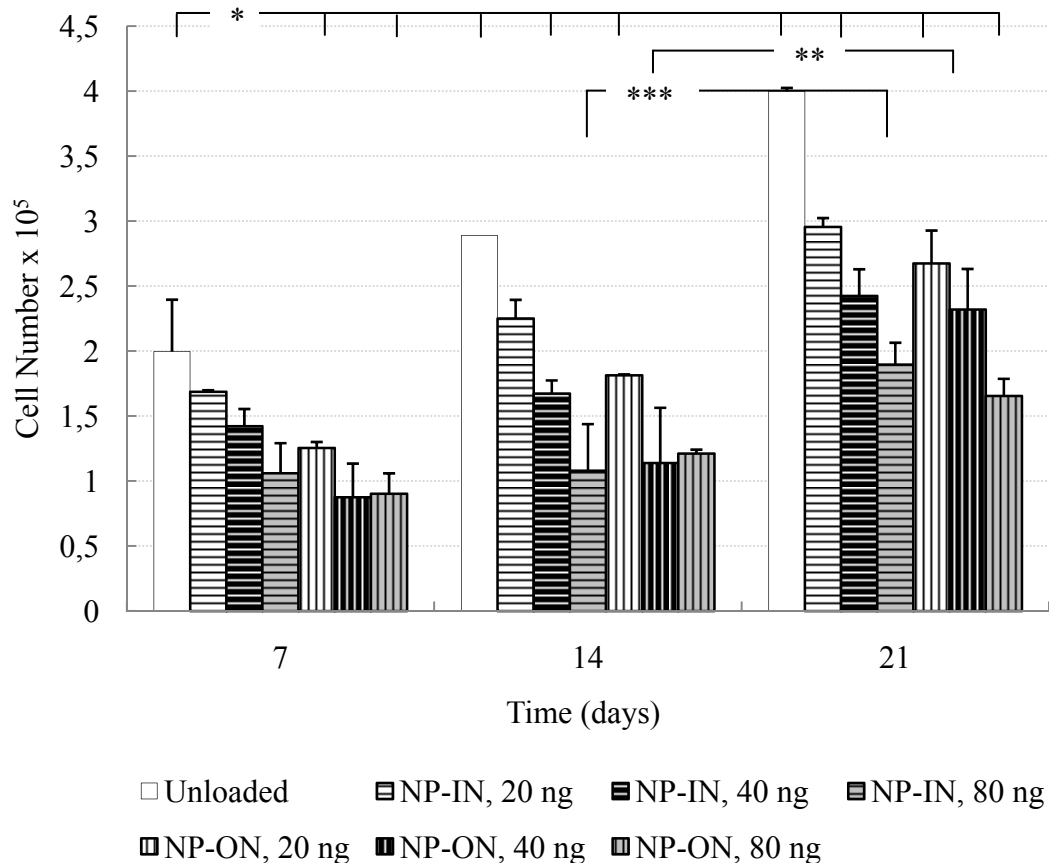


Figure 3.21. Effect of BMP-2 dose carried in PLGA nanocapsule loaded scaffolds on the proliferation of MSCs ($n=3$, $*p < 0.001$, $**p < 0.01$, $***p < 0.05$).

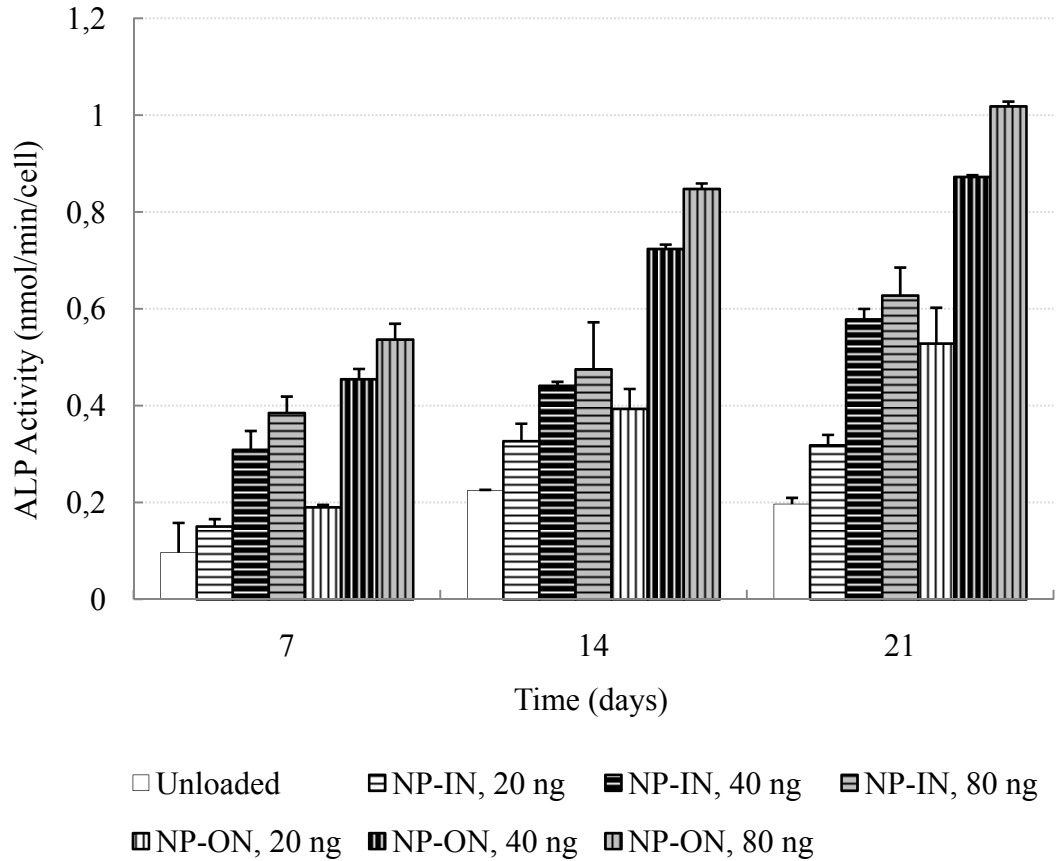


Figure 3.22. Effect of BMP-2 dose on the differentiation of MSCs.

3.2.7. Influence of BMP-2/BMP-7 Delivery from Constructs on MSC Proliferation and Differentiation

The effect of single, simultaneous and sequential delivery of BMP-2 and BMP-7 released from constructs was investigated *in vitro* using rat bone marrow MSCs with two different incorporation methods. Only the CHI4-HAc2 scaffold (smooth fiber surface, higher initial MSC differentiation (Figures 3.10 and 3.16)), was used for the incorporation of BMP loaded nanoparticle incorporation studies. The simultaneous delivery of the two growth factors was achieved by encapsulating both growth factors in PLGA nanocapsules. Therefore, in this condition, both the BMP-2 and BMP-7 were released to the medium from the very beginning of the

culturing. The difference observed in cell proliferation and differentiation through different administration approaches of BMPs suggested that the growth factors were released in a bioactive form from the constructs for an extended period.

In every condition tested, particles incorporated on the fiber surfaces (NP-ON) led to higher cell numbers compared to NP-IN indicating higher concentration of the growth factors under these conditions due to higher rate of release of the growth factors (Figure 3.23).

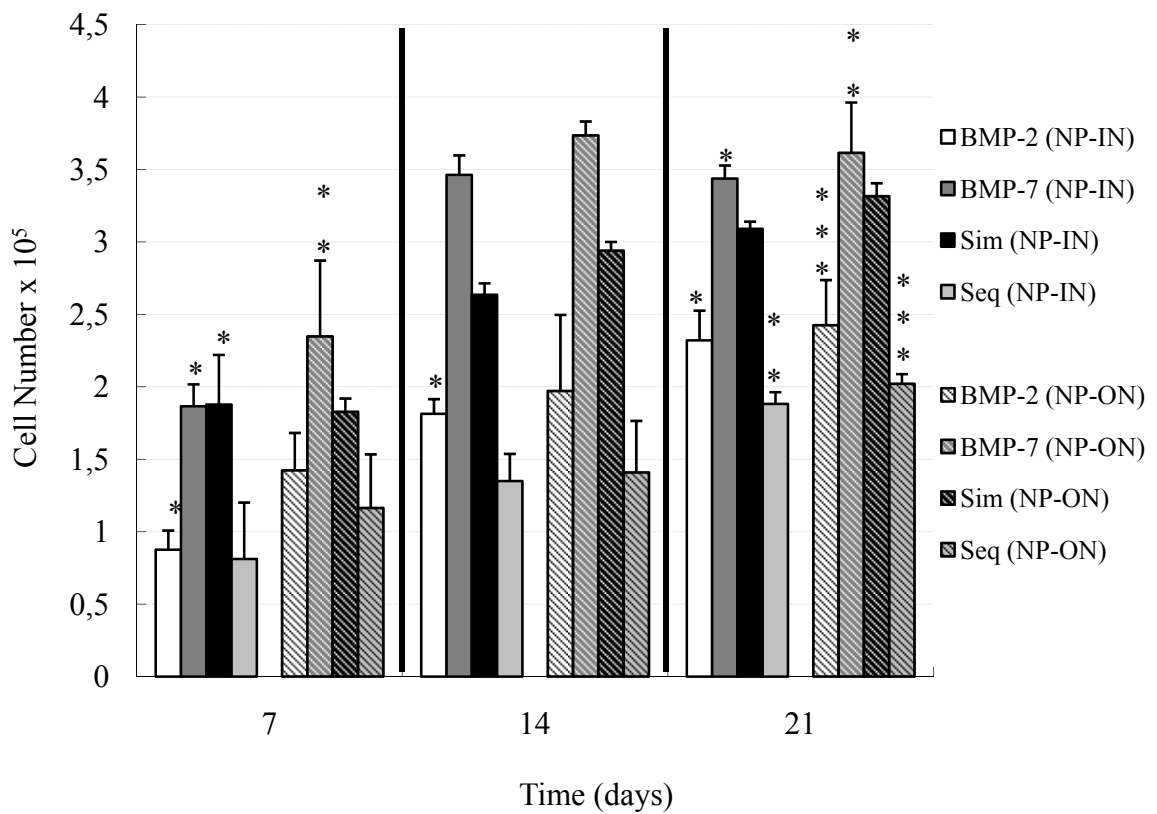


Figure 3.23. MSC proliferation on chitosan scaffolds carrying BMP loaded nanocapsules. (n=3, *p<0.001, **p<0.01, ***p<0.05).

The change in cell proliferation was significant at all times for all conditions ($p < 0.05$, details given on the figure). For both NP-IN and NP-ON cases, single delivery of BMP-7 lead to highest MSC proliferation followed by simultaneous BMP-2/BMP-7, single BMP-2 and sequential BMP-2/BMP-7 delivery. This indicated that the presence of BMP-2 suppressed MSC proliferation compared to BMP-7. This was also apparent when single BMP-7 and simultaneous cases were compared, the latter leading to lower cell numbers. In the case of sequential delivery of these two growth factors, the lowest cell numbers were obtained for both NP-IN and NP-ON cases. The reason for this was observed with highest ALP activity results (Figure 3.24) indicating higher cellular differentiation in case of sequential delivery of BMP-2 and BMP-7. BMP-2 was more effective in inducing differentiation compared to BMP-7. Simultaneous delivery of two growth factors failed to give high ALP activity results basically because proliferation was the stimulated biological mechanism rather than differentiation. The differences between ALP activity results were statistically significant at all time points for all conditions ($p < 0.001$).

Cell number on chitosan fiber mesh scaffolds without loaded with any BMPs (CHI4-HAc2) on day 7, 14 and 21 were $7.8 \cdot 10^5 \pm 8.6 \cdot 10^4$, $8 \cdot 10^5 \pm 7 \cdot 10^4$ and $1 \cdot 10^6 \pm 1 \cdot 10^5$ respectively (Figure 3.15), being much higher compared to the loaded scaffolds also indicated the suppression of cell proliferation in the presence of BMPs regardless of the delivery condition.

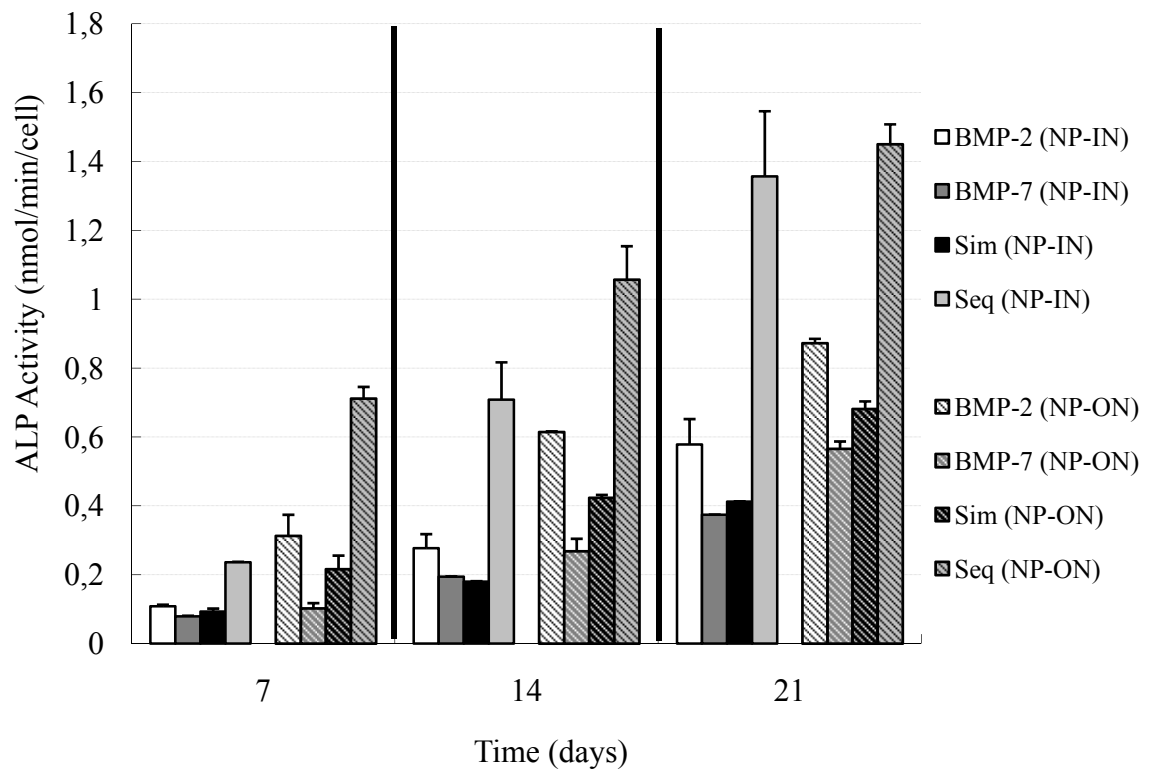


Figure 3.24. Specific ALP Activity on BMP loaded particle incorporated chitosan fiber mesh scaffolds.

3.3. Growth Factor Delivery from PCL Scaffolds

3.3.1. PCL Scaffold Production and Characterization

Oriented and random PCL scaffolds were produced by 3-D plotting and wet spinning, respectively. Oriented PCL scaffolds were prepared with four different standard architectures designated as basic (B), basic-offset (BO), crossed (C) and crossed-offset (CO) structures, where random PCL scaffold was abbreviated as random (R). SEM in Figure 3.25 showed the fiber orientation of the PCL scaffolds and the overall architecture of the 3-D scaffolds.

3.3.1.1. Scaffold Porosity

The porosity and porosity distribution throughout the thickness of the PCL scaffolds were investigated by μ -CT. The 3-D representations of PCL scaffolds were also obtained with μ -CT showing the 3-D architecture of the fibers that constitute the 3-D structures (Figure 3.26).

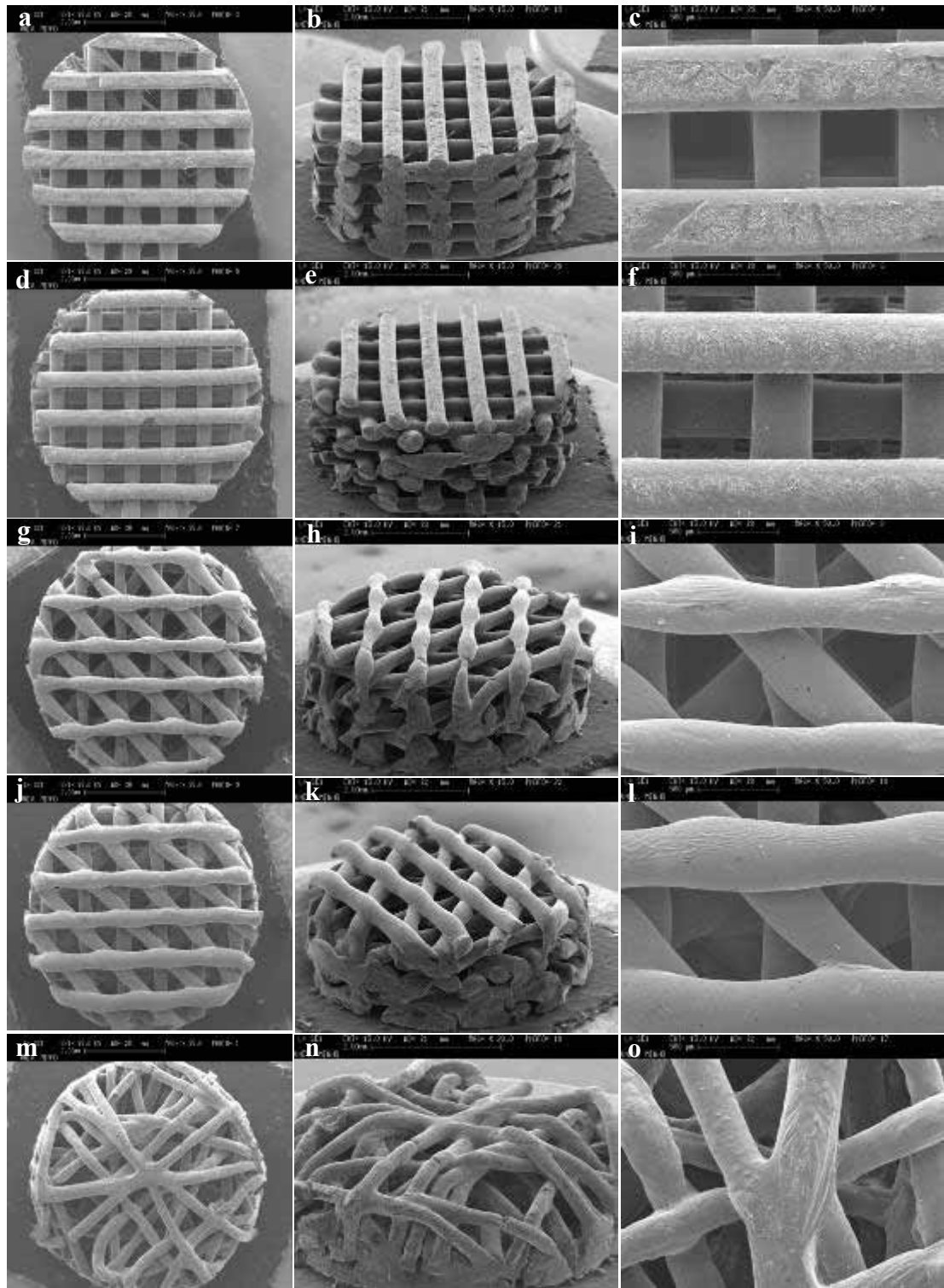


Figure 3.25. SEM images of PCL scaffolds produced with 3-D plotting and wet spinning with different architectures, **B:** (a) and (b) x15, (c) x50; **BO:** (d) and (e) x15, (f) x50; **C:** (g) and (h) x15, (i) x50; **CO:** (j) and (k) x15, (l) x50; **R:** (m) and (n) x15, (o) x50.

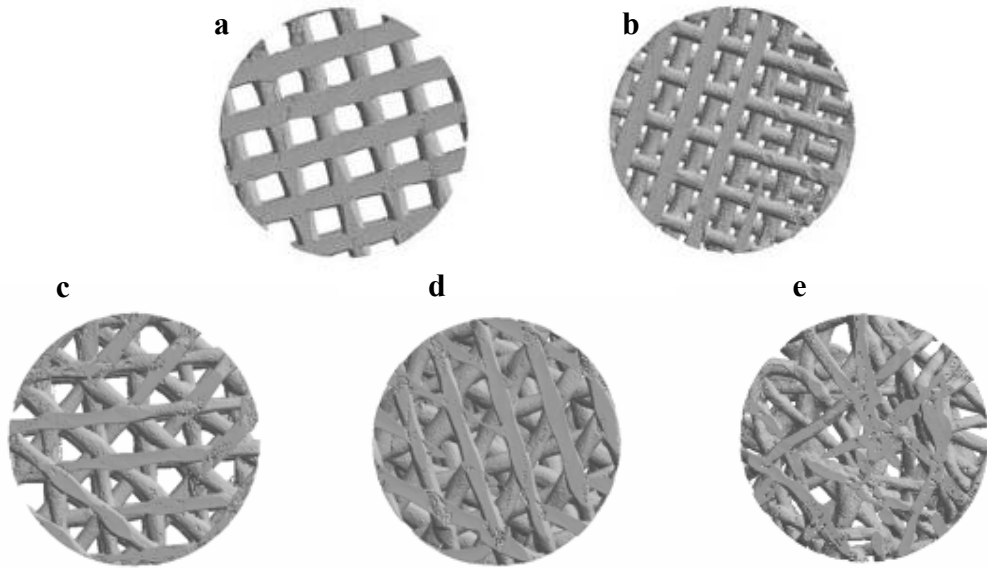


Figure 3.26. 3-D representations of PCL scaffolds. (a) B, (b) BO, (c) C, (d) CO, (e) R.

The porosity (%) values of the scaffolds indicate that the porosity of the scaffolds are about 50-70% and are to some extent dependent on the fiber orientation within the construct (Table 3.4).

Table 3.4. The porosity of the PCL scaffolds (n=3).

Sample	Porosity (%)
B	50.98±3.16
BO	66.31±4.35
C	65.00±6.01
CO	56.80±6.78
R	66.83±5.82

The porosity profiles showed that the porosity from top to bottom of the scaffolds did not change significantly as expected from the precision of the production of the scaffolds by the Bioplotter (Figure 3.27). It could be also observed that the pores were completely interconnected throughout the whole structure. This is especially important when most scaffolds produced by other methods do not have complete connectivity and the porosity decreases from the surface towards the core leading to insufficient population by cells and oxygen/nutrient concentrations at the core.

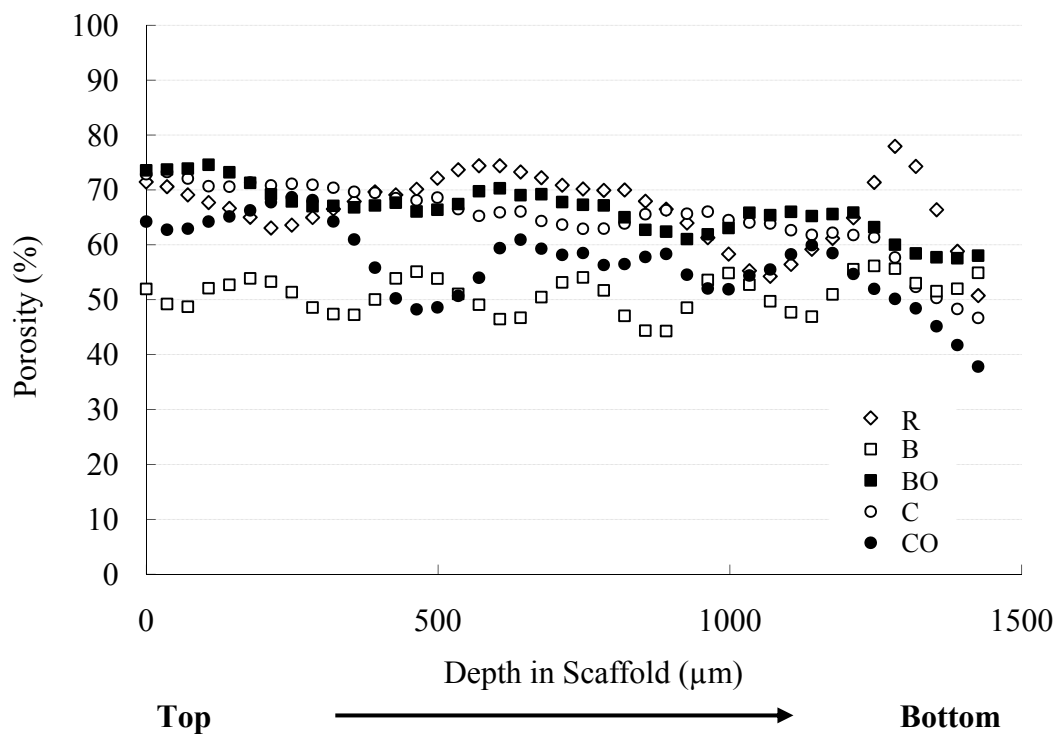


Figure 3.27. Porosity distribution within PCL scaffolds.

3.3.1.2. Mechanical Properties

The stiffness, the storage and loss modulus values of the samples were calculated by dynamic mechanical analysis (DMA) (Table 3.5). It was observed that the change in fiber orientation in the scaffold from BO to B architecture increased the storage modulus almost 5 fold from $3.48 \pm 0.08 \cdot 10^6$ Pa to $1.85 \pm 0.19 \cdot 10^7$ Pa. The loss modulus, on the other hand, increased from $2.64 \pm 0.07 \cdot 10^5$ Pa to $8.80 \pm 0.01 \cdot 10^5$ Pa for the same. Therefore, it can be stated that the mechanical properties of a 3-D plotted scaffold can be, to some extent, tuned through the adjustment of the fiber positioning within the scaffold architecture, allowing its adaptation for different mechanical requirements.

The storage moduli for cortical, demineralized cortical and trabecular bone were reported to be $8 \cdot 10^9$, $2 \cdot 10^9$ and $8 \cdot 10^5$ Pa, respectively (Wang and Feng, 2005). The loss moduli for the same samples were $2 \cdot 10^8$, $7.5 \cdot 10^7$ and $5.2 \cdot 10^4$ Pa, respectively (Toyraş *et. al.*, 2002). Therefore, the PCL scaffolds exhibit higher stiffness as compared to trabecular bone and lower stiffness relative to cortical bone. In order to resist to the mechanical stresses a cortical bone implant is subjected to, these scaffolds need to be stiffer. It should be kept in mind that the stiffness and strength in bone are the result of the organization of mineral and organic fractions at the nano-scale. Since the current scaffolds cannot match the high mechanical properties of the cortical bones, it is expected that upon cell proliferation and ECM secretion the construct to attain mechanical properties comparable to that of a living bone.

Table 3.5. Storage and loss modulus of PCL scaffolds (n=3).

Sample	Storage Modulus (Pa)	Loss Modulus (Pa)
B	$1.85 \pm 0.19 \cdot 10^7$	$8.80 \pm 0.01 \cdot 10^5$
BO	$3.48 \pm 0.08 \cdot 10^6$	$2.64 \pm 0.07 \cdot 10^5$
C	$1.15 \pm 0.09 \cdot 10^7$	$6.12 \pm 0.05 \cdot 10^5$
CO	$9.69 \pm 0.14 \cdot 10^6$	$5.32 \pm 0.07 \cdot 10^5$
R	$6.76 \pm 0.18 \cdot 10^6$	$5.96 \pm 0.03 \cdot 10^5$

This analysis also showed that the PCL scaffolds exhibit a viscoelastic behavior and that although influential, the porosity is not the sole determinant of the stiffness as other factors and that the number of junction points between the fibers and their relative orientation can also influence mechanical properties. For example, structures BO and C demonstrated almost similar porosities (about 65%), but their storage moduli differed by about 3.3 times (from $3.48 \cdot 10^6$ to $1.15 \cdot 10^7$ Pa). When the structures are compared, it is observed that scaffolds without offset had higher compressive stiffnesses due to the juxtaposition of the consecutive filaments along the Z axis (Figure 3.28).

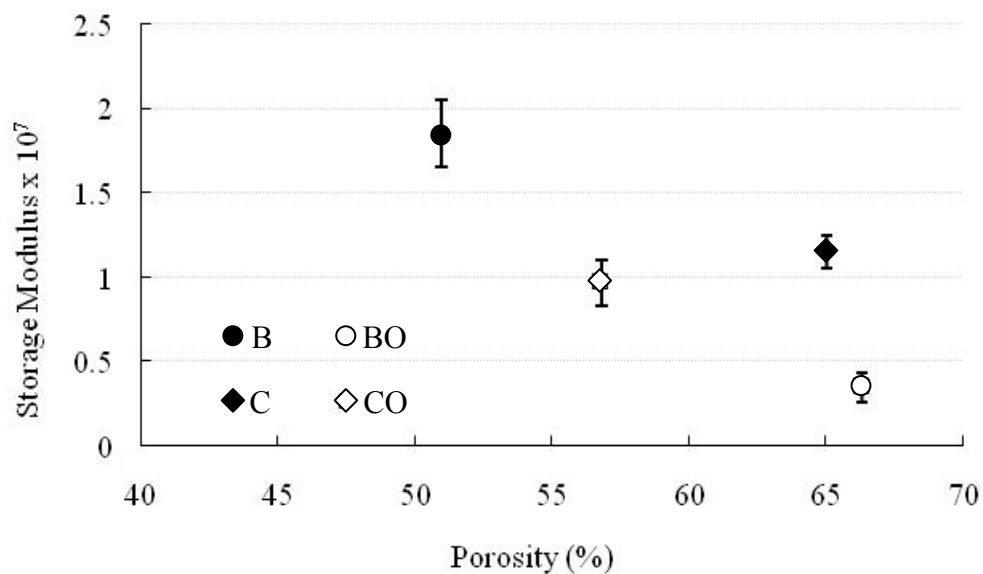


Figure 3.28. Relation between storage moduli and porosity of the oriented PCL scaffolds.

3.3.2. Degradation of PCL Scaffolds

Oriented PCL scaffolds with the “B” architecture were used to study PCL scaffold degradation for 6 weeks in PBS. It was observed that at the end of the incubation period, there was no change in the weight of the scaffolds that could be detected gravimetrically. However, the medium pH decreased gradually from 7.40 to ca. 7.16 (Figure 3.29) indicating an acidic by-product formation probably due to the hydrolytic degradation of PCL fibers.

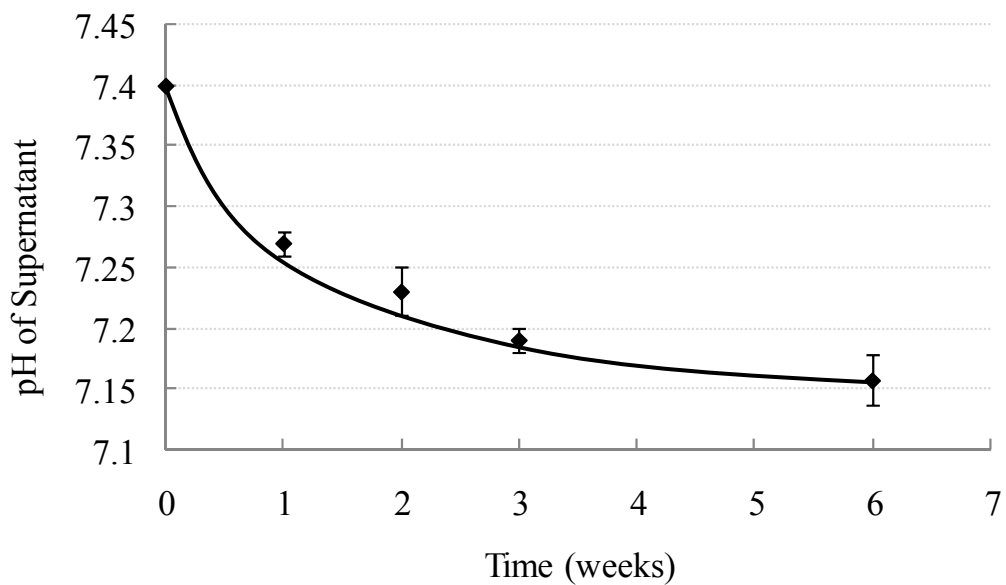


Figure 3.29. pH change of the medium during incubation of “B” PCL scaffold in PBS (T= 37°C).

Signs of PCL scaffold degradation were also examined by SEM. It was observed that at the end of the incubation period, PCL fiber surfaces had partially eroded, and gaps and cracks were apparent on their surfaces (Figure 3.30).

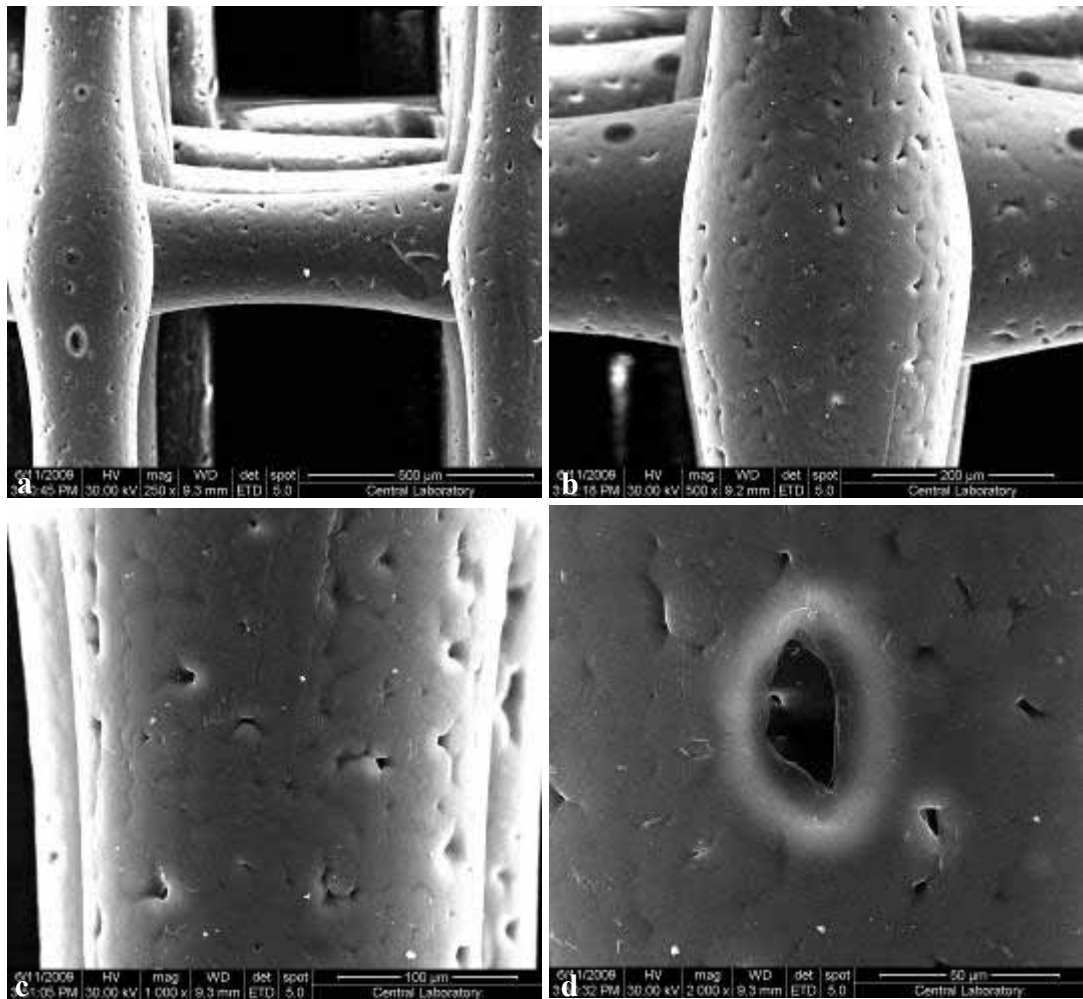


Figure 3.30. SEM of degradation of “B” PCL scaffold after 6 weeks of incubation in sterile PBS, (a) x250, (b) x500, (c) x1,000, (d) x2,000.

3.3.3. MSC Culture on PCL Scaffolds

PCL scaffolds were seeded with rat bone marrow MSCs at a density of 50,000 cells per scaffold to assess suitability for use in bone tissue engineering applications. Proliferation and ALP activity were tested after 7, 14 and 21 days of incubation.

Cell proliferation tests demonstrated that both scaffolds with the offset (BO and CO compared to B and C) resulted in significantly higher cell proliferation (Figure 3.31). This might be related to the tortuosity of the flow path of the media. During cell seeding, the relative positioning of the fibers will determine the path of flow of the media and, to a certain extent, the cell seeding efficiency. When there is no offset, cells have a straight and open path which increases the likelihood of cells passing through the scaffold, and very few would move laterally during seeding. On the contrary, when there is an offset structure, fibers act as obstacles in the path and also provide a higher surface area for cells to attach to. This leads to increased initial adhesion and subsequent higher cell numbers. The initial cell attachment trend observed on day 1 continued for the rest of the incubation period, offset scaffolds housing higher number of cells, with the random scaffold having a value in between the regular and offset scaffolds. The overall difference in cell proliferation was statistically significant for all scaffold types ($n=3$, $p<0.001$). The increase in the number of cells was not statistically significant between days 7 and 14 for scaffolds BO, C, CO and R.

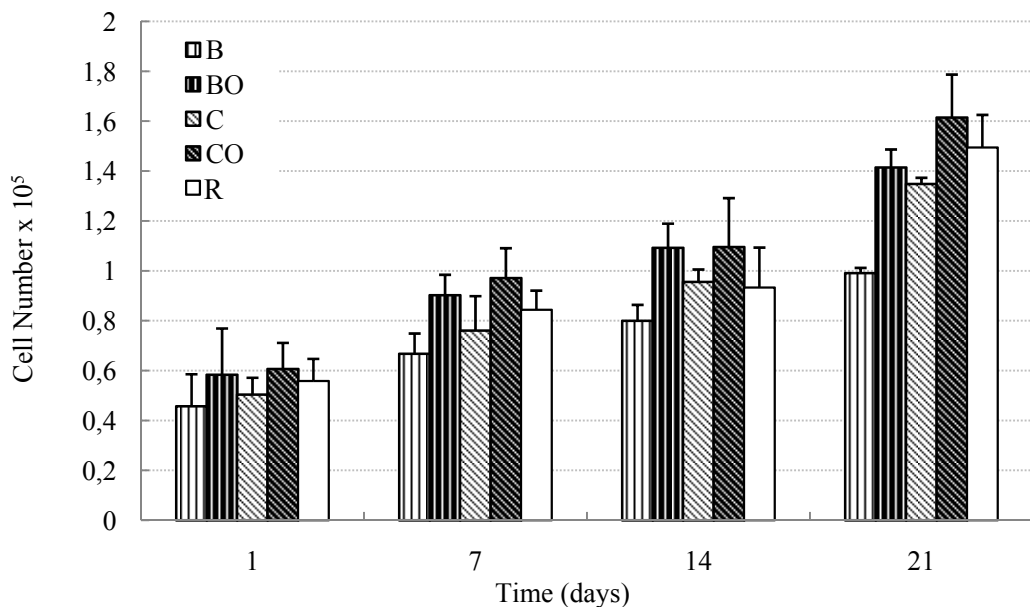


Figure 3.31. MSC proliferation on PCL scaffolds.

In order to determine the cell behavior and to qualitatively monitor cell growth, the samples were fixed and the actin filaments of the cells were stained on day 21 of the culture (Figure 3.32 and 3.33). It was observed that the cells attach and proliferate well on the fiber surfaces of the scaffolds regardless of fiber geometry.

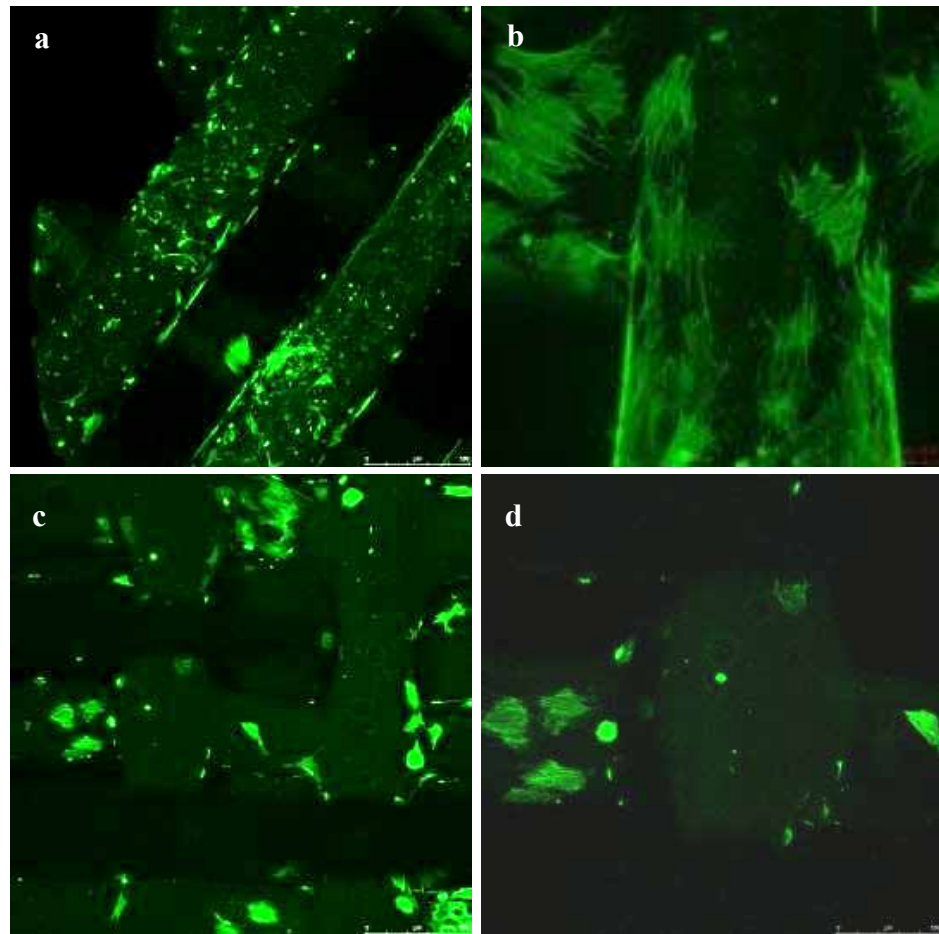


Figure 3.32. Fluorescence microcopy of MSC seeded PCL scaffolds, (a) B (x5), (b) B (x10), (c) BO (x5), (d) BO (x10). Stain: FITC-labeled phalloidin. Time: Day 21.

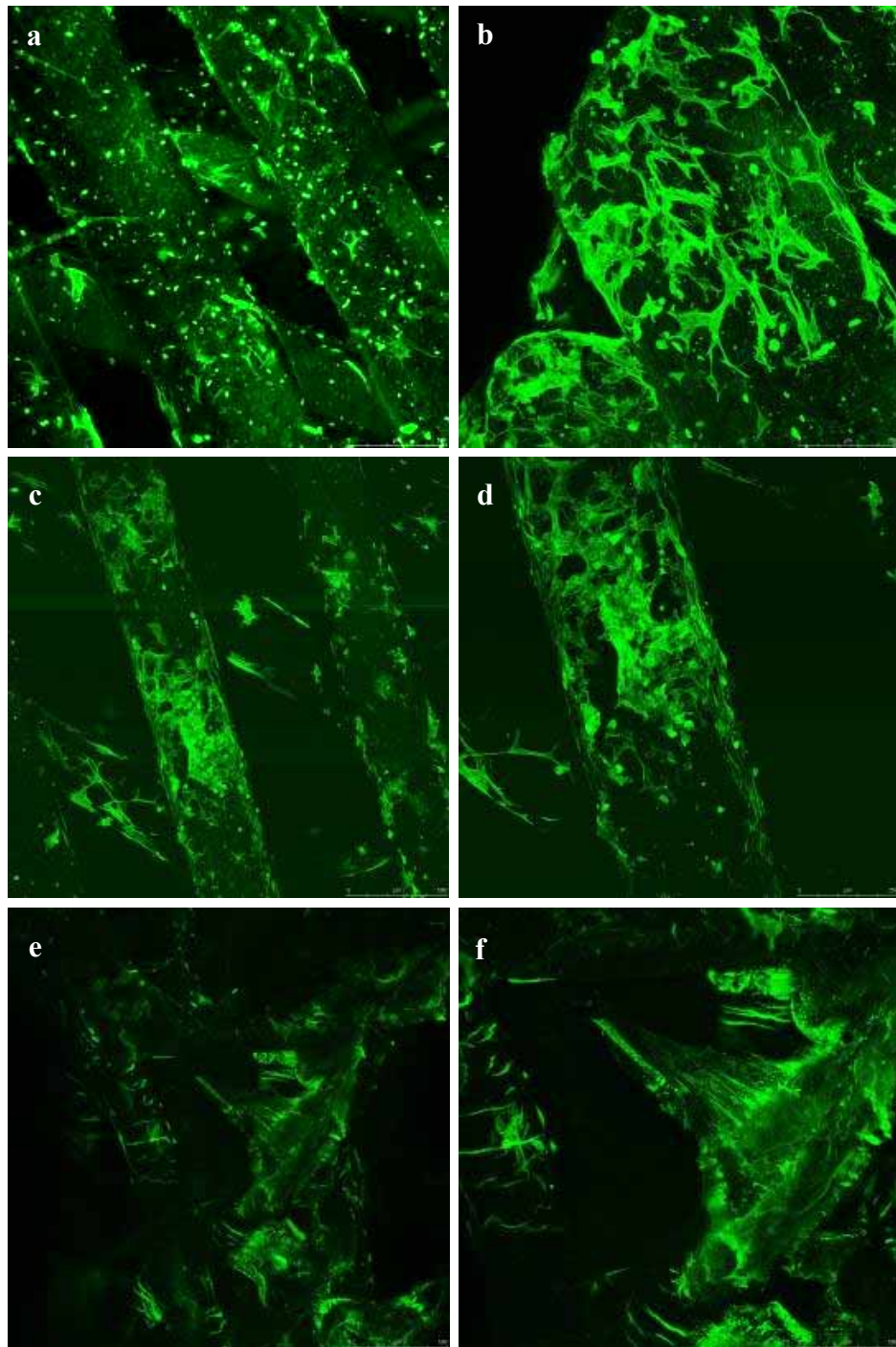


Figure 3.33. Fluorescence microscopy of MSC seeded PCL scaffolds, (a) C (x5), (b) C (x10), (c) CO (x5), (d) CO (x10), (e) R (x5), (f) R (x10). Stain: FITC-labeled phalloidin. Time: Day 21.

Cell attachment and spreading on fiber surfaces were also observed by SEM (Figure 3.34). SEM revealed proper cell adhesion and spreading on PCL fibers as was also verified by fluorescence microscopy.

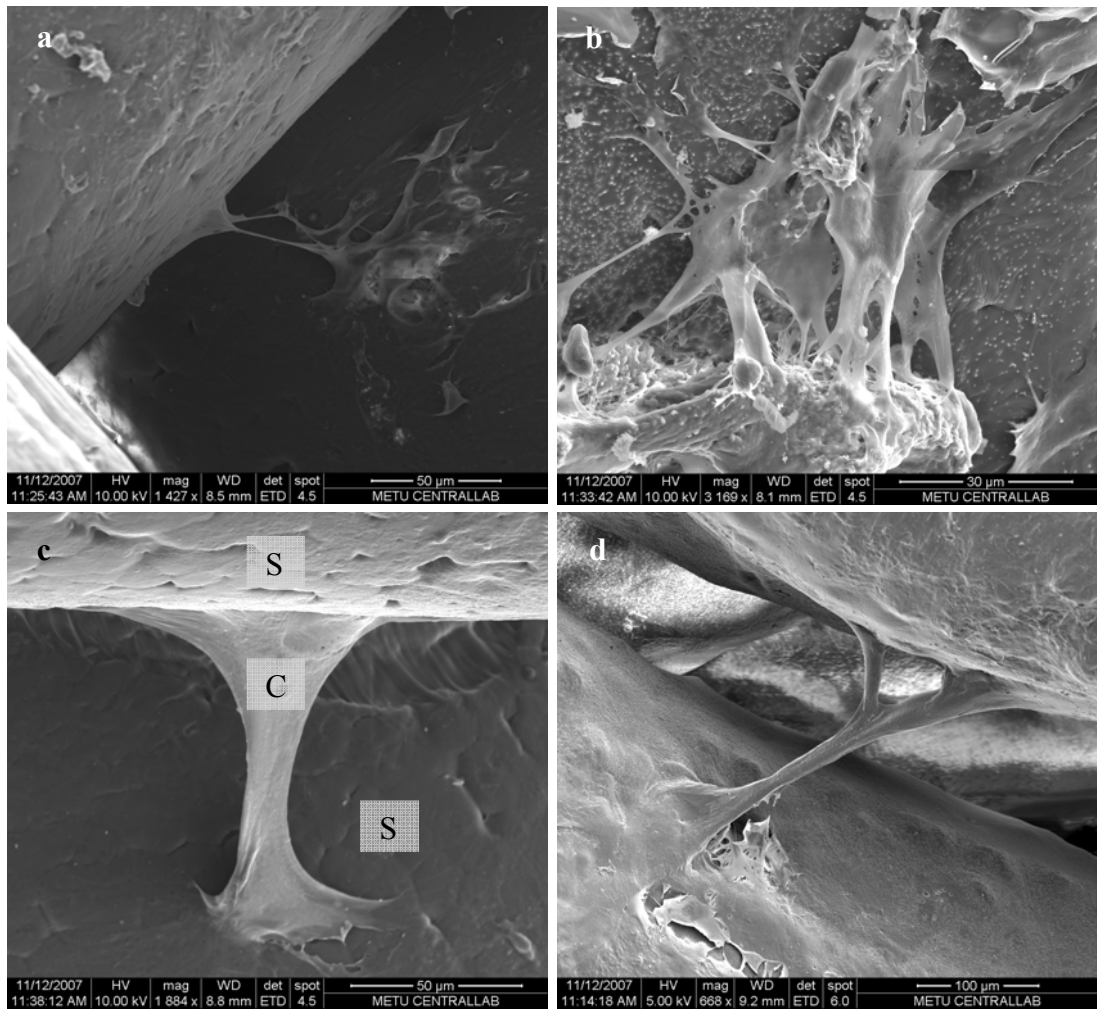


Figure 3.34. SEM of MSC attachment and spreading on PCL scaffolds. (a) BO, (b) C, (c) CO, (d) R. In these figures especially the cell stretching between different fibers is shown. Time: Day 21.

ALP activity per cell (specific activity) at specific time points during incubation was measured in order to investigate the effect of fiber orientation on the differentiation of MSCs into osteoblastic cells (Figure 3.35). In general, ALP results were in agreement with the cell proliferation results; higher ALP activity values were obtained for samples with lower cell proliferation. Highest MSC differentiation (highest ALP activity) was observed for crossed scaffold (C). These results indicate that scaffold architecture influences cell response, in terms of both seeding efficiency and proliferation. Furthermore, cell differentiation, as measured by ALP activity, appears to be also affected by scaffold structure, indicating that scaffold geometry can be fine-tuned to obtain the optimum scaffold.

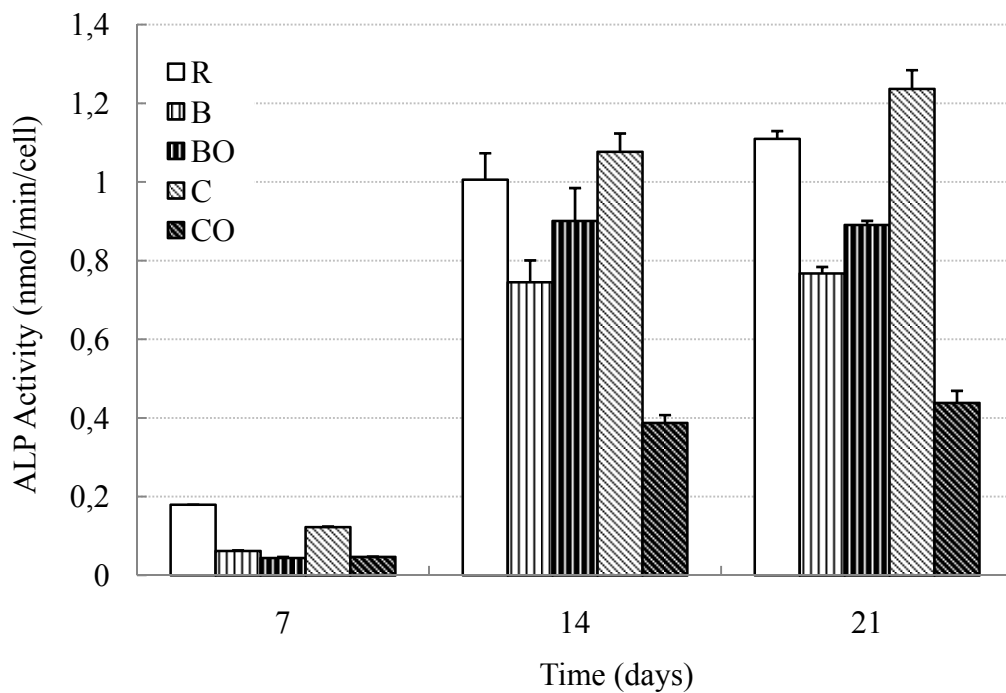


Figure 3.35. Specific ALP activity on PCL scaffolds.

3.3.4. Incorporation of Delivery System onto PCL Scaffolds

PLGA and PHBV nanocapsules were incorporated onto the fiber surfaces of PCL scaffolds by using a post-seeding method. Nanocapsules suspended in an aqueous alginic acid solution were applied onto the PCL fibers which were then stabilized with CaCl₂. Nanocapsule application was done from both sides of the scaffold to ensure proper dispersion of the nanocapsules throughout the structure.

For nanocapsule incorporation studies, three types of PCL scaffolds, B, BO and R, were selected out of the five (B, BO, C, CO and R) in order to decrease the number of samples to study the relation between fiber orientation and nanocapsule retention capability.

SEM micrographs revealed that nanocapsules in alginic acid were coated onto the surfaces of PCL fibers as a thin layer (few micrometers), without affecting the porosity of the scaffold in all the scaffold architectures tested (Figure 3.36).

PLGA and PHBV nanocapsule incorporated PCL scaffolds were incubated under normal culture conditions (37°C, 5% CO₂) for 21 days and were examined with SEM for signs of potential change in the construct. It was observed with loaded “B” scaffold that the nanocapsules were still present on the fiber surfaces at the end of the culture while the alginic acid layer was substantially removed (Figure 3.37).

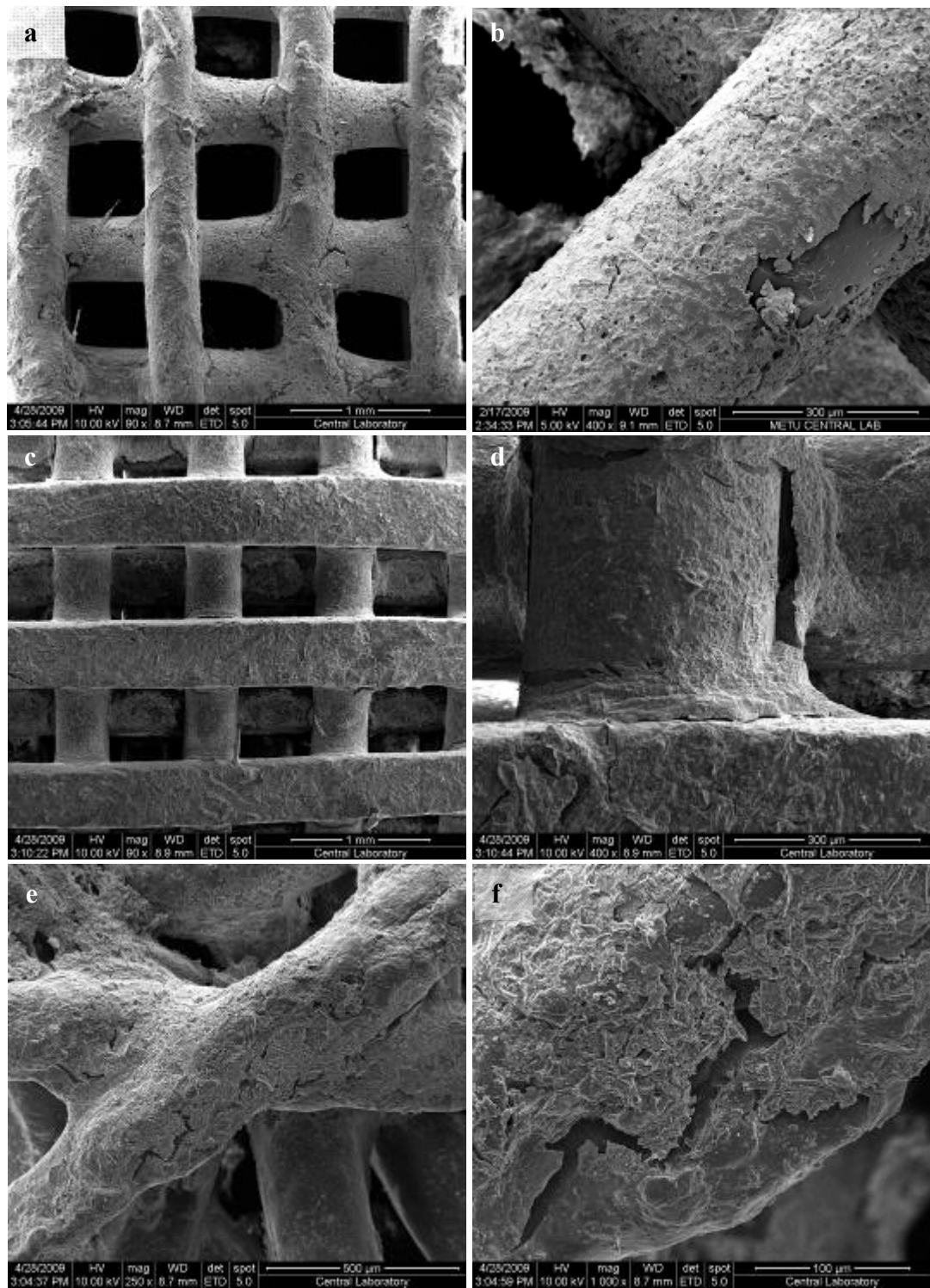


Figure 3.36. SEM of PLGA nanocapsules incorporated onto the fiber surfaces of PCL scaffolds. **B:** (a) x90, (b) x400; **BO:** (c) x90, (d) x400; **R:** (e) x250, (f) x1,000.

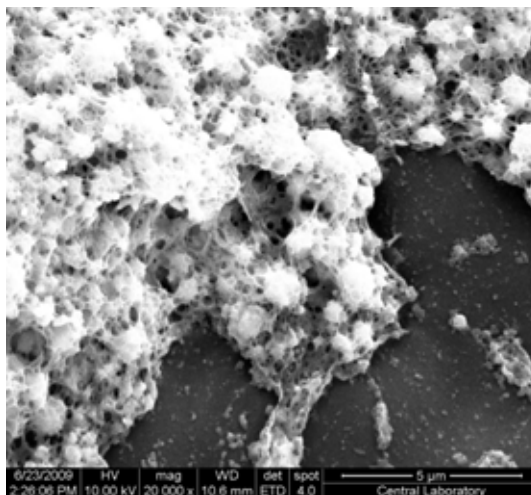


Figure 3.37. SEM of “B” scaffold loaded with PLGA and PHBV nanocapsules after 21 days of culture (x20,000).

3.3.5. The Release Behavior

Release of BSA, the model protein, from PLGA and PHBV nanocapsules incorporated onto PCL scaffolds was studied (Figures 3.38 and 3.39). It was observed in Figure 3.38 that the free nanocapsules had a slightly higher release followed by BO, R and B. The suppression of release could be due to the thin alginic acid layer surrounding the nanocapsules and also due to the matrix structure creating a more stagnant environment. The general trend in all was that within 1 day there was about 50% release which then significantly slowed down leading to 70-90% release in about 3 weeks.

The release of BSA from PHBV nanocapsules followed a similar trend but burst was around 25% and the total release in 3 weeks was about 45%, much lower than with PLGA (Figure 3.39). Like the previous case, rate of release from BO was higher than with B and R.

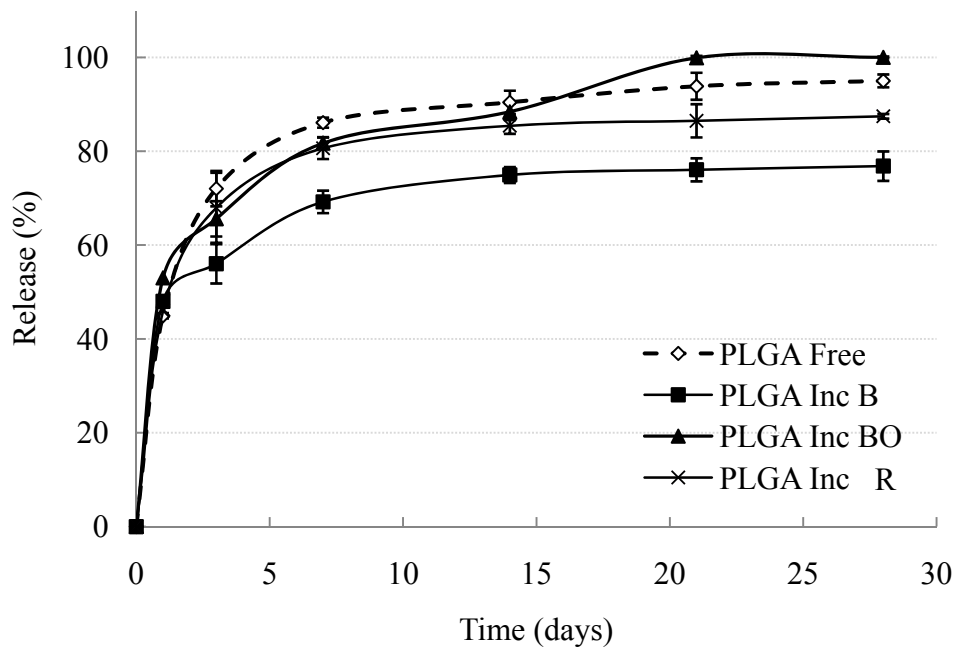


Figure 3.38. BSA release from PLGA nanocapsules incorporated on PCL scaffolds and free.

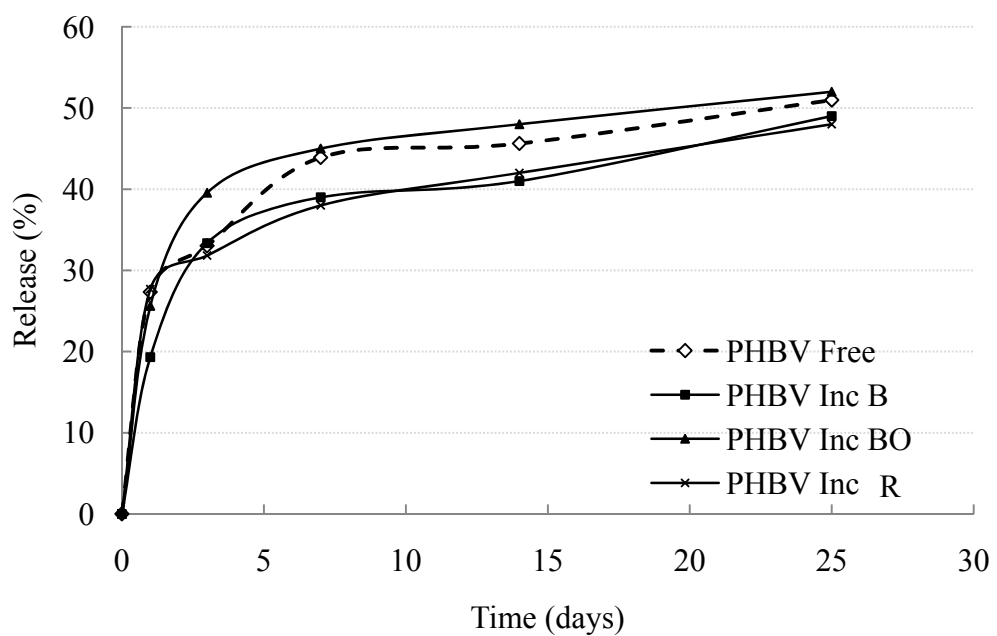


Figure 3.39. BSA release from PHBV nanocapsules incorporated on PCL scaffolds and free.

3.3.6. Effect of Sequential BMP-2/BMP-7 Delivery from PCL Scaffolds with Different Fiber Orientations on the Proliferation and Differentiation of MSCs

After the preliminary studies using BSA as the model protein and assuring that the growth factors behave similar to BSA, the effect of single, simultaneous and sequential delivery of BMP-2 and BMP-7 from PCL scaffolds was studied by using rat bone marrow MSCs. The effect of both the fiber orientation and the combination of BMP-2 and BMP-7 delivery systems were investigated.

Cell proliferation tests (Figure 3.40) revealed that a similar trend to that was observed with chitosan scaffolds was prevalent; presence of BMP-2 suppressed MSC proliferation compared to the unloaded PCL scaffolds (Figure 3.32) and higher than BMP-7 so all three BMP-2 carrying systems were suppressed. The most suppressed was the sequential BMP-2/BMP-7 delivery system. This trend did not change for the 3 weeks test period.

Although it was shown with the model protein that the 3-D orientation of the fibers of the PCL scaffold do not have a significant effect on the nanocapsule retention and the release rate, it affected MSC proliferation. Especially after the first week of incubation, cell proliferation on R scaffolds were significantly higher compared to B and BO structures, probably due to the higher initial attachment ratio.

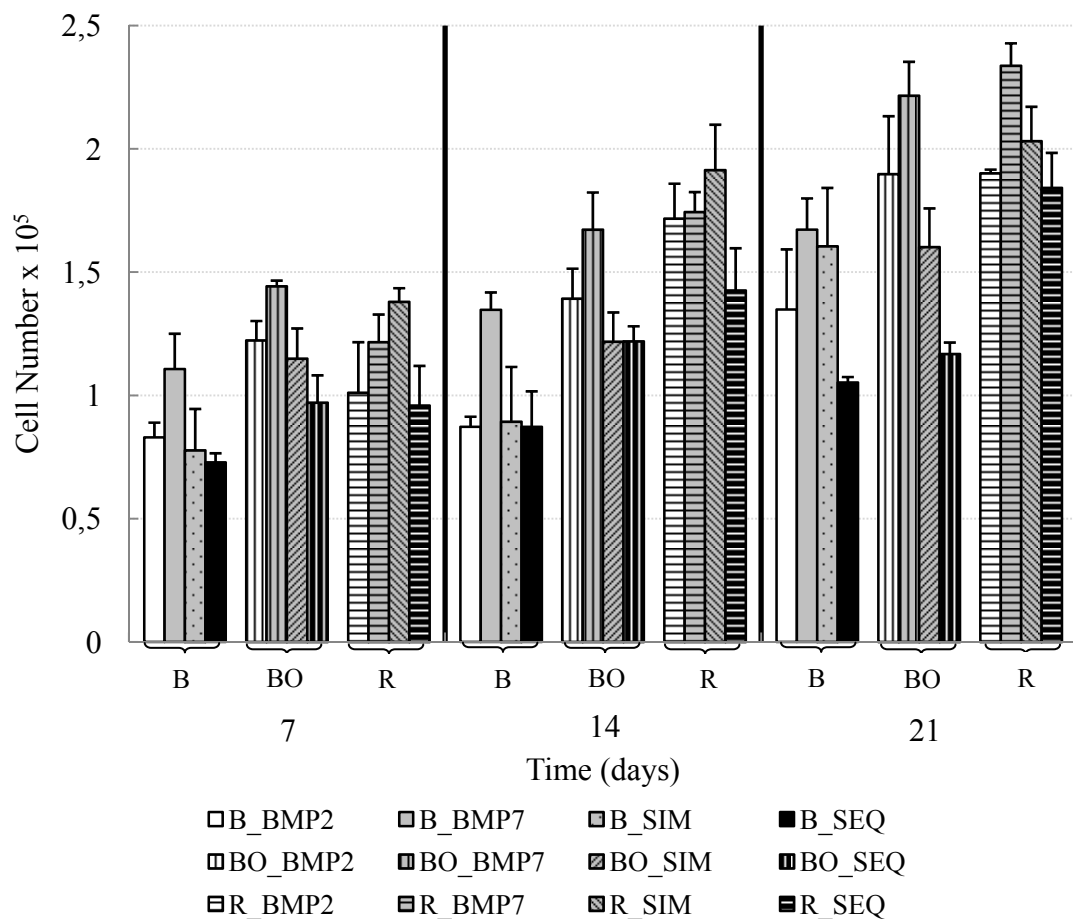


Figure 3.40. Cell proliferation on BMP loaded particle incorporated PCL scaffolds.

Once the cell number counts were completed, the samples were fixed (day 21) and the actin filaments of the cells were stained with FITC-phalloidin in order to monitor cell spreading on the PCL fiber surfaces (Figure 3.41). Proper cell attachment and spread was verified on the PLGA and PHBV nanocapsule incorporated PCL fibers.

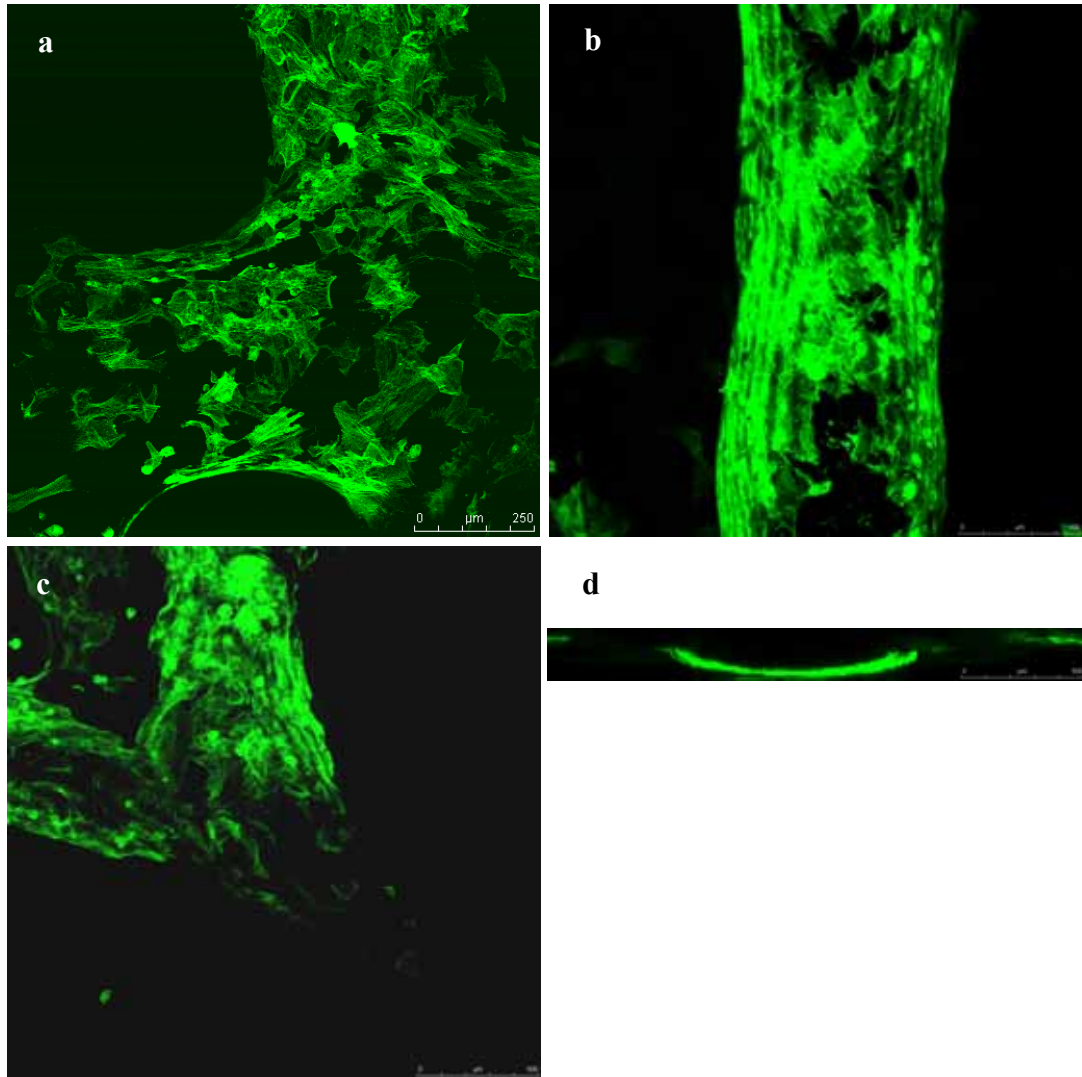


Figure 3.41. PCL scaffolds seeded with MSC on day 21 of incubation incorporated with PLGA and/or PHBV nanocapsules to provide sequential BMP-2/BMP-7 delivery. (a) scaffold B, (b) scaffold BO, (c) scaffold R, (d) x-section of the fiber of BO scaffold showing complete coverage of the fiber surface with MSCs. x10.

Cell spread on the scaffolds was also investigated by SEM with BMP-2 loaded PLGA nanocapsule incorporated constructs (Figure 3.42). Proper cell spread as well as the presence of nanocapsules on the fiber surfaces could be clearly seen in the micrographs.

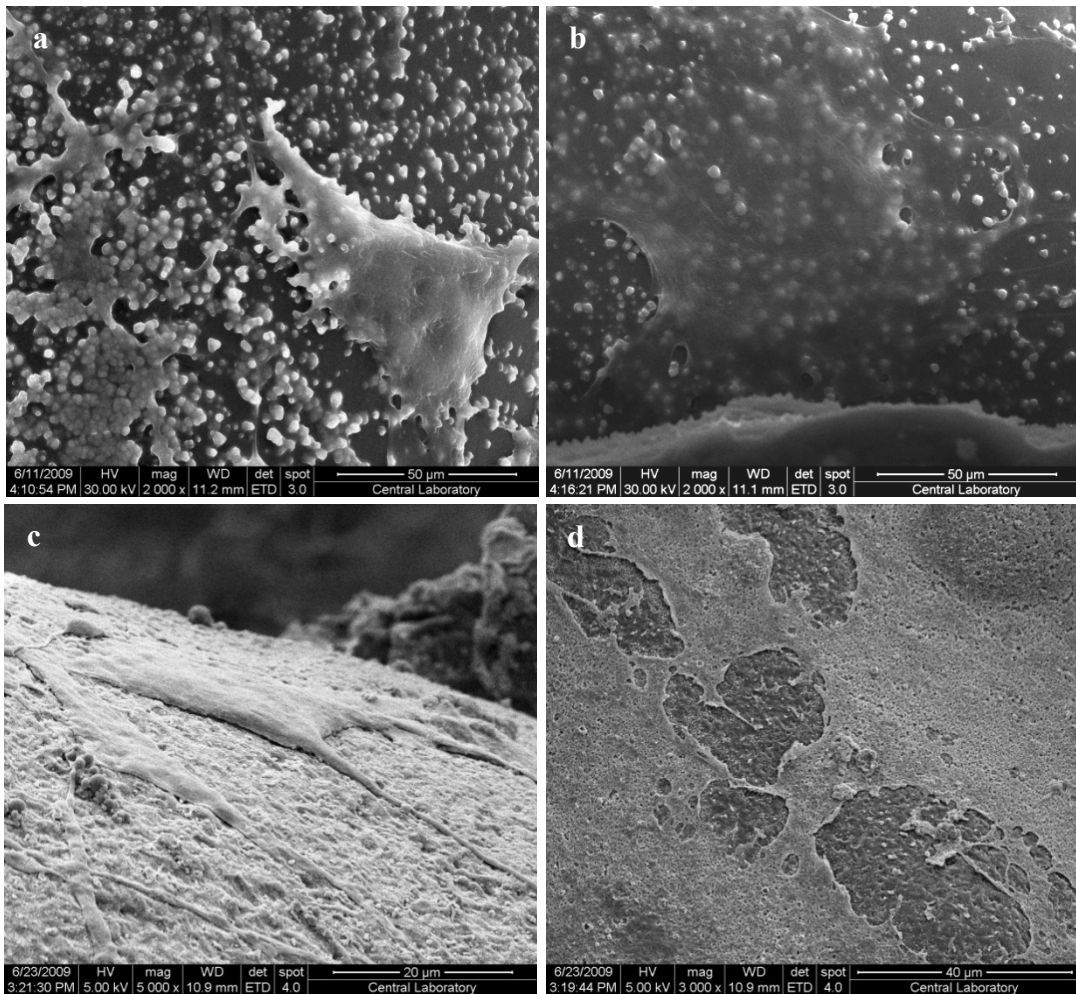


Figure 3.42. MSCs on BMP-2 loaded PLGA nanocapsule incorporated (a) B, (b) BO, (c, d) R PCL scaffolds at the end of 21 days of culture.

MSC differentiation test with incorporated PCL scaffolds revealed, as also was observed with the proliferation, ALP activity trend was similar to that observed in chitosan scaffolds (Figure 3.43). Here also, the ALP activity reached its highest level when BMP-2 and BMP-7 were supplemented to the growth medium in a sequential manner regardless of scaffold fiber orientation and time. ALP activity increased gradually for all scaffolds (B, BO and R) and every delivery condition tested (single, simultaneous and sequential delivery) during the 21 days of incubation. When the ALP activity for sequential delivery case was compared

among the various scaffold types, it was observed that R scaffolds had a higher ALP activity compared to B and BO as was the case with the unloaded scaffolds (Figure 3.35).

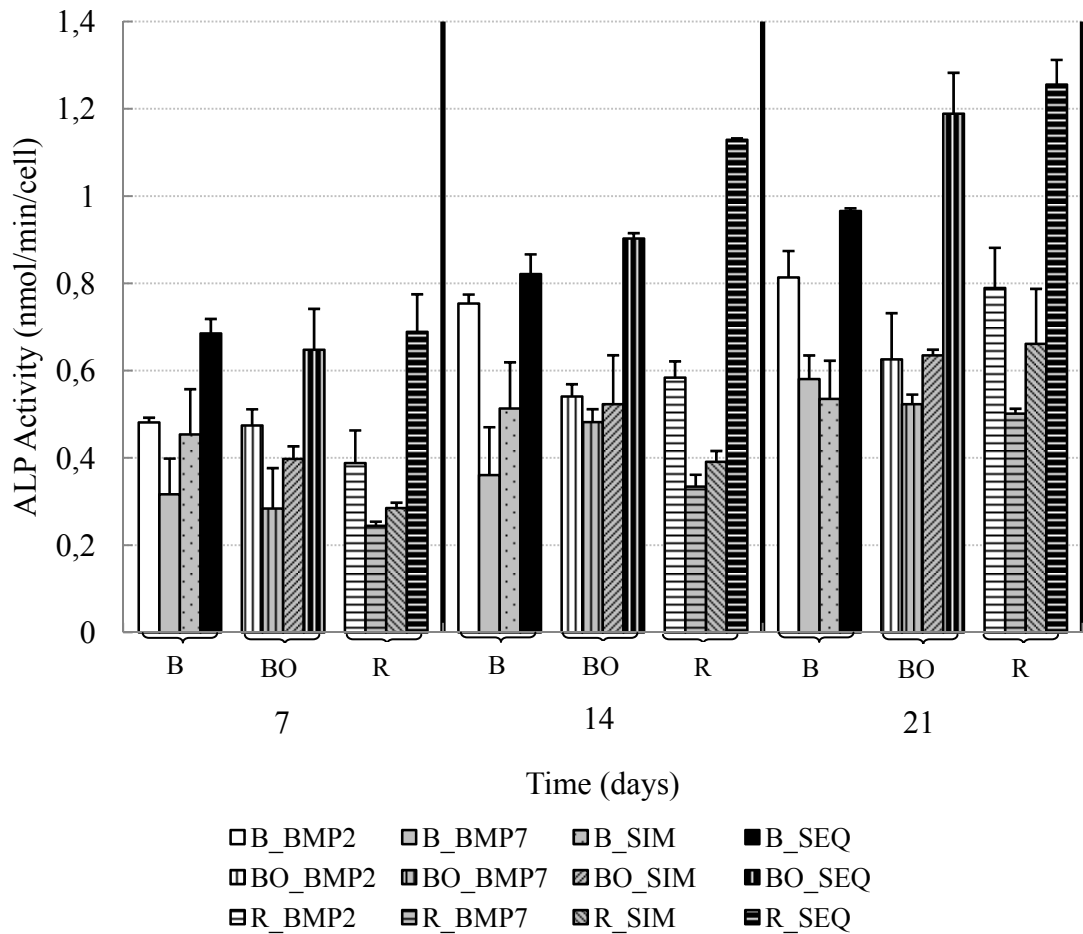


Figure 3.43. Specific ALP activity of MSCs on BMP loaded particle incorporated PCL scaffolds.

3.4. *In vivo* Application of BMP-2 Loaded PLGA Nanocapsules with no Scaffold

The *in vivo* effectiveness of BMP-2 loaded PLGA nanocapsules was investigated by subcutaneous implantation in Wistar rats (Figure 3.44). The *in vivo* compatibility of the nano-sized particles as well as their *in vivo* degradation behavior and the effect of BMP-2 on the peri-implant tissue were assessed as signs for a successful implant.

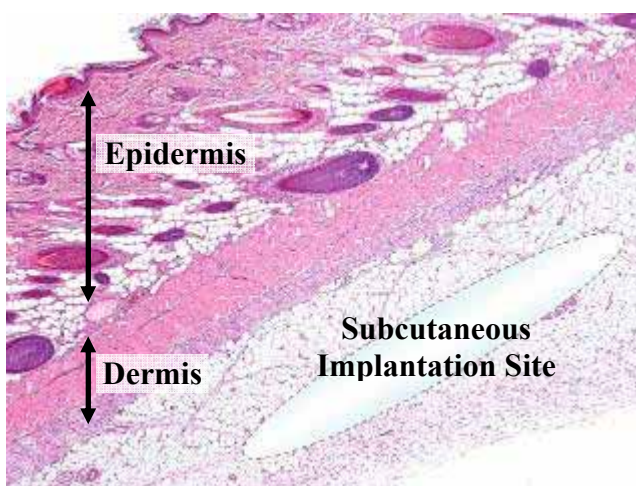


Figure 3.44. Histology of the subcutaneous implantation site in a Wistar rat. Haematoxylin-Eosin staining, x40.

Starting with day 3 of implantation, the BMP-2 loaded PLGA nanocapsules were covered by a fibrin-rich tissue and a few sporadic neutrophil granulocytes were observed. At this time, numerous macrophages and foreign body giant cells in concert with an increased number of fibroblasts could be observed in the peri-implant site.

On day 10 of implantation, the acute inflammatory response observed on day 3 declined. The number of the macrophages and foreign body giant cells around partly degraded nanocapsules increased. Together with clearly detectable blood vessels in the margin of the biomaterial, multinucleated tartrate-resistant acid phosphatase (TRAP)-positive cells appeared adjacent to the nanocapsules. At this time point, already a decline in the number of the inflammatory cells other than macrophages and multinucleated giant cells could be observed.

On day 30, continuation of increased vascularization of the biomaterial and the decrease of the amount of the TRAP-positive cells were observed. Meanwhile, the degradation of the biomaterial continued until 40 days after implantation. The nanocapsules had a clear round shape and were in direct contact with the multinucleated giant cells. There were no signs of activated fibroblasts and fibrosis.

In brief, the signs of vascularization and nanoparticle degradation increased between 3 to 40 days while the signs of inflammation decreased (Figure 3.45). Although no bone formation could be observed in the first 40 days after implantation, the mild inflammatory response and the formation of TRAP-positive cells could be interpreted as a response to the BMP-2 release from the nanocapsules.

The mild inflammatory response with a few sporadic neutrophils followed by the accumulation of macrophages in the early phase after the implantation reflects an acceptable inflammatory response. The early transformation of macrophages and multinucleated giant cells to TRAP-positive cells on day 10 could be interpreted as a response to the BMP-2 release from the nanocapsules. BMP-2 is known to be able to induce differentiation and also to activate osteoclasts. No bone formation could be observed in the first 40 days, which is possibly due to the low concentration of BMP-2 in the extracellular matrix. These results are encouraging and the PLGA nanocapsules appear to have a potential as a functional drug delivery system for tissue engineering.

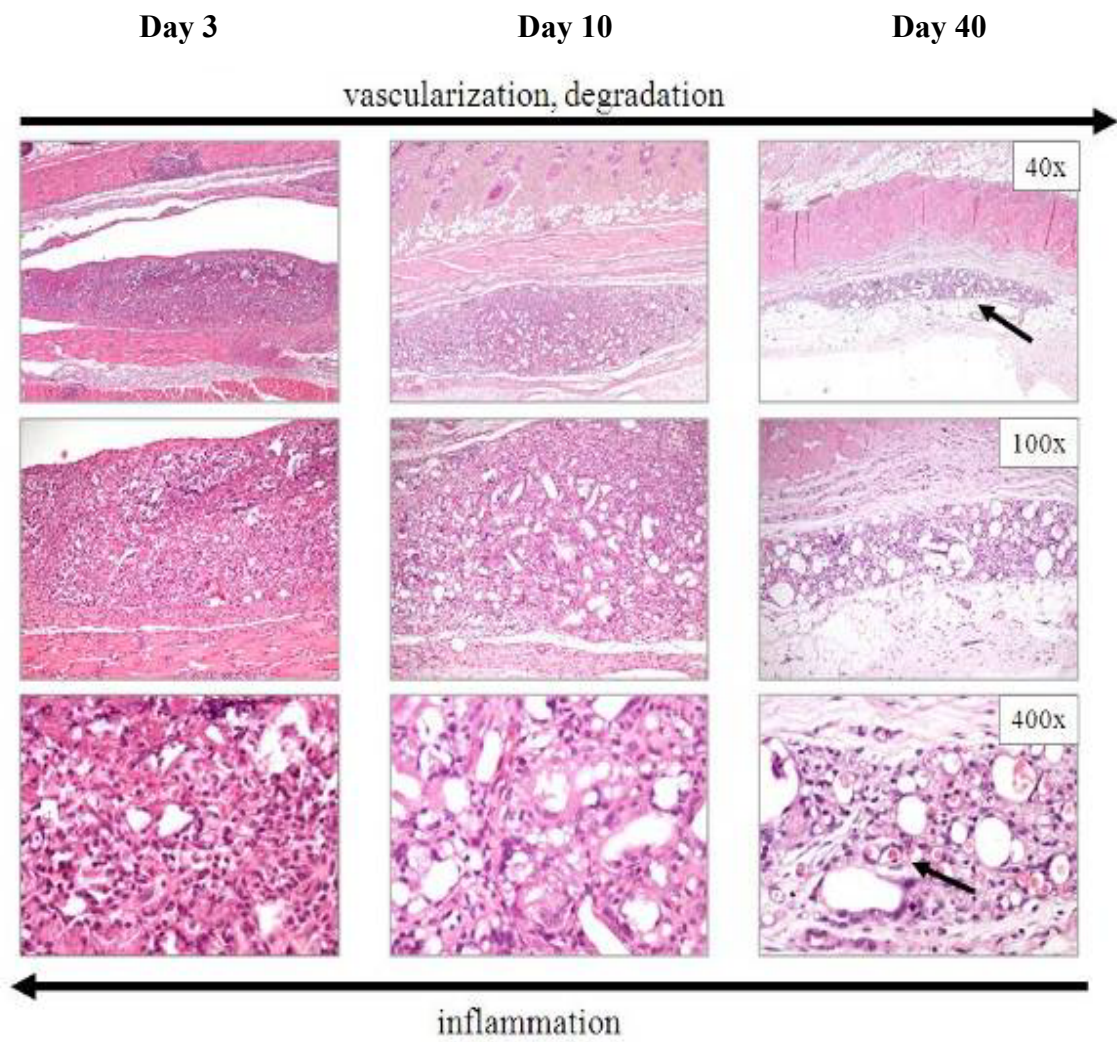


Figure 3.45. The overall evaluation of the *in vivo* performance of BMP-2 loaded PLGA nanocapsules.

CHAPTER 4

CONCLUSION

Tissue engineering offers a solution to the worldwide shortage of bone substitutes for clinical implantation. Although the technique has been greatly improved since its first inception, one of the current problems it encounters is the lack of functionality. This functionality could be achieved through the induction and control of cellular behavior within the tissue engineered construct to provide differentiation, mineralization and vascularization. It is well documented that cellular activities in the body are strictly controlled and regulated by growth factors of several types. It was revealed that BMPs are particularly important in bone formation and regeneration, being the most osteoinductive growth factors presently described. Moreover, it was shown that growth factors act in a time and dose dependent manner during natural bone regeneration process.

In this study, the hypothesis was that bone regeneration could be maximized by mimicking the timing of the natural bioavailability of BMP-2 and BMP-7. Due to the fact that BMP-2 is an early appearing factor after fracture and BMP-7 follows it after 2 weeks, a delivery system was constructed that could mimic this timing. To protect the fragile growth factors from degradation, as well as to control their release rates, they were encapsulated in two different polymeric nanocapsules. Moreover, the advantage of using nano-scale carriers was that the delivery system could be incorporated into a variety of scaffolds without affecting their structure.

After achieving the sequential delivery through the nanoparticles and verifying the maximized osteogenic activity through this delivery condition; the

carriers were incorporated into two different polymeric (chitosan and PCL) scaffold systems. Beforehand, the applicability of these scaffolds prepared by wet spinning and 3-D plotting was shown for bone tissue engineering applications *in vitro*. Then, the effect of incorporation on the release behavior of the growth factors compared to the free nanocapsules was studied. The successful release of the growth factors from the constructs was shown *in vitro* with differences in proliferation and differentiation rates of bone marrow mesenchymal stem cells. For both scaffold systems (chitosan and PCL), the positive effect of co-administration of BMP-2 and BMP-7 in a sequential manner was shown with maximized osteogenic activity.

As a conclusion, it was possible to obtain multi-functional bioactive tissue engineering constructs capable of delivering osteogenic factors in a sequential manner.

Ongoing and Future Work:

The sequential delivery systems produced in this study (both free and incorporated) were proven to be effective *in vitro* on maximizing the osteogenic activity. However, *in vivo* results should also be seen. The preliminary results of implantation of free nanocapsules indicated proper biocompatibility and promising results due to BMP-2 release. However, detailed testing needs to be done in order to verify the effect of sequential delivery on bone formation *in vivo*. Tissue engineered PCL scaffolds capable of sequential BMP-2/BMP-7 delivery were implanted into the iliac crest of rats in our ongoing study. The effect of sequential BMP-2/BMP-7 delivery on the healing of bone defects are being studied with radiological and histological analysis. Preliminary gross observation at 6 weeks revealed no significant inflammatory response and show proper integration of the scaffolds with the newly formed tissue.

REFERENCES

- Abboud S.L. A bone marrow stromal cell line is a source and target for platelet-derived growth factor. *Blood* 1993; 81: 2547-2553.
- Agrawal C.M., Ray R.B. Biodegradable polymeric scaffolds for musculoskeletal tissue engineering. *J Biomed Mater Res* 2001; 55: 141–150.
- Akazawa T., Murata M., Sasaki T., Tazaki J., Kobayashi M., Kanno T., Nakamura K., Arisue M. Biodegradation and bioabsorption innovation of the functionally graded bovine bone–originated apatite with blood permeability. *J Biomed Mater Res* 2006; 76A: 44 –51.
- Akhtar S. Physicochemical properties of bacterial P(HB-HV) polyesters and their uses in drug delivery. PhD Thesis for the University of Bath. 1990
- Allori A.C., Sailon A.M., Warren S.M. Biological Basis of Bone Formation, Remodeling, and Repair- Part I: Biochemical Signaling Molecules. *Tissue Eng Part B* 2008; 14(3): 259-273.
- Almirall A., Larrecq G., Delgado J.A., Martínez S., Planell J.A., Ginebra M.P. Fabrication of low temperature macroporous hydroxyapatite scaffolds by foaming and hydrolysis of an α -TCP paste. *Biomaterials* 2004; 25: 3671-3680.
- Altman G.H., Diaz F., Jakuba C., Calabro T., Horan R.L., Chen J., Lu H., Richmond J., Kaplan L. Silk-based biomaterials. *Biomaterials* 2003; 24(3): 401-416.
- Ambrosio A.M., Sahota J.S., Khan Y., Laurencin C.T. A novel amorphous calcium phosphate polymer ceramic for bone repair: I. Synthesis and characterization. *J Biomed Mater Res* 2001; 58(3): 295-301.
- Anselme K. Osteoblast adhesion on biomaterials. *Biomaterials* 2000; 21(7): 667-681.
- Ashammakhi N., Mäkelä E.A., Törmälä P., Waris T., Rokkanen P. Effect of self-reinforced polyglycolide membrane on osteogenesis: An experimental study in rats. *Eur J Plast Surg* 2000; 23(8): 423-428.
- Bakos D., Soldán M., Hernández-Fuentes I. Hydroxyapatite-collagen-hyaluronic acid composite. *Biomaterials* 1999; 20(2): 191-195.

- Bandyopadhyay A., Tsuji K., Cox K., Harfe B.D., Rosen V., Tabin C.J. Genetic analysis of the roles of BMP2, BMP4, and BMP7 in limb patterning and skeletogenesis. *PLoS Genet* 2006; 2(12): e216. doi:10.1371/journal.pgen.0020216.
- Baran E.T., Ozer N., Hasirci V. In vivo half life of nanoencapsulated L-asparaginase. *J Mater Sci Mater Med* 2002; 13: 1113-1121.
- Basmanav F.B., Kose G.T., Hasirci V. Sequential growth factor delivery from complexed microspheres for bone tissue engineering. *Biomaterials* 2008; 29: 4195–4204.
- Benya P.D., Schaffer J.D. Dedifferentiated chondrocytes reexpress the differentiated collagen phenotype when cultured in agarose gels. *Cell* 1982; 30: 215-224.
- Ber S., Kose G.T., Hasirci V. Bone tissue engineering on patterned collagen films: An in vitro study. *Biomaterials* 2005; 26(14): 1977-1986.
- Bessa P.C., Casal M., Reis R.L. Bone morphogenetic proteins in tissue engineering: the road from the laboratory to the clinic, part I (basic concepts). *J Tissue Eng Regen Med* 2008; 2: 1–13.
- Bibb R., Freeman P., Brown R., Sugar A., Evans P., Bocca A. An investigation of three-dimensional scanning of human body surfaces and its use in the design and manufacture of prostheses. *Proc Inst Mech Eng H* 2000; 214 (6): 589-94
- Boccaccini A.R., Roether J.A., Hench L.L., Maquet V., Jerome R.A. composites approach to tissue engineering. *Ceram Eng Sci Proc* 2002; 23: 805–816.
- Bonewald L.F., Mundy G.R. Role of transforming growth factor beta in bone remodeling: a review. *Connect Tissue Res* 1989; 23: 201-208.
- Brigger I., Dubernet C., Couvreur P. Nanoparticles in cancer therapy and diagnosis. *Adv Drug Deliv Rev* 2002; 54: 631-651.
- Buckwalter J.A., Glimcher M.J., Cooper R.R, Recker R. Bone biology Part II: Formation, form, modeling, remodeling, and regulation of cell function. *J Bone Joint Surg* 1995; 77-A: 1276-1283.
- Burgess D.J., Hickey A.J. Microsphere technology and applications. In: Swarbrick, Boylan, editors. *Encyclopedia of Pharmaceutical Technology*. New York:Marcel Dekker; 1994. p 1–29.
- Buttafoco L., Boks N.P., Poot A.A., Dijkstra P.J., Vermes I., Feijen J. Melt spinning and fibre winding of Trimethylenecarbonate (TMC)-based polymers for tissue engineering small diameter blood vessels. *Transactions - 7th World Biomaterials Congress* 2004; 711.

Cao H., Chen X., Huang L., Shao Z. Electrospinning of reconstituted silk fiber from aqueous silk fibroin solution. *Mater Sci Eng C* 2009, article in press.

Cao T., Ho K.H., Teoh S.H. Scaffold design and in vitro study of osteochondral coculture in a three-dimensional porous polycaprolactone scaffold fabricated by fused deposition modeling. *Tissue Eng* 2003; 9(1): 103-112.

Caplan A.I. Adult Mesenchymal Stem Cells for Tissue Engineering Versus Regenerative Medicine. *J Cell Physiol* 2007; 213: 341–347.

Caplan A.I., Dennis J.E. Genetically Linked Scientists: The One-Two Punch For NFATp Knockout. *J Exp Med* 2000; 191(1); 1-4.

Caplan A.L. Method for enhancing the implantation and differentiation of marrow-derived mesenchymal stem cells. 1993. US patent 5197985.

Carano R.A.D., Filvaroff E.H. Angiogenesis and bone repair. *Drug Discovery Today* 2003; 8: 980-989.

Centrella M., Casinghino S., Ignatz R., McCarthy T.L. Multiple regulatory effects by transforming growth factor-beta on type I collagen levels in osteoblast-enriched cultures from fetal rat bone. *Endocrinology* 1992; 131: 2863- 2872.

Centrella M., Horowitz M.C., Wozney J.M., McCarthy T.L. Transforming growth factor-beta gene family members and bone. *Endocr Rev* 1994; 15: 27-39.

Chau A.M.T., Mobbs R.J. Bone graft substitutes in anterior cervical discectomy and fusion. *Eur Spine J* 2009; 18: 449–464.

Chen F.M., Zhao Y.M., Zhang R., Jin T., Sun H.H., Wu Z.F., Jin Y. Periodontal regeneration using novel glycidyl methacrylated dextran (Dex- GMA)/gelatin scaffolds containing microspheres loaded with bone morphogenetic proteins. *J Contr Release* 2007; 121: 81-90.

Chen G., Okamura A., Sugiyama K., Wozniak M.J., Kawazoe N., Sato S., Tateishi T. Surface modification of porous scaffolds with nanothick collagen layer by centrifugation and freeze-drying. *J Biomed Mater Res Part B Appl Biomater* 2009; 90(2): 864-872.

Chen G., Zhou P., Mei N., Chen X., Shao Z., Pan L., Wu C. Silk fibroin modified porous poly(ϵ -caprolactone) scaffold for human fibroblast culture in vitro. *J Mater Sci Mater Med* 2004; 15(6): 671-677.

Chen L.J., Wang M. Production and evaluation of biodegradable composites based on PHB-PHV copolymer. *Biomaterials* 2002; 23(13): 2631-2639.

Chen R.R., Mooney D.J. Polymeric growth factor delivery strategies for tissue engineering. *Pharmaceutical Research* 2003; 20(8): 1103-1112.

Chen Z., Li D., Lu B., Tang Y., Sun M., Xu S. Fabrication of osteo-structure analogous scaffolds via fused deposition modeling. *Scr Mater* 2005; 52:157-161.

Chenu C., Pfeilschifter J., Mundy G.R., Roodman G.D. Transforming growth factor beta inhibits formation of osteoclast-like cells in long-term human marrow cultures. *Proc Natl Acad Sci USA* 1988; 85: 5683- 5687.

Chim H., Hutmacher D.W., Chou A.M., Oliveira A.L., Reis R.L., Lim T.C., Schantz J.T. A comparative analysis of scaffold material modifications for load-bearing applications in bone tissue engineering. *Int J Oral Maxillofac Surg* 2006; 35(10): 928-934.

Cho T.J., Gerstenfeld L.C., Einhorn T.A. Differential temporal expression of members of the transforming growth factor beta superfamily during murine fracture healing. *J Bone Miner Res* 2002; 17: 513–520.

Choong C., Triffitt J.T., Cui Z.F. Polycaprolactone scaffolds for bone tissue engineering: Effects of a calcium phosphate coating layer on osteogenic cells. *Food and Bioproducts Processing* 2004; 82(2 C): 117-125.

Chua C.K., Leong K.F., Tan K.H., Wiria F.E., Cheah C.M. Development of tissue scaffolds using selective laser sintering of polyvinyl alcohol/hydroxyapatite biocomposite for craniofacial and joint defects. *J Mater Sci Mater Med* 2004; 15(10): 1113-1121.

Chung Y.S., Kang S.I., Kwon O.W., Shin D.S., Lee S.G., Shin E.J., Min B.G., Lyoo W.S. Preparation of hydroxyapatite/poly(vinyl alcohol) composite fibers by wet spinning and their characterization. *J App Polym Sci* 2007; 106(5): 3423-3429.

Ciccone W., Motz C., Bentley C., Tasto J. Bioabsorbable implants in orthopaedics: new developments and clinical applications. *J Am Acad Orthop Surg* 2001; 9: 280-288.

Coelho M.J., Carbal A.T., Fernandes M.H. Human bone cell cultures in biocompatibility testing. Part I: osteoblastic differentiation of serially passaged human bone marrow cells cultured in α -MEM and in DMEM. *Biomaterials* 2000; 21: 1087-1094.

Corden T.J., Jones I.A., Rudd C.D., Christian P., Downes S., McDougall K.E. Physical and biocompatibility properties of poly- ϵ -caprolactone produced using in situ polymerisation: A novel manufacturing technique for long-fibre composite materials. *Biomaterials* 2000; 21(7): 713-724.

Costa R.O.R., Pereira M.M., Lameiras F.S., Vasconcelos W.L. In vitro study of apatite precipitation on poly(2-hydroxyethyl methacrylate)-silica hybrids with controlled surface areas. *Key Engineering Materials* 2003; 240-242: 195-198.

Cowan C.M., Aghaloo T., Chou Y.F., Walder B., Zhang X., Soo C., Ting K., Wu B. MicroCT evaluation of three-dimensional mineralization in response to BMP-2 doses in vitro and in critical sized rat calvarial defects. *Tissue Eng* 2007; 13(3): 501-512.

Cowan C.M., Soo C., Ting K., Wu B. Evolving concepts in bone tissue engineering. *Curr Top Dev Biol* 2005; 66: 239-285.

Cui F., Cun D., Tao A., Yang M., Shi K., Zhao M., Guan Y. Preparation and characterization of melittin-loaded poly(DL-lactic acid) or poly(DL-lactic-co-glycolic acid) microspheres made by the double emulsion method. *J Contr Release* 2005; 107: 310–319.

Davies S., Tighe B. Cell attachment to gel-spun polyhydroxybutyrate fibres. *Polym Prep Am Chem Soc Div Polym Chem* 1995; 36: 103-109.

Deckers M.M., Karperien M., van der Bent C., Yamashita T., Papapoulos S.E., Lowik C.W. Expression of vascular endothelial growth factors and their receptors during osteoblast differentiation. *Endocrinology* 2000; 141: 1667-1674.

Demirci U., Montesano G. Single cell epitaxy by acoustic picolitre droplets. *Lab on a Chip - Miniaturisation for Chemistry and Biology* 2007; 7(9): 1139-1145.

Deschamps A. Transactions of the Sixth World Biomaterials Congress, Society for Biomaterials, Minneapolis, 2000, 364.

Drury J.L., Mooney D.J. Hydrogels for tissue engineering: scaffold design variables and applications. *Biomaterials* 2003; 24: 4337-4351.

Duan Y., Wang Z., Yan W., Wang S., Zhang S., Jia J. Preparation of collagen-coated electrospun nanofibers by remote plasma treatment and their biological properties. *J Biomater Sci Polymer Ed* 2007; 18(9): 1153-1164.

Ebraheim N.A., Elgafy H., Xu R. Bone-Graft Harvesting From Iliac and Fibular Donor Sites: Techniques and Complications. *J Am Acad Orthop Surg* 2001; 9(3): 210-218.

Eckardt H., Ding M., Lind M., Hansen E.S., Christensen K.S., Hvid I. Recombinant human vascular endothelial growth factor enhances bone healing in an experimental nonunion model. *J Bone Joint Surg* 2005; 87: 1434-1438.

Eingartner C., Coerper S., Fritz J., Gaissmaier C., Koveker G., Weise K. Growth factors in distraction osteogenesis. Immuno-histological pattern of TGF-beta1 and

IGF-I in human callus induced by distraction osteogenesis. *Int Orthop* 1999; 23: 253-259.

Ellis M.J., Chaudhuri J.B. Poly(lactic-co-glycolic acid) hollow fibre membranes for use as a tissue engineering scaffold. *Biotechnol Bioeng* 2007; 96(1): 177-187.

Erbe E.M., Clineff T.D., Bagga C.S., Nagvajara G.M., Koblish A. Biocompatible bone graft material. US Patent 7189263, 2007.

Fedorovich N.E., De Wijn J.R., Verbout A.J., Alblas J., Dhert W.J.A. Three-dimensional fiber deposition of cell-laden, viable, patterned constructs for bone tissue printing. *Tissue Eng* 2008; 14A(1): 127-133.

Fernandez D.L., Ring D., Jupiter J.B. Surgical management of delayed union and nonunion of distal radius fractures. *J Hand Surg* 2001; 26(2): 201-209.

Filmon R., Baslé M.F., Barbier A., Chappard D. Poly(2-hydroxy ethyl methacrylate)-alkaline phosphatase: A composite biomaterial allowing in vitro studies of bisphosphonates on the mineralization process. *J Biomater Sci Polymer Ed* 2000; 11(8): 849-868

Fisher J., Dowson D. Tribology of total artificial joints. *Proc Inst Mech Eng J Eng Med* 1991; 205: 73-79.

Freyman T.M., Yannas I.V., Gibson L.J. Cellular materials as porous scaffolds for tissue engineering. *Prog in Mater Sci* 2001; 46: 273-282

Friedenstein A.J., Chailakhyan R.K., Gerasimov U.V. Bone marrow osteogenic stem cells: In vitro cultivation and transplantation in diffusion chambers. *Cell Tissue Kinet* 1987; 20: 263-272.

Fuchs S., Jiang X., Schmidt H., Dohle E., Ghanaati S., Orth C., Hofmann A., Motta A., Migliaresi C., Kirkpatrick C.J. Dynamic processes involved in the pre-vascularization of silk fibroin constructs for bone regeneration using outgrowth endothelial cells. *Biomaterials* 2009; 30(7): 1329-1338.

Fuller R.C. Microbial inclusions with special reference to PHA inclusions and intracellular boundary envelopes. *Int J Biol Macromol* 1999; 25: 21-29.

Funakoshi T., Majima T., Iwasaki N., Yamane S., Masuko T., Minami A., Harada K., Nishimura S.I. Novel chitosan-based hyaluronan hybrid polymer fibers as a scaffold in ligament tissue engineering. *J Biomed Mater Res* 2005; 74A(3): 338-346

Geng L., Feng W., Hutmacher D.W., Wong Y.S., Loh H.T., Fuh J.Y.H. Direct writing of chitosan scaffolds using a robotic system. *Rapid Prototyping Journal* 2005; 11(2): 90-97.

Goldstein A.S., Zhu G., Morris G.E., Meszlenyi R.K., Mikos A.G. Effect of osteoblastic culture conditions on the structure of poly(DL-lactic-co-glycolic acid) foam scaffolds. *Tissue Eng* 1999; 5(5): 421-433.

Gomes M.E., Holtorf H.L., Reis R.L., Mikos A.G. Influence of the porosity of starch-based fiber mesh scaffolds on the proliferation and osteogenic differentiation of bone marrow stromal cells cultured in a flow perfusion bioreactor. *Tissue Eng* 2006; 12: 801-809.

Gomes M.E., Reis R.L., Mikos A.G. Bone tissue engineering constructs based on starch scaffolds and bone marrow cells cultured in a flow perfusion bioreactor. *Mater Sci Forum* 2006; 514-516: 980-984.

Gray, H. *Anatomy of the Human Body*. Twentieth ed. Revised and re-edited by Lewis W.H., Lea & Febiger, New York, USA, 2000.

Grellier M., Granja P.L., Fricain J.C., Bidarra S.J., Renard M., Bareille R., Bourget C., Amedee J., Barbosa M.A. The effect of the co-immobilization of human osteoprogenitors and endothelial cells within alginate microspheres on mineralization in a bone defect. *Biomaterials* 2009; 30(19): 3271-3278.

Guarino V., Ambrosio L. The synergic effect of polylactide fiber and calcium phosphate particle reinforcement in poly ϵ -caprolactone-based composite scaffolds. *Acta Biomater* 2008; 4(6): 1778-1787.

Guarino V., Causa F., Taddei P., di Foggia M., Ciapetti G., Martini D., Fagnano C., Ambrosio L. Polylactic acid fibre-reinforced polycaprolactone scaffolds for bone tissue engineering. *Biomaterials* 2008; 29(27): 3662-3670.

Guelcher S.A. Biodegradable polyurethanes: Synthesis and applications in regenerative medicine. *Tissue Eng Part B: Reviews* 2008; 14(1): 3-17.

Hacking S.A., Khademhosseini A. Applications of microscale technologies for regenerative dentistry. *Journal of Dental Research* 2009; 88(5): 409-421.

Hasirci V., Litman A.E., Trantolo D.J., Gresser J.D., Wise D.L., Margolis H.C. PLGA bone plates reinforced with crosslinked PPF. *J Mater Sci Mater Med* 2002; 13(2): 159-167.

Hasirci V., Yucel D. Polymers Used in Tissue Engineering, in *Encyclopedia of Biomaterials and Biomedical Engineering* 2007, 1:1, 1-17.

Hauschka P.V., Mavrakos A.E., Iafrafi M.D., Doleman S.E., Klagsbrun M. Growth Factors in Bone Matrix. *J Biol Chem* 1986; 261(27): 12665-12674.

Haynesworth S.E., Goshima J., Goldberg V.M., Caplan A. Characterization of cells with osteogenic potential from human marrow. *Bone* 1992; 13: 81-88.

Hench L., Polak J. Third generation biomedical materials. *Science* 2002; 295: 1014–1017.

Hench L.L. *Biomaterials*. *Science* 1980; 208: 826–831.

Higuchi T. Rate of Release of Medicaments from Ointment Bases Containing Drugs in Suspensions. *J Pharm Sci* 1961; 50: 874-875.

Hiltunen A., Aro H.T., Vuorio E. Regulation of extracellular matrix genes during fracture healing in mice. *Clin Orthop Rel Res* 1993; 297: 23-27.

Ho M.H., Wang D.M., Hsieh H.J., Liu H.C., Hsien T.Y., Lai J.Y., Hou L.T. Preparation and characterization of RGD-immobilized chitosan scaffolds. *Biomaterials* 2005; 26(16): 3197-3206.

Hogan BL. Bone morphogenetic proteins: Multifunctional regulators of vertebrate development. *Genes Dev* 1996; 10: 1580–1594.

Hoque M.E., Hutmacher D.W., Feng W., Li S., Huang M.H., Vert M., Wong Y.S. Fabrication using a rapid prototyping system and in vitro characterization of PEG-PCL-PLA scaffolds for tissue engineering. *J Biomater Sci Polymer Edn* 2005; 16: 1595–1610.

Huang L., Nagapudi K., Apkarian R.P., Chaikof E.L. Engineered collagen-PEO nanofibers and fabrics. *J Biomater Sci Polym Ed* 2001; 12 (9): 979-93

Hughes F.J., Aubin J.E., Heersche J.N. Differential chemotactic responses of different populations of fetal rat calvaria cells to platelet-derived growth factor and transforming growth factor beta. *Bone Miner* 1992; 19: 63-74.

Hutmacher D., Hurzeler M.B., Schliephake H. A review of material properties of biodegradable and bioresorbable polymer for GTR and GBR. *J Oral Maxillofac Implants* 2000; 11: 667–678.

Hutmacher D.W., Sittinger M., Risbud M.V. Scaffold-based tissue engineering: Rationale for computer-aided design and solid free-form fabrication systems. *Trends Biotechnol* 2004; 22(7): 354-362.

Jaklenec A., Hinckfuss A., Bilgen B., Ciombor D.M., Aaron R., Mathiowitz E. Sequential release of bioactive IGF-I and TGF- β 1 from PLGA microsphere-based scaffolds. *Biomaterials* 2008; 29: 1518-1525.

Jeon O., Song S.J., Yang H.S., Bhang S.H., Kang S.W., Sung M.A., Lee J.H., Kim B.S. Long-term delivery enhances in vivo osteogenic efficacy of bone morphogenetic protein-2 compared to short-term delivery. *Biochem Biophys Res Comm* 2008; 369: 774-780.

Jose M.V., Thomas V., Dean D.R., Nyairo E. Fabrication and characterization of aligned nanofibrous PLGA/Collagen blends as bone tissue scaffolds, *Polymer* 2009; 50(15): 3778-3785

Jukes J.M., Both S.K., Leusink A., Sterk L.M., van Blitterswijk C.A., de Boer J. Endochondral bone tissue engineering using embryonic stem cells. *PNAS* 2008; 105(19): 6840-6845.

Kang S.W., Lim H.W., Seo S.W., Jeon O., Lee M., Kim B.S. Nanosphere-mediated delivery of vascular endothelial growth factor gene for therapeutic angiogenesis in mouse ischemic limbs. *Biomaterials* 2008; 29: 1109-1117.

Kato K., Eika Y., Ikada Y. Deposition of hydroxiapatite thin layer onto a polymer surface carrying grafted phosphate polymer chains. *J Biomed Mater Res* 1996; 32: 687-691.

Kawaguchi H., Kurokawa T., Hanada K., Hiyama Y., Tamura M., Ogata E., Matsumoto T. Stimulation of fracture repair by recombinant human basic fibroblast growth factor in normal and streptozotocin-diabetic rats. *Endocrinology* 1994; 135: 774-781.

Kawai T., Mieki A., Ohno Y., Umemura M., Kataoka H., Kurita S., Koie M., Jinde T., Hasagawa J., Urist MR. Osteoinductive activity of composites of bone morphogenetic protein and pure titanium. *Clin Orthop* 1993; 290: 296-305.

Kawakami T., Antoh M., Hasegawa H., Yamagishi T., Ito M., Eda S. Experimental study on osteoconductive properties of a chitosan-bonded hydroxyapatite self-hardening paste. *Biomaterials* 1992; 13: 759-763.

Kellomäki M., Niiranen H., Puumanen K., Ashammakhi N., Waris T., Törmälä P. Bioabsorbable scaffolds for guided bone regeneration and generation. *Biomaterials* 2000; 21(24): 2495-2505.

Kempen D.H.R., Lu L., Hefferan T.E., Creemers L.B., Maran A., Classic K.L., Dhert W.J.A., Yaszemski M.J. Retention of in vitro and in vivo BMP-2 bioactivities in sustained delivery vehicles for bone tissue engineering. *Biomaterials* 2008; 29: 3245-3252.

Kenar H., Torun Kose G., Hasirci V. Tissue Engineering Of Bone On Micropatterned Biodegradable Polyester Films. *Biomaterials* 2006; 27: 885-95.

Kenar H., Kocabas A., Aydinli A., Hasirci V. Chemical and topographical modification of PHBV surface to promote osteoblast alignment and confinement, *J Biomed Mater Res A* 2008; 85(4): 1001-1010.

Khan S.N., Fraser J.F., Sandhu H.S., Cammisa F.P., Girardi F.P., Lane J.M. Use of Osteopromotive Growth Factors, Demineralized Bone Matrix, and Ceramics to Enhance Spinal Fusion. *J Am Acad Orthop Surg* 2005; 13(2): 129-137.

Khor E., Lim L.Y. Implantable applications of chitin and chitosan. *Biomaterials* 2003; 24(13): 2339-2349.

Kim H.K., Chung H.J., Park T.G. Biodegradable polymeric microspheres with “open/closed” pores for sustained release of human growth hormone. *J Contr Release* 2006; 112: 167–174.

Kim S.S., Gwak S.J., Kim B.S. Orthotopic bone formation by implantation of apatite-coated poly(lactide-co-glycolide)/hydroxyapatite composite particulates and bone morphogenetic protein-2. *J Biomed Mater Res* 2008; 87A(1): 245-253.

Kimoto T., Hosokawa R., Kubo T., Maeda M., Sano A., Akagawa Y. Continuous administration of basic fibroblast growth factor (FGF-2) accelerates bone induction on rat calvaria—an application of a new drug delivery system. *J Dent Res* 1998; 77: 1965-1969.

Kinoshita Y., Kobayashi M., Hidaka T., Ikada Y. Reconstruction of mandibular continuity defects in dogs using poly (L- lactide) mesh and autogenic particulate cancellous bone and marrow: Preliminary report. *J Oral Maxillofac Surg* 1997; 55(7): 718-724.

Kok F., Hasirci V. Polyhydroxybutyrate And Its Copolymers: Applications In The Medical Field. In: Yaszemski, Trantolo, Lewandrovski, Hasirci, Altobelli, Wise, editors. *Tissue Engineering and Novel Delivery Systems*. CRC Press; 2003. p 543-562.

Kose G.T., Kenar H., Hasirci N, Hasirci V. Macroporous poly(3-hydroxybutyrate-co-3-hydroxyvalerate) matrices for bone tissue engineering. *Biomaterials* 2003; 24(11): 1949-1958.

Kose G.T., Korkusuz F., Korkusuz P., Hasirci V. In vivo tissue engineering of bone using poly(3-hydroxybutyric acid-co-3-hydroxyvaleric acid) and collagen scaffolds. *Tissue Eng* 2004; 10(7-8): 1234-1250.

Kose G.T., Korkusuz F., Korkusuz P., Purali N., Ozkul A., Hasirci V. Bone generation on PHBV matrices: An in vitro study. *Biomaterials* 2003; 24(27): 4999-5007.

Kose G.T., Korkusuz F., Ozkul A., Ber S., Kenar H., Hasirci V. Tissue engineering of bone using collagen and PHBV matrices. *Technology and Health Care* 2002; 10(3-4): 299-301.

Kumar R., Bakowsky U., Lehr C.M. Preparation and characterization of cationic PLGA nanospheres as DNA carriers. *Biomaterials* 2004; 25: 1771.

La Gatta A., De Rosa A., Laurienzo P., Malinconico M., De Rosa M., Schiraldi C. A novel injectable poly(ϵ -caprolactone)/calcium sulfate system for bone regeneration: Synthesis and characterization. *Macromol Biosci* 2005; 5(11): 1108-1117.

Lahiji A., Sohrabi A., Hungerford D.S., Frondoza C.G. Chitosan supports the expression of extracellular matrix proteins in human osteoblasts and chondrocytes. *J Biomed Mater Res* 2000; 51(4): 586-595.

Lam C.X.F., Mo X.M., Teoh S.H., Hutmacher D.W. Scaffold development using 3D printing with a starch-based polymer. *Mater Sci Eng C* 2002; 20(1): 49–56.

Lammens J., Liu Z., Aerssens J., Dequeker J., Fabry G. Distraction bone healing versus osteotomy healing: a comparative biochemical analysis. *J Bone Miner Res* 1998; 13: 279-286.

Landers R., Hübner U., Schmelzeisen R., Mülhaupt R. Rapid prototyping of scaffolds derived from thermoreversible hydrogels and tailored for applications in tissue engineering. *Biomaterials* 2002; 23(23): 4437-4447.

Langer R., Vacanti J.P. Tissue engineering. *Science* 1993; 260: 920-926.

Laurencin C, Khan Y., El-Amin S.F. Bone graft substitutes. *Expert Rev Med Devices* 2006; 3(1): 49-57.

Lazzeri L., Cascone M.G., Quiriconi S., Morabito L., Giusti P. Biodegradable hollow microfibres to produce bioactive scaffolds. *Polymer International* 2005; 54(1): 101-107.

Lee J.Y., Nam S.H., Im S.Y., Park Y.J., Lee Y.M., Seol Y.J., Chung C.P., Lee S.J. Enhanced bone formation by controlled growth factor delivery from chitosan-based biomaterials. *J Contr Rel* 2002; 78(1-3): 187-197.

Lee S.C., Shea M., Battle M.A., Kozitza K., Ron E., Turek T., Schaub R.G., Hayes W.C. Healing of large segmental defects in rat femurs is aided by RhBMP-2 in PLGA matrix. *J Biomed Mater Res* 1994; 28: 1149-1156.

Lee S.H., Shin H. Matrices and scaffolds for delivery of bioactive molecules in bone and cartilage tissue engineering. *Adv Drug Deliv Rev* 2007; 59: 339–359.

Lee S.J., Park Y.J., Park S.N., Lee Y.M., Seol Y.J., Ku Y., Chung C.P. Molded porous poly (L-lactide) membranes for guided bone regeneration with enhanced effects by controlled growth factor release. *J Biomed Mater Res* 2001; 55(3): 295-303.

Lemaire V., Belair J., Hildgen P. Structural modeling of drug release from biodegradable porous matrices based on a combined diffusion/erosion process. *Int J Pharm* 2003; 258: 95–107.

Lewandrowski K.U., Bondre S., Hile D.D., Thompson B.M.J., Wise D.L., Tomford W.W., Trantolo D.J. Porous poly(propylene fumarate) foam coating of orthotopic cortical bone grafts for improved osteoconduction. *Tissue Eng* 2002; 8(6): 1017-1027.

Leyh R.G., Wilhelmi M., Rebe P., Fischer S., Kofidis T., Haverich A., Mertsching H. In vivo repopulation of xenogeneic and allogeneic acellular valve matrix conduits in the pulmonary circulation. *Ann Thorac Surg* 2003; 75(5): 1457-1463.

Li M., Mondrinos M.J., Chen X., Gandhi M.R., Ko F.K., Lelkes P.I. Co-electrospun poly(lactide-co-glycolide), gelatin, and elastin blends for tissue engineering scaffolds. *J Biomed Mater Res* 2006; 79A(4): 963-973.

Li R.H., Wozney J.M. Delivering on the promise of bone morphogenetic proteins. *Trends Biotechnol* 2001; 19: 255–265.

Li W.J., Tuli R., Okafor C., Derfoul A., Danielson K.G., Hall D.J., Tuan R.S. A three-dimensional nanofibrous scaffold for cartilage tissue engineering using human mesenchymal stem cells. *Biomaterials* 2005; 26: 599-609.

Linkhart T.A., Mohan S., Baylink D.J. Growth factors for bone growth and repair: IGF, TGF beta and BMP. *Bone* 1996; 19(1): 1-12.

Lisignoli G., Fini M., Giavaresi G., Nicoli Aldini N., Toneguzzi S., Facchini A. Osteogenesis of large segmental radius defects enhanced by basic fibroblast growth factor activated bone marrow stromal cells grown on non-woven hyaluronic acid-based polymer scaffold. *Biomaterials* 2002; 23(4): 1043-1051.

Liu L., Zhang L., Ren B., Wang F., Zhang Q. Preparation and Characterization of Collagen-Hydroxyapatite Composite Used for Bone Tissue Engineering Scaffold. *Artificial Cells, Blood Substitutes, and Immobilization Biotechnology* 2003; 31(4): 435-448.

Liu Z., Luyten F.P., Lammens J., Dequeker J. Molecular signaling in bone fracture healing and distraction osteogenesis. *Histol Histopathol* 1999; 14: 587-595.

Lootz D., Behrend D., Kramer S., Freier T., Haubold A., Benkieser G., Schmitz K.P., Becher B. Laser cutting: Influence on morphological and physicochemical properties of polyhydroxybutyrate. *Biomaterials* 2001; 22(18): 2447-2452.

Lu L., Peter S.J., Lyman M.D., Lai H.L., Leite S.M., Tamada J.A., Uyama S., Vacanti J.P., Ma Z., Gao C., Gong Y., Ji J., Shen J. Immobilization of natural

macromolecules on poly-L-lactic acid membrane surface in order to improve its cytocompatibility. *J Biomed Mater Res* 2002; 63: 838–847.

Lu L., Peter S.J., Lyman M.D., Lai H.L., Leite S.M., Tamada J.A., Uyama S., Vacanti J.P., Langer R., Mikos A.G. In vitro and in vivo degradation of porous poly(DL-lactic-co-glycolic acid) foams. *Biomaterials* 2000; 21(18): 1837-1845.

Ma Z., Gao C., Gong Y., Ji J., Shen J. Immobilization of natural macromolecules on poly-l-lactic acid membrane surface in order to improve its cytocompatibility. *J Biomed Mater Res* 2002; 63: 838–847.

Ma Z., He W., Yong T., Ramakrishna S. Grafting of gelatin on electrospun poly(caprolactone) nanofibers to improve endothelial cell spreading and proliferation and to control cell orientation. *Tissue Eng* 2005; 11(7-8): 1149-1158.

Maatz R., Bauermeister A., A Method of Bone Maceration: Results in Animal Experiments. *J Bone Joint Surg Am* 1957; 39: 153-166.

Maher P.S., Keatch R.P., Donnelly K., MacKay R.E., Paxton J.Z. Construction of 3D biological matrices using rapid prototyping technology. *Rapid Prototyping Journal* 2009; 15(3): 204-210.

Mankin H.J., Springfield D.S., Gebhardt B.C., Tomford W. Current status of allografting for bone tumors. *Orthopedics* 1992; 15: 1147-1154.

Marden L.J., Fan R.S., Pierce G.F., Reddi A.H., Hollinger J.O. Platelet-derived growth factor inhibits bone regeneration induced by osteogenin, a bone morphogenetic protein, in rat craniotomy defects. *J Clin Invest* 1993; 92: 2897-2905.

Marieb E.N., Hoehn K. *Human Anatomy & Physiology* 7th Edition, San Francisco, Benjamin Cummings, 2007.

Marques A.P., Reis R.L., Hunt J.A. The biocompatibility of novel starch-based polymers and composites: In vitro studies. *Biomaterials* 2002; 23(6): 1471-1478.

Marra K.G., Szem J.W., Kumta P.N., DiMilla P.A., Weiss L.E. In Vitro Analysis of Biodegradable Polymer Blend/Hydroxyapatite Composites for Bone Tissue Engineering. *J Biomed Mater Res* 1999; 47: 324–335.

Martino A.D., Sittinger M., Risbud M.V. Chitosan: a versatile biopolymer for orthopaedic tissue-engineering. *Biomaterials* 2005; 26: 5983–5990.

Martins A., Chung S., Pedro A.J., Sousa R.A., Marques A.P., Reis R.L., Neves N.M. Hierarchical starch-based fibrous scaffold for bone tissue engineering applications. *J Tissue Eng Regen Med* 2009; 3(1): 37-42.

Matsumoto T., Okazaki M., Inoue M., Yamaguchi S., Kusunose T., Toyonaga T., Hamada Y., Takahashi J. Hydroxyapatite particles as a controlled release carrier of protein. *Biomaterials* 2004; 25: 3807-3812.

Matthews J.A., Wnek G.E., Simpson D.G., Bowlin G.L. Electrospinning of collagen nanofibers. *Biomacromolecules*. 2002; 3 (2): 232-8

Mayer H., Scutt A.M., Ankenbauer T. Subtle differences in the mitogenic effects of recombinant human bone morphogenetic proteins-2 to -7 on DNA synthesis in primary bone-forming cells and identification of BMP-2/4 receptor. *Calcif Tissue Int* 1996; 58: 249-255.

McKay W.F., Peckham S.M., Badura J.M. A comprehensive clinical review of recombinant human bone morphogenetic protein-2 (INFUSE® Bone Graft). *Int Orthop* 2007; 31: 729-734.

Mehrara B.J., Rowe N.M., Steinbrech D.S., Dudziak M.E., Saadeh P.B., McCarthy J.G., Gittes G.K., Longaker M.T. Rat mandibular distraction osteogenesis: II. Molecular analysis of transforming growth factor beta-1 and osteocalcin gene expression. *Plast Reconstr Surg* 1999; 103: 536-547.

Meinel L., Fajardo R., Hofmann S., Langer R., Chen J., Snyder B., Vunjak-Novakovic G., Kaplan D. Silk implants for the healing of critical size bone defects. *Bone* 2005; 37(5): 688-698.

Mikos A.G., Sarakinos G., Leite S.M., Vacanti J.P., Langer R. Laminated three-dimensional biodegradable foams for use in tissue engineering. *Biomaterials* 1993; 14: 323-330.

Mironov V., Boland T., Trusk T., Forgacs G., Markwald R.R. Organ printing: computer-aided jet-based 3D tissue engineering. *Trends Biotechnol* 2003; 21 (4): 157-61

Miura Y., O'Driscoll S.W. Culturing periosteum in vitro: The influence of different sizes of explants. *Cell Transplant* 1998; 7: 453-457.

Mori T., Okumura M., Matsuura M., Ueno K., Tokura S., Okamoto Y. Effects of chitin and its derivatives on the proliferation and cytokine production of fibroblasts in vitro. *Biomaterials* 1997; 18: 947-951.

Moroni L., Curti M., Welti M., Korom S., Weder W., De Wijn J.R., Van Blitterswijk C.A. Anatomical 3D fiber-deposited scaffolds for tissue engineering: designing a neotrachea. *Tissue Eng* 2007; 13(10): 2483-2493.

Moroni L., de Wijn J.R., van Blitterswijk C.A. 3D fiber-deposited scaffolds for tissue engineering : Influence of pores geometry and architecture on dynamic mechanical properties. *Biomaterials* 2006; 27: 974-985.

- Navarro M., Michiardi A., Castano O., Planell J.A. Biomaterials in orthopaedics. *R Soc Interface* 2008; 5: 1137–1158.
- Ndreu A., Nikkola L., Ylikauppila H., Ashammakhi N., Hasirci V. Electrospun biodegradable nanofibrous mats for tissue engineering. *Nanomedicine* 2008; 3: 45-60.
- Nefussi J.R., Brami G., Modrowski D., Oboeuf M., Forest N. Sequential expression of bone matrix proteins during rat calvaria osteoblast differentiation and bone nodule formation in vitro. *J Histochem Cytochem* 1997; 45: 493–503.
- Nelson K.D., Romero A., Waggoner P., Crow B., Borneman A., Smith G.M. Technique Paper for Wet-Spinning Poly(L-lactic acid) and Poly(DL-lactide-co-glycolide) Monofilament Fibers. *Tissue Eng* 2003; 9(6): 1323-1330.
- Nigiam M., Liao S., Patil A.J., Cheng Z., Chan C.K., Ramakrishna S. The fabrication of nano-hydroxyapatite on PLGA and PLGA/collagen nanofibrous composite scaffolds and their effects in osteoblastic behavior for bone tissue engineering. *Bone* 2009; 45(1): 4-16.
- Niemeyer P., Seckinger A., Simank H.G., Kasten P., Sudkamp N., Krause U. Allogenic transplantation of human mesenchymal stem cells for tissue engineering purposes: an in vitro study. *Orthopade* 2004; 33 (12): 1346-1353.
- Nishimura K., Nishimura S., Nishi N., Saiki I., Tokura S., Azuma I. Immunological activity of chitin and its derivatives. *Vaccine* 1984; 2: 93–99.
- Nishimura T., Utsunomiya Y., Hoshikawa M., Ohuchi H., Itoh N. Structure and expression of a novel human FGF, FGF-19, expressed in the fetal brain. *Biochim Biophys Acta* 1999; 1444: 148-151.
- Norotte C., Marga F.S., Niklason L.E., Forgacs G. Scaffold-free vascular tissue engineering using bioprinting. *Biomaterials* 2009; Article in Press.
- Nystrom E., Ahlqvist J., Legrell P.E., Kahnberg K.E. Bone graft remodelling and implant success rate in the treatment of the severely resorbed maxilla: a 5-year longitudinal study. *Int J Oral Maxillofac Surg* 2002; 31(2): 158-164.
- Oh S.H., Kim J.H., Kim J.M., Lee J.H. Asymmetrically porous PLGA/Pluronic F127 membrane for effective guided bone regeneration. *J Biomater Sci Polymer Ed* 2006; 17(12): 1375-1387.
- Ohlendorf C., Tomford W., Mankin H.J. Chondrocyte survival in cryopreserved osteochondral articular cartilage. *J Orthop Res* 1996; 14: 413-416.

Okamoto Y., Minami S., Matsushashi A., Sashiwa H., Saimoto H., Shigemasa Y. Polymeric N acetyl-d-glucosamine (Chitin) induces histionic activation in dogs. *J Vet Med Sci* 1993; 55: 739–742.

Oliveira A.L., Malafaya P.B., Costa S.A., Sousa R.A., Reis R.L. Micro-computed tomography (micro-CT) as a potential tool to assess the effect of dynamic coating routes on the formation of biomimetic apatite layers on 3D-plotted biodegradable polymeric scaffolds. *J Mater Sci Mater Med* 2007; 18(2): 211-223.

Olivier J.C. *The Journal of the American Society for Experimental NeuroTherapeutics* 2005; 2: 108.

Oyane A., Uchida M., Yokoyama Y., Choong C., Triffitt J., Ito A. Simple surface modification of poly(ϵ -caprolactone) to induce its apatite-forming ability. *J Biomed Mater Res* 2005a; 75A(1): 138-145.

Oyane A., Uchida M., Choong C., Triffitt J., Jones J., Ito A. Simple surface modification of poly(ϵ -caprolactone) for apatite deposition from simulated body fluid. *Biomaterials* 2005b; 26(15): 2407-2413.

Parikh S.N. Bone graft substitutes: past, present, future. *J Postgrad Med* 2002; 48: 142-148.

Park E.K., Lee S.B., Lee Y.M. Preparation and characterization of methoxy poly(ethylene glycol)/poly(ϵ -caprolactone) amphiphilic block copolymeric nanospheres. *Biomaterials* 2005; 26: 1053-1061.

Park H., Lee K.Y., Lee S.J., Park K.E., Park W.H. Plasma-treated poly(lactic-co-glycolic acid) nanofibers for tissue engineering. *Macromolecular Research* 2007; 15(3): 238-243.

Park Y.J., Lee Y.M., Park S.N., Lee J.Y., Ku Y., Chung C.P., Lee S.J. Enhanced guided bone regeneration by controlled tetracycline release from poly(L-lactide) barrier membranes. *J Biomed Mater Res* 2000; 51(3): 391-397.

Patel Z.S., Yamamoto M., Ueda H., Tabata Y., Mikos A.G. Biodegradable gelatin microparticles as delivery systems for the controlled release of bone morphogenetic protein-2. *Acta Biomater* 2008a; 4: 1126–1138.

Patel Z.S., Young S., Tabata Y., Jansen J.A., Wong M.E.K., Mikos A.G. Dual delivery of an angiogenic and an osteogenic growth factor for bone regeneration in a critical size defect model. *Bone* 2008b; 43: 931–940.

Payne R.G., McGonigle J.S., Yaszemski M.J., Yasko A.W., Mikos A.G. Development of an injectable, in situ crosslinkable, degradable polymeric carrier for osteogenic cell populations. Part 3. Proliferation and differentiation of encapsulated

marrow stromal osteoblasts cultured on crosslinking poly(propylene fumarate). *Biomaterials* 2002; 23(22): 4381–4387.

Peltola S.M., Melchels F.P.W., Grijpma D.W., Kellomäki M. A review of rapid prototyping techniques for tissue engineering purposes. *Ann Med* 2008; 40(4): 268-280.

Peter S.J., Lu L., Kim D.J., Stamatias G.N., Miller M.J., Yaszemski M.J., Mikos A.G. Effects of transforming growth factor b1 released from biodegradable polymer microparticles on marrow stromal osteoblasts cultured on poly(propylene fumarate) substrates. *J Biomed Mater Res* 2000; 50: 452–462.

Peterson B., Whang P.G., Iglesias R., Wang J.C., Lieberman J.R. Osteoinductivity of Commercially Available Demineralized Bone Matrix. *J Bone Joint Surg Am* 2004; 86: 2243-2250.

Pfeilschifter J., Seyedin S.M., Mundy G.R. Transforming growth factor beta inhibits bone resorption in fetal rat long bone cultures. *J Clin Invest* 1988; 82: 680-685.

Pitt C.G. Poly(ϵ -caprolactone) and its copolymers. in: *Biodegradable Polymers as Drug Delivery Systems*, M. Chasin and R. Langer (Eds) Marcel Dekker, New York, NY, 1990, p. 71-120.

Porter J.R., Henson A., Popat K.C. Biodegradable poly(ϵ -caprolactone) nanowires for bone tissue engineering applications. *Biomaterials* 2009; 30(5): 780-788.

Qiu Y., Zhang N., Kang Q., An Y., Wen X. Chemically modified light-curable chitosans with enhanced potential for bone tissue repair. *J Biomed Mater Res A* 2009; 89(3): 772-779.

Rai B., Teoh S.H., Hutmacher D.W., Cao T., Ho K.H. Novel PCL-based honeycomb scaffolds as drug delivery systems for rhBMP-2. *Biomaterials* 2005; 26: 3739-3748.

Raiche A.T., Puleo D.A. In vitro effects of combined and sequential delivery of two bone growth factors. *Biomaterials* 2004; 25: 677–685.

Raisz, L.G., Simmons, H.A., Sandberg, A.L., and Canalis, E. Direct stimulation of bone resorption by epidermal growth factor. *Endocrinology* 1980; 107: 270-273.

Raschke M., Wildemann B., Inden P., Bail H., Flyvbjerg A., Hoffmann J., Haas N.P., Schmidmaier G. Insulin-like growth factor-1 and transforming growth factor- β 1 accelerates osteotomy healing using polylactide-coated implants as a delivery system: a biomechanical and histological study in minipigs. *Bone* 2002; 30: 144–151.

Rasubala L., Yoshikawa H., Nagata K., Iijima T., Ohishi M. Platelet-derived growth factor and bone morphogenetic protein in the healing of mandibular fractures in rats. *Br J Oral Maxillofac Surg* 2003; 41: 173-178.

Ren T., Ren J., Jia X., Pan K. The bone formation in vitro and mandibular defect repair using PLGA porous scaffolds. *J Biomed Mater Res* 2005; 74A(4): 562-569.

Robey P.G., Termine J.D. Human bone cells in vitro. *Calcif Tissue Int* 1985; 37: 453-460.

Rohner D., Huttmacher D.W., Cheng T.K., Oberholzer M., Hammer B., J. In vivo efficacy of bone marrow coated polycaprolactone scaffolds for the reconstruction of orbital defects in the pig. *J Biomed Mater Res Part B: Appl Biomater* 2003; 66B: 574-580.

Sahoo S.K., Labhassetwar V. Nanotech approaches in drug delivery and Imaging. *Drug Discovery Today* 2003; 8(24): 1112-1120.

Saito N, Murakami N, Takahashi J, Horiuchi H, Ota H, Kato H, Okada T, Nozaki K, Takaoka K. Synthetic biodegradable polymers as drug delivery systems for bone morphogenetic proteins. *Adv Drug Deliv Rev* 2005; 57:1037- 1048.

Salgado A.J., Coutinho O.P., Reis R.L., Davies J.E. In vivo response to starch-based scaffolds designed for bone tissue engineering applications. *J Biomed Mater Res A* 2007; 80(4): 983-989.

Sandberg M.M., Aro H.T., Vuorio E.I. Gene expression during bone repair. *Clin Orthop Rel Res* 1993; 289: 292-312.

Santos M.I., Fuchs S., Gomes M.E., Unger R.E., Reis R.L., Kirkpatrick C.J. Response of micro- and macrovascular endothelial cells to starch-based fiber meshes for bone tissue engineering. *Biomaterials* 2007; 28: 240-248.

Santos M.I., Tuzlakoglu K., Fuchs S., Gomes M.E., Peters K., Unger R.E., Piskin E., Reis R.L., Kirkpatrick C.J., Endothelial cell colonization and angiogenic potential of combined nano- and micro-fibrous scaffolds for bone tissue engineering. *Biomaterials* 2008; 29(32): 4306-4313.

Schantz J.-T., Brandwood A., Huttmacher D.W., Khor H.L., Bittner K. Osteogenic differentiation of mesenchymal progenitor cells in computer designed fibrin-polymer-ceramic scaffolds manufactured by fused deposition modeling. *J Mater Sci Mater Med* 2005; 16(9): 807-819.

Schieker M., Seitz H., Drosse I., Seitz S., Mutschler W. Biomaterials as Scaffold for Bone Tissue Engineering. *Eur J Trauma* 2006; 32: 114-124.

Schrier J.A., Fink B.F., Rodgers J.B., Vasconez H.C., DeLuca P.P. Effect of a Freeze-Dried CMC/PLGA Microsphere Matrix of rhBMP-2 on Bone Healing. *AAPS PharmSciTech* 2001; 2: article 18.

Schug T., Rodemer H., Neupert W., Dumbach J. Treatment of complex mandibular fractures using titanium mesh. *J Craniomaxillofac Surg* 2000; 28(4): 235-237.

Se H.O., Soung G.K., Jin H.L. Degradation behavior of hydrophilized PLGA scaffolds prepared by melt-molding particulate-leaching method: Comparison with control hydrophobic one. *J Mater Sci Mater Med* 2006; 17: 131-137.

Seetharam L., Gotoh N., Maru Y., Neufeld G., Yamaguchi S., Shibuya M. A unique signal transduction from FLT tyrosine kinase, a receptor for vascular endothelial growth factor VEGF. *Oncogene* 1995; 10: 135-147.

She H., Xiao X., Liu R. Preparation and characterization of polycaprolactone-chitosan composites for tissue engineering applications. *Journal of Materials Science* 2007; 42(19): 8113-8119

Shen H., Hu X., Bei J., Wang S. The immobilization of basic fibroblast growth factor on plasma-treated poly(lactide-co-glycolide). *Biomaterials* 2008; 29(15): 2388-2399.

Sherwood J.K., Riley S.L., Palazzolo R., Brown S.C., Monkhouse D.C., Coates M., Griffith L.G., Ratcliffe A. A three-dimensional osteochondral composite scaffold for articular cartilage repair. *Biomaterials* 2002; 23(24): 4739-4751.

Shishatskaya E.I., Khlusov I.A., Volova T.G. A hybrid PHB-hydroxyapatite composite for biomedical application: Production, in vitro and in vivo investigation. *J Biomater Sci Polymer Ed* 2006; 17(5): 481-498.

Shor L., Güçeri S., Wen X., Gandhi M., Sun W. Fabrication of three-dimensional polycaprolactone/hydroxyapatite tissue scaffolds and osteoblast-scaffold interactions in vitro. *Biomaterials* 2007; 28(35): 5291-5297.

Simmons C.A., Alsberg E., Hsiong S., Kim W.J., Mooney D.J. Dual growth factor delivery and controlled scaffold degradation enhance in vivo bone formation by transplanted bone marrow stromal cells. *Bone* 2004; 35: 562-569.

Singla A.K., Chawla M. Chitosan: some pharmaceutical and biological aspects—an update. *Pharm Pharmacol* 2001; 53: 1047–1067.

Spaans C.J., Belgraver V.W., Rienstra O., de Groot J.H., Veth R.P.H., Pennings A.J. Solvent-free fabrication of micro-porous polyurethane amide and polyurethane-urea scaffolds for repair and replacement of the knee-joint meniscus. *Biomaterials* 2000; 21: 2453–2460.

Spence A. Basic Medical Anatomy 1990, 3rd ed. Redwood City, CA: Benjamin/Cummings.

Spencer E.M., Liu C.C., Si E.C., Howard G.A. In vivo actions of insulin-like growth factor-I (IGF-I) on bone formation and resorption in rats. *Bone* 1991; 12: 21-26.

Stein G.S., Lian J.B. Molecular mechanisms mediating proliferation/differentiation interrelationships during progressive development of the osteoblast phenotype. *Endocrine Reviews* 1993; 14(4): 424-441.

Sun W., Darling A., Starly B., Nam J. Computer aided tissue engineering: overview, scope and challenges. *J Biotech Appl Biochem* 2004a; 39: 29-47.

Sun W., Starly B., Darling A., Gomez C. Computer-aided tissue engineering: application to biomimetic modelling and design of tissue scaffolds. *J Biotech Appl Biochem* 2004b; 39: 49-58.

Sutherland D., Bostrom M., *Grafts and Bone Graft Substitutes, from Bone regeneration and Repair: Biology and Clinical Applications.* Ed. Lieberman J.B., Friedlaender G.E, Humana Press, USA, 133-156. 2005.

Sutula L.C., Collier J.P., Saum K.A., Currier B.H., Currier J.H., Sanford W.M., Mayor M.B., Wooding R.E., Sperling D.K., Williams I.R. Impact of gamma sterilization on clinical performance of polyethylene in the hip. *Clin Orthop* 1995; 319: 28-40.

Tabata Y., Yamada K., Miyamoto S., Nagata I., Kikuchi H., Aoyama I., Tamura M., Ikada Y. Bone regeneration by basic fibroblast growth factor complexed with biodegradable hydrogels. *Biomaterials* 1998; 19: 807-815.

Tamama K., Fan V.H., Griffith L.G., Blair H.C., Wells A. Epidermal growth factor as a candidate for ex vivo expansion of bone marrow-derived mesenchymal stem cells. *Stem Cells* 2006; 24: 686-695.

Tanigawa T., Tanaka Y., Sashiwa H., Saimoto H., Shigemasa Y. Various biological effects of chitin derivatives. In: C.J. Brine, P.A. Sandford and J.P. Zikakis, Editors, *Advances in chitin and chitosan*, Elsevier, pp. 206-215, 1992.

Tavakoli K., Yu Y., Shahidi S., Bonar F., Walsh W.R., Poole M.D. Expression of growth factors in the mandibular distraction zone: a sheep study. *Br J Plast Surg* 1999; 52: 434-439.

Temenoff J.S., Mikos A.G. Tissue engineering for regeneration of articular cartilage. *Biomaterials* 2000; 21: 431-440.

Tesema Y., Raghavan D., Stubbs J. Bone cell viability on collagen immobilized poly (3-hydroxybutrate-co-3-hydroxyvalerate) membrane: effect of surface chemistry. *J Appl Polym Sci* 2004; 93: 2445-53.

Tokura S., Ueno K., Miyazaki S., Nishi N. Molecular weight dependent antimicrobial activity by chitosan. *Macromol Symp* 1997; 120: 1-9.

Tombran-Tink J., Barnstable C.J. Osteoblasts and osteoclasts express PEDF, VEGF-A isoforms, and VEGF receptors: possible mediators of angiogenesis and matrix remodeling in the bone. *Biochem Biophys Res Commun* 2004; 316: 573-579.

Tomford W., Springfield D.S., Mankin H.J. Fresh and frozen articular cartilage allografts. *Orthopedics* 1992; 15: 1183-1188.

Tuzlakoglu K., Alves C.M., Mano J.F., Reis R.L., Production and characterization of chitosan fibers and 3-D fiber mesh scaffolds for tissue engineering applications, *Macromol Biosci* 2004; 4(8): 811-819.

Tuzlakoglu K., Bolgen N., Salgado A.J., Gomes M.E., Piskin E., Reis R.L. Nano- and micro-fiber combined scaffolds: A new architecture for bone tissue engineering. *J Mater Sci Mater Med* 2005; 16: 1099-1104.

Tuzlakoglu K., Reis R.L., Formation of bone-like apatite layer on chitosan fiber mesh scaffolds by a biomimetic spraying process. *J Mater Sci Mater Med* 2007; 18(7): 1279-1286.

Urist M.R. Bone morphogenetic protein: the molecularization of skeletal system development. *J Bone Miner Res* 1997; 12: 332-342.

Urist MR. Bone: Formation by autoinduction. *Science* 1965;150:893-899.

van der Zee E., Jansen I., Hoeben K., Beertsen W., Everts V. EGF and IL-1 alpha modulate the release of collagenase, gelatinase and TIMP-1 as well as the release of calcium by rabbit calvarial bone explants. *J Periodontal Res* 1998; 33: 65-72.

van Meekeren, J. Heel-en Geneeskunstige Aanmerkingen. Commelijjn, 1668.

Vandevord P.J., Matthew H.W.T., Desilva S.P., Mayton L., Wu B., Wooley P.H. Evaluation of the biocompatibility of a chitosan scaffold in mice. *J Biomed Mater Res* 2002; 59(3): 585-590.

Venugopal J., Vadgama P., Sampath Kumar T.S., Ramakrishna S. Biocomposite nanofibres and osteoblasts for bone tissue engineering. *Nanotechnology* 2007; 18(5): art. no. 055101

Verma D., Katti K., Katti D. Bioactivity in in situ hydroxyapatite-polycaprolactone composites. *J Biomed Mater Res* 2006; 78A(4): 772-780.

Wada Y., Kataoaka H., Yokose S., Ishizuya T., Miyazono K. Changes in osteoblast phenotype during differentiation of enzymatically isolated rat calvaria cells. *Bone* 1998; 22: 479-485.

Walsh D., Furuzono T., Tanaka J. Preparation of porous composite implant materials by in situ polymerization of porous apatite containing ϵ -caprolactone or methyl methacrylate. *Biomaterials* 2001; 22(11): 1205-1212.

Wang E.A., Rosen V., D'Alessandro J.S., Bauduy M., Cordes P., Harada T., Israel D.I., Hewick R.M., Kerns K.M., LaPan P., Luxenberg D.P., McQuaid D., Moutsatsos I.K., Nove J., Wozney J.M. Recombinant human bone morphogenetic protein induces bone formation. *Proc Natl Acad Sci USA* 1990; 87: 2220-2224.

Wang L., Shelton R.M., Cooper P.R., Lawson M., Triffitt J.T., Barralet J.E. Evaluation of sodium alginate for bone marrow cell tissue engineering. *Biomaterials* 2003; 24(20): 3475-3481.

Wang Y., Lu L., Zheng Y., Chen X. Improvement in hydrophilicity of PHBV films by plasma treatment. *J Biomed Mater Res A* 2006; 76: 589-595.

Wang Y.J., Lin F.H., Sun J.S., Huang Y.C., Chueh S.C., Hsu F.Y. Collagen-hydroxyapatite microspheres as carriers for bone morphogenetic protein-4. *Artif Organs* 2003; 27: 162-168.

Webb P.A. A review of rapid prototyping (RP) techniques in the medical and biomedical sector. *J Med Eng Tech* 2000; 24(4): 149-153.

Wei G., Jin Q., Giannobile W.V., Ma P.X. The enhancement of osteogenesis by nano-fibrous scaffolds incorporating rhBMP-7 nanospheres. *Biomaterials* 2007; 28: 2087-2096.

White A.P., Vaccaro A.R., Hall J.A., Whang P.G., Friel B.C., McKee M.D. Clinical applications of BMP-7/OP-1 in fractures, non-unions and spinal fusion. *Int Orthop* 2007; 31: 735-741.

Williams J.M., Adewunmi A., Schek R.M., Flanagan C.L., Krebsbach P.H., Feinberg S.E., Hollister S.J., Das S. Bone Tissue Engineering using Polycaprolactone Scaffolds Fabricated via Selective Laser Sintering. *Biomaterials* 2005; 26: 4817-4827.

Williamson M.R., Coombes A.G.A. Gravity spinning of polycaprolactone fibres for applications in tissue engineering. *Biomaterials* 2004; 25(3): 459-465.

Wiria F.E., Leong K.F., Chua C.K., Liu Y. Poly- ϵ -caprolatone/hydroxyapatite for tissue engineering scaffold fabrication using selective laser sintering. *Acta Biomater* 2007; 3: 1–12.

Wu Q., Wang Y., Chen G.Q. Medical application of microbial biopolyesters polyhydroxyalkanoates. *Artificial Cells, Blood Substitutes, and Biotechnology* 2009; 37(1): 1-12.

Wu T.P., Hu P., Zhang X.B., Li W., Chen F. Biocompatibility of modified poly beta-hydroxybutyric acid to adrenocortical cells. *J Wuhan Univ Tech-Mater Sci Ed* 2004; 19: 38-40.

Xiao Y., Qian H., Young W.G., Bartold P.M. Tissue Engineering for Bone Regeneration Using Differentiated Alveolar Bone Cells in Collagen Scaffolds. *Tissue Eng* 2003; 9(6): 1167-1177.

Xiong Z., Yan Y., Wang S., Zhang R., Zhang C. Fabrication of porous scaffolds for bone tissue engineering via low-temperature deposition. *Scr Mater* 2002; 46: 771-776.

Yang Q., Peng J., Guo Q.Y., Huang J.X., Yang F., Wang S.G., Lu, S.-B. Preparation and assessment of plasma-treated collagen-anchored poly(lactic-co-glycolic acid)/acellular bone matrix bilayered scaffold. *Journal of Clinical Rehabilitative Tissue Engineering Research* 2007; 11(48): 9646-9650.

Yang X., Shah J.D., Wang H. Nanofiber enabled layer-by-layer approach toward three-dimensional tissue formation. *Tissue Eng Part A* 2009; 15(4): 945-956.

Ye S.H., Watanabe J., Takai M., Iwasaki Y., Ishihara K. Design of functional hollow fiber membranes modified with phospholipid polymers. *Biomaterials* 2005; 26(24): 5032-5041.

Yeh L.C., Zavala M.C., Lee J.C. Osteogenic protein-1 and interleukin-6 with its soluble receptor synergistically stimulate rat osteoblastic cell differentiation. *J Cell Physiol* 2002; 190: 322–31.

Yeong W.Y., Chua C.K., Leong K.F., Chandrasekaran M. Rapid prototyping in tissue engineering: challenges and potential. *Trends Biotechnol* 2004; 22: 643-652.

Yildirim E.D., Gandhi M., Fridman A., Güçeri S., Sun W. Plasma surface modification of three dimensional poly (ϵ -caprolactone) scaffolds for tissue engineering application. *NATO Security through Science Series A: Chemistry and Biology* 2008; 191-201.

Yin Y., Ye F., Cui J., Zhang F., Li X., Yao K. Preparation and characterization of macroporous chitosan-gelatin/ β -tricalcium phosphate composite scaffolds for bone tissue engineering. *J Biomed Mater Res* 2003; 67A(3): 844-855.

Yoon E., Dhar S., Chun D.E., Gharibjanian N.A., Evans G.R.D. In vivo osteogenic potential of human adipose-derived stem cells/poly lactide-co-glycolic acid constructs for bone regeneration in a rat critical-sized calvarial defect model. *Tissue Eng* 2007; 13(3): 619-627.

Younger E.M., Chapman M. Morbidity at bone graft donor sites. *J Orthop Trauma* 1989; 3: 192-195.

Yu H.S., Jang J.H., Kim T.I., Lee H.H., Kim H.W. Apatite-mineralized polycaprolactone nanofibrous web as a bone tissue regeneration substrate. *J Biomed Mater Res* 2009; 88(3): 747-754

Zhang H., Lin C.Y., Hollister S.J., The interaction between bone marrow stromal cells and RGD-modified three-dimensional porous polycaprolactone scaffolds. *Biomaterials* 2009; 30(25): 4063-4069.

Zhang K., Zhang M. Calcium phosphate/chitosan composite scaffolds for controlled in vitro antibiotic drug release. *J Biomed Mater Res* 2002; 62: 378–786.

Zhang Z., Chen J., Jin D. Platelet-derived growth factor (PDGF)-BB stimulates osteoclastic bone resorption directly: the role of receptor beta. *Biochem Biophys Res Commun* 1998; 251: 190.

Zhao J., Zhang Z., Wang S., Sun X., Zhang X., Chen J., Kaplan D.L., Jiang X. Apatite-coated silk fibroin scaffolds to healing mandibular border defects in canines. *Bone* 2009, article in press.

Zimmerman L.B., de Jesus-Escobar J.M., Harland R.M. The Spemann organizer signal noggin binds and inactivates bone morphogenetic protein 4. *Cell* 1996; 86: 599.

Zolnik B.S., Leary P.E., Burgess D.J. Elevated temperature accelerated release testing of PLGA microspheres. *J Contr Release* 2006; 112: 293–300.

APPENDIX A

CALIBRATION CURVE FOR BSA CONCENTRATION DETERMINATION

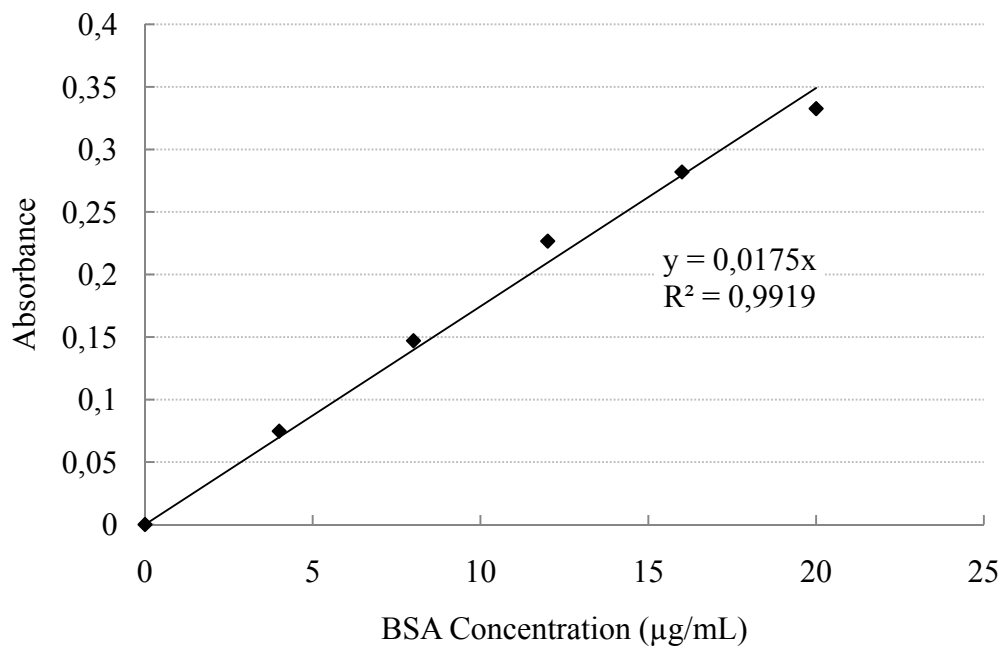


Figure A.1. Calibration curve of BSA concentration for Micro-Bradford Assay.

APPENDIX B

CALIBRATION CURVE FOR CELL NUMBER DETERMINATION

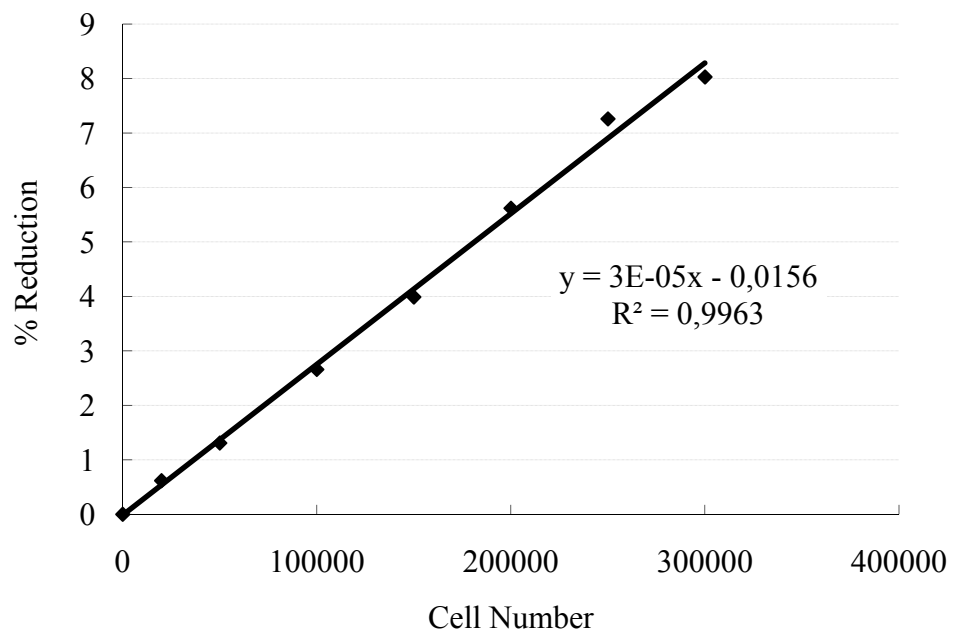


Figure B.1. Calibration curve of rat bone marrow MSCs for Alamar Blue Assay.

APPENDIX C

ETHICAL COMMITTEE APPROVAL

 T.C.
GAZİ ÜNİVERSİTESİ
REKTÖRLÜĞÜ
Hayvan Deneyleri Yerel Etik Kurul Başkanlığı

SAYI : B.30.2.GÜN.0.05.06.00/13-2561
KONU:
Sayın
Prof.Dr.Vasif HASIRCI
ODTÜ Biyolojik Bilimler Bölümü
Biyoteknoloji Araştırma Birimi
Öğretim Üyesi

13.02.2009

G.Ü.ET-09.005 kod numaralı ve "*Kemik Doku Mühendisliğinde Kullanılmak Üzere "3D Plotting"(3 boyutlu basım) Tekniği ile Hazırlanan Poli (ε-caprolactone) Hücre Taşıyıcılarının In vivo Çalışmalarla Değerlendirilmesi*" başlıklı araştırma öneriniz incelenmiş ve Gazi Üniversitesi Hayvan Deneyleri Yerel Etik Kurul Yönergesindeki ilkelere uygun olduğu saptanarak onaylanmasına oybirliği ile karar verilmiştir.

Bilgilerinizi saygılarımla rica ederim.

It is unanimously approved that the research project numbered G.Ü.ET-09.005 and entitled "*In vivo Evaluation of 3D Plotted Poly (ε-caprolactone) Scaffolds for Bone Tissue Engineering*" is in compliance with Gazi University Animal Experiments Local Ethics Committee regulations.

With my best regards.


Prof.Dr.Gökhan ALPASLAN
Gazi Üniversitesi
Hayvan Deneyleri Yerel Etik Kurul Başkanı

Figure C.1. Ethical Committee Approval

CURRICULUM VITAE

PERSONAL INFORMATION

Surname, Name: Yılgör Huri, Pınar

Nationality: Turkish (T.C.)

Date and Place of Birth: 9 October 1981, Mersin, Turkey

Marital Status: Married

Phone: +90 312 210 51 93

Fax: +90 312 210 15 42

E-mail: pyilgor@yahoo.com

EDUCATION

Degree	Institution	Year of Graduation
MS	METU, Dept. of Chemical Engineering	2004
BS	Gazi Univ., Dept. of Chemical Engineering	2002
High School	Mersin Toros College	1998

ACADEMIC EXPERIENCE

Year	Place	Enrollment
2004-2009	METU, Biotechnology Research Unit	Full time Researcher
2006 (6 months)	3B's Research Group, Department of Polymer Engineering, Univ.Minho, Portugal	Visiting Researcher
2002-2004	METU, Chemical Engineering Dept., Industrial Biotechnology and Metabolic Engineering Research Lab	Full time Researcher

FOREIGN LANGUAGES: Advanced English

PUBLICATIONS

1. P.Yilgor, N.Hasirci, V.Hasirci, Sequential BMP-2/BMP-7 Delivery from Polyester Nanocapsules, *Journal of Biomedical Materials Research Part A*, doi: 10.1002/jbm.a.32520, 2009.
2. P.Yilgor, K.Tuzlakoglu, R.L.Reis, N.Hasirci, V.Hasirci, Incorporation of a Sequential BMP-2/BMP-7 Delivery System into Chitosan-Based Scaffolds for Bone Tissue Engineering, *Biomaterials*, 30, 3551–3559, 2009.
3. P.Zorlutuna, P.Yilgor, F.B.Basmanav, V.Hasirci, Biomaterials and Tissue Engineering Research in Turkey: The METU BIOMAT Center Experience, *Biotechnology Journal*, doi:10.1002/biot.200800335, 2009.

4. P.Yilgor, D.Yucel, H.Kenar, V.Hasirci. Polyhydroxyalkanoates: a Versatile Class of Biopolymers, and Their Biomedical Potential, In *Brazilian Network On Green Chemistry: Awareness, Responsibility And Action*, Ed. J.O.B.Carioca, Chapter 20, 415-431, 2008.
5. P.Yilgor, R.A.Sousa, R.L.Reis, N.Hasirci, V.Hasirci. 3D Plotted PCL Scaffolds for Stem Cell Based Bone Tissue Engineering, *Macromolecular Symposia*, 269, 92-99, 2008.
6. P.Yilgor, K.Tuzlakoglu, R.L.Reis, N.Hasirci, V.Hasirci, Nano/Microparticle Incorporated Chitosan Fibers as Tissue Engineering Scaffolds, *Tissue Engineering Part A*, 14(5), 759-759, Meeting Abstract, 2008.
7. P.Yilgor, C.Orth, S.Ghanaati, N.Hasirci, J.Kirkpatrick, V.Hasirci, PLGA Based BMP-2 Nanocapsules for Bone Tissue Engineering, *Tissue Engineering Part A*, 14(5), 896-897, Meeting Abstract, 2008.
8. V.Hasirci, E.Vrana, P.Zorlutuna, A.Ndreu, P.Yilgor, B.Basmanav, E.Aydin. Nano biomaterials; A review of the existing science and technology, and new approaches, *Journal of Biomaterials Science Polymer Edition*, 17(11), 1241-1268, 2006.
9. P.Calik, P.Yilgor, A.S.Demir. Influence of controlled-pH and uncontrolled-pH operations on recombinant benzaldehyde lyase production by *Escherichia coli*, *Enzyme and Microbial Technology*, 38(5), 617-627, 2006.
10. P.Calik, P.Yilgor, P.Ayhan, A.S.Demir. Oxygen Transfer Effects On Recombinant Benzaldehyde Lyase Production, *Chemical Engineering Science*, 59, 5075-5083, 2004.